

CLUSTERING OF MOTILE BACTERIA AROUND PHYTOPLANKTON
IN A TURBULENT OCEAN

by

JAMES DOUGLAS BOWEN

A.B. Botany, Duke University
(1979)

M.S. Civil and Environmental Engineering, Vanderbilt University
(1983)

Submitted to the Department of
Civil Engineering in Partial Fulfillment of
the Requirements for the
Degree of

DOCTOR OF PHILOSOPHY

at the

Massachusetts Institute of Technology

February 1990

© Massachusetts Institute of Technology
All Rights Reserved

Signature Redacted

Signature of Author _____
Department of Civil Engineering
January 15, 1990

Certified by _____
Signature Redacted
Keith D. Stolzenbach
Associate Professor, Civil Engineering
Thesis Co - Supervisor

Signature Redacted

Signature Redacted
Sallie W. Chisholm
Professor, Civil Engineering
Thesis Co - Supervisor

Accepted by _____
Ole S. Madsen
Departmental Committee on Graduate Studies

MASSACHUSETTS INSTITUTE
OF TECHNOLOGY

FEB 28 1990

LIBRARIES

ARCHIVES

Clustering of Motile Bacteria Around Phytoplankton in a Turbulent Ocean

by

James D. Bowen

Submitted to the Department of Civil Engineering
on January 16, 1990
in partial fulfillment of the requirements for the
Degree of Doctor of Philosophy

Abstract

Bacteria in the oligotrophic ocean live in a world where the bulk concentrations of the dissolved organic compounds important in metabolism are exceedingly low (10^{-8} to 10^{-13} M) yet recent measurements show bacteria generation times as short as eleven hours. Clustering of motile bacteria around phytoplankton cells that are exuding dissolved organic carbon might help explain this paradox. The non-random association between bacteria and phytoplankton may have important consequences to the exchange of nutrients and energy in the microbial food web. While swarming of bacteria around phytoplankton cells in culture can be observed under the microscope, there is no practical way to observe or sample clusters in situ. A simulation model of each of the relevant biological and physical processes was therefore developed to study the interactions between phytoplankton and motile bacteria in fluids with relative motions due to phytoplankton sinking and turbulent shearing.

A non-sinking phytoplankter in the upper mixed layer can be considered to be a continuous point source of mass into a fluid with a steady linear velocity distribution. Concentration distributions surrounding the phytoplankton cell are distorted by the flow at distances greater than $\gamma/E_b^{\frac{1}{2}}$, where γ is the molecular diffusion coefficient and E_b is a characteristic shear rate. The distributions have two distinct shapes depending on the number of principal axes of fluid strain that are expansive and the relative magnitude of irrotational and rotational shears. For irrotational flows a single expansive principal axis of strain results in tube-like structures while two expansive axes results in disk-like structures. Approximate analytical solutions, derived by neglecting diffusion along the expansive axes, agree well with concentrations calculated by numerically convolving the exact instantaneous source solution. The effect of fluid vorticity is generally to reorient the distributions away from the principal axes of strain and to reduce the asymmetry of the concentration distributions. The shape and structure of the concentration distribution varies little until the vorticity approaches a critical value defined by a kinematic condition for equilibrium orientation in the presence of rotation. For larger values of vorticity the concentrations distributions gradually become axisymmetric around the axis of rotation. Application of these results to numerical simulations of isotropic turbulence suggests that tubes are more common than disks and that vorticity exceeds the critical value throughout a significant portion of the fluid.

An analysis of published experiments on the pattern of bacterial swimming shows that a chemotactic bacteria's approach to a continuous point source of attractant can be described with a hyperbolic function of the temporal change in chemoreceptor occupancy experienced by the bacteria. In motionless fluid, the population density of chemotactic bacteria surrounding the source shows a characteristic form resulting from a balance between random and chemotactic bacterial motions. Near the source the population density decreases exponentially with distance at a rate dependent on the swimming speed and a characteristic run time of the bacteria. The population density approaches a uniform value at a distance dependent on the attractant input rate and bacterial chemotaxis sensitivity, but independent of the bacterial swimming speed. Peak bacterial population density near the source therefore decreases with increasing bacterial swimming speed in motionless fluids. When the source is in relative motion, bacterial densities approach background levels at a distance where effective chemotactic motion balances fluid motion. The bacterial population density distribution near the source varies as in the motionless case according to the swimming speed and characteristic run time.

Results of the simulation model of bacterial chemotaxis towards an exuding phytoplankton indicate that bacteria may attain population densities orders of magnitude above background levels in microzones occupying less than 0.1 percent of the total fluid volume. The degree of clustering varies with phytoplankton exudation rate, and bacterial swimming speed and chemotactic sensitivity, but it does not depend directly on phytoplankton cell size. At turbulence intensities expected in the upper mixed layer of the oceans (shear rate of $.15 \text{ sec}^{-1}$) as much as twenty percent of the chemotactic bacteria population can be clustered around exuding phytoplankton cells even though individual encounters last only seconds. The time-averaged exudate concentration experienced by the chemotactic population is as much as ten times higher than that experienced on average by non-chemotactic bacteria. At shear intensities of $.15 \text{ sec}^{-1}$ or phytoplankton sinking speeds of $10 \mu\text{m sec}^{-1}$ the bacteria's ability to stay near a phytoplankton depends on both the random and effective chemotactic components of bacterial motion, such that an intermediate swimming speed of approximately $40 \mu\text{m sec}^{-1}$ maximizes the time-averaged exudate exposure. Unsteady turbulent mixing in the oceanic surface layer disperses clusters during bursts of mixing but intervening calm periods are long enough to allow clusters to reform. The bacteria in a cluster may take up as much as seventy percent of the exuded photosynthate assuming diffusion limited bacterial uptake, but the spatial distribution of bacteria does not significantly affect competition for limiting nutrients between phytoplankton and bacteria.

Thesis Co - Supervisor: Keith D. Stolzenbach
Title: Associate Professor of Civil Engineering

Thesis Co - Supervisor: Sallie W. Chisholm
Title: Professor of Civil Engineering

To Mom, whose energy, courage, and charity continue to inspire me
and
To Dad, who taught me to do my best

Acknowledgements

This research was partially supported by the National Science Foundation under Grant Nos. OCE-8614488 and CES-8801767 and from a Hugh Hampton Young Fellowship.

I would like to thank the members of my thesis committee: Penny Chisholm, Keith Stolzenbach, John Waterbury, and Phil Gschwend for the time and effort invested in assisting my research. I would also like to thank these members of the Parsons Lab community whose friendship and assistance have made graduate school a little more bearable: Pat and Brian Dixon, Sheila Frankel, Vicki Murphy, Ginger Armbrust, and Deb Backhus.

Finally, I would like to thank my wife, Carol Bowen, for the love and support over the last five years of graduate school and the last ten years of our marriage. Her faith and encouragement got me through the bad times. I am truly thankful for her presence in my life.

TABLE OF CONTENTS

Chapter 1.	Introduction and Summary of Thesis Research	7
Chapter 2.	Concentration Distributions Around Continuous Point Sources in a Fluid with a Steady Linear Velocity Distribution	22
Chapter 3.	Strong Rotation Produces Vortex Tubes in Homogeneous, Isotropic Turbulence	73
Chapter 4.	Microbial Chemotaxis Towards a Continuous Point Source of Attractant	82
Chapter 5.	Simulating Bacterial Clustering Around Phytoplankton Cells in a Turbulent Ocean	103
Appendix A.	Model Validation and Sensitivity Analysis	154
Appendix B.	Computer Codes	177

Chapter 1.

Introduction and Summary of Thesis Research

Recent measurements of bacterial biomass, growth rates and heterotrophic activity have forced microbial ecologists to reevaluate the coupling between organic matter production and heterotrophic activity. Bacterioplankton were originally regarded primarily as either dormant (Stevenson 1978) or as remineralizers attached to detrital organic material (Steele 1974). Free-living bacteria were thought to have population densities below that of phytoplankton and have the slow growth rates consistent with the dilute nature of the dissolved organic compounds important to metabolism, which typically have concentrations in the nanomolar range (Williams 1976, Mopper and Lindroth 1982, Carlucci et al. 1984). With advances in techniques for measuring bacterioplankton biomass and productivity came the discoveries that bacterial biomass approaches phytoplankton biomass (Williams 1981), that bacteria generation times may be as short as ten hours (Hagstrom et al. 1979, Fuhrman and Azam 1980) and that bacterial secondary production can be 10 - 50 percent of primary production (Fuhrman and Azam 1982, Williams 1984, Scavia et al. 1986). Bacterioplankton are now recognized as an important component of the planktonic food web (Fenchel 1988).

The major sources of the reduced organic material metabolized by free-living bacterioplankton in oligotrophic waters are phytoplankton and zooplankton exudation, sloppy feeding by zooplankton, and dissolution of detrital material (Williams 1981). The relative importance of these sources is a matter of some controversy. Measurements of *in situ* exudation, expressed as a percentage of the primary productivity rate, have varied widely (Sharp 1977, Jones and Cannon 1986), and many *in situ* exudation measurements exceed those performed on phytoplankton in culture. In addition, Jumars et al. (1989) have pointed out that the *in situ* exudation measurements often do not discriminate between phytoplankton exudation and phytoplankton releases associated with grazing, either from damaged phytoplankton (Lampert 1978) or from dissolution of fecal pellets

(Jumars et al. 1989). Nonetheless, it is generally accepted that in marine systems 5 - 30 percent of the carbon fixed through photosynthesis is lost from phytoplankton cells. Since bacterial productivity has been measured to be 10 - 50 percent of primary productivity, it seems likely that the loss of organic material from phytoplankton cells is a major source of nutrition to free-living marine bacteria.

Reduced carbon released by phytoplankton is introduced to the bacterioplankton from a finite number of concentrated sources. The concentrated nature of the source and the observation that some bacterioplankton are motile has prompted the hypothesis that chemotactic bacteria may be clustered around phytoplankton cells that are releasing dissolved organic carbon into the fluid (Bell and Mitchell 1972). Bell and Mitchell (1972) used capillary chemotactic assays to demonstrate that some motile marine bacteria are attracted to algal exudate. Chemotaxis to the small chain alcohols, sugars, and amino acids known to be in algal exudate (Hellebust 1965) has been observed repeatedly for marine and freshwater bacteria (Chet and Mitchell 1976, Geesey and Morita 1979, Gallucci and Paerl 1994, Hazen et al. 1984). In addition, swarming of bacteria around phytoplankton cells can be observed in mixed cultures of phytoplankton and bacteria, but at present there is no way to observe bacterial clusters *in situ*. While the chemotaxis assays demonstrate the possibility of clustering, an assessment of clustering in the upper mixed layer must also account for the effects of fluid motion resulting from sinking of phytoplankton cells or from turbulent shearing of the fluid.

The objective of the following thesis research is to develop a better understanding of the physical and biological processes affecting the clustering of motile bacteria around phytoplankton cells. The primary tool in the analysis of bacterial clustering is a simulation model of bacterial chemotaxis surrounding a phytoplankton cell. Concentration distributions surrounding the phytoplankton cell are simulated for the fluid motions expected either from sinking of the

phytoplankton or from turbulent shearing of the fluid. Bacterial chemotactic swimming is simulated using models of chemotaxis developed from experiments on enteric and photosynthetic bacteria (e.g., MacNab and Koshland 1972, Brown and Berg 1974, Armitage and MacNab 1987). The relative motion of the bacteria is also affected by the relative motion of the fluid.

Previous investigations of clustering have relied on order of magnitude estimates of the physical processes (Mitchell et al. 1985) or have focused on the short-term, transient response of chemotactic bacteria (Jackson 1987, 1989). While these studies have provided necessary background information, they have not adequately simulated the effects of turbulent shear on exudation distributions or bacterial movement. The simulation model presented here relies on new information developed as part of the thesis research describing analytically the exudate concentration distributions surrounding phytoplankton in fluids with the shearing motion expected in the mixed layer. The study then extends Jackson's analysis of the initial response of a bacteria population by simulating behavior over periods long enough to quantify the population density and time-averaged exudate exposure of the chemotactic bacteria population. These two parameters are critical in assessing the ecological implications of non-random interactions between phytoplankton and chemotactic bacteria. The population density and time-averaged exudate exposure are examined for the range of phytoplankton exudation rates, marine bacteria chemotaxis abilities, and fluid motion conditions expected in the mixed layer. The utility of chemotactic behavior is examined by comparing time-averaged exudate exposures for populations of chemotactic and non-chemotactic bacteria. The calculated bacterial population densities are used to estimate clustering effects on the exudate spatial distributions, on the bacteria population's effect, on the phytoplankton's uptake of inorganic nutrient, and on the flow of carbon through the microbial food web.

The first phase of the research asked the following question: How does shearing fluid motion around individual phytoplankton cells affect exudate concentration distributions? While much is known about how shearing motion modifies the mass transfer rate from particles (Batchelor 1979, 1980), there is little information on concentration distributions surrounding sources of mass or heat in shearing flows. Concentration distributions are known only for the simple case of two-dimensional simple shear (Frankel and Acrivos 1968), and numerical solutions have also been reported for this type of flow (Csanady 1966, Okubo and Karweit 1969). No analytical solutions are available for a general shearing flow, although concentrations at points in space can be calculated by summing the contributions of many instantaneous point sources, for which analytical solutions are available for a general linear velocity distribution (Foister and Van de Ven 1980).

Chapter 2 describes the concentration distributions that might be expected around a phytoplankton cell assumed to be a continuous point source of mass into a fluid with a steady linear velocity distribution. For the shear rates expected in the upper mixed layer, phytoplankton that exude dissolved organic carbon and have cell radii less than 30 μm can be considered point sources of mass, and their exudation rate can be considered steady if the time scale for variation exceeds a few seconds. In analyzing the concentration distributions, the general linear velocity distribution is divided into irrotational and rotational flow cases. For the irrotational case, approximate analytical solutions are derived in the region where advection dominates the mass transfer by neglecting diffusive transport along the axes where fluid moves directly away from the phytoplankton. The shear pattern is specified with a characteristic shear strength that determines the spatial scale of the concentration distributions and a symmetry factor that determines the shape of the concentration distributions. Qualitatively, the analytical solutions predict

concentration distributions having either tube or disk like shapes depending on the sign of the symmetry factor.

Rotational effects are analyzed by systematically varying the strength of rotational motion, while fixing the alignment of the rotation axis, the shear intensity, and the shear symmetry factor. Concentration distributions along axes defining the equilibrium orientation of an instantaneous pulse are calculated by summing the contributions of many instantaneous point sources. Rotation effects on the concentration distributions are found to be minor until the rotation rate approaches a critical value equal to the rate necessary to give imaginary eigenvectors for the velocity gradient tensor. When the rotation axis is aligned with a principal axis of strain, the critical rotation rate is simply one-half the difference in the principal strain rates perpendicular to the rotation axis. As the rotation rate increases beyond the critical value, concentration distributions approach an axisymmetric configuration with a characteristic shear strength equal to the strain rate along the rotation axis.

An examination of exudate distributions surrounding phytoplankton in the upper mixed layer must also account for the unsteadiness in shear intensity characteristic of turbulent flows. Lumley (1972) has hypothesized that each shear rate in homogeneous, isotropic turbulence lasts for a time corresponding to the large scale motions. In the upper mixed layer this time is long compared to the time it takes for the establishment of a steady concentration distribution which scales with the inverse of the shear rate. The time history of exudate concentration distributions in turbulent shearing can therefore be seen as a collection of steady state distributions separated by short transition periods. The equations developed for steady shearing are appropriate for the relatively long period after the short transition to a new shearing rate.

The research described in Chapter 3 examines whether regions of strongly rotational flow are concentrated in disk or tube like structures for flows assumed to have homogeneous, isotropic turbulence. Recent turbulence theory is often based on a conceptualization of turbulence as a collection of coherent structures (Liu 1989). The thesis research contributes to our understanding of how these coherent structures are distorted by shear and rotation. Recent numerical simulations of turbulence have shown that regions of strong rotation are concentrated in tube shaped structures (Kerr 1985, Ashurst et al. 1987), yet predictions based solely on the irrotational component of the flow predict that disk shaped structures should be more common than tubes (Townsend 1951). It is shown in Chapter 3 how strong rotation can modify the distortion of fluid elements from that predicted by the irrotational component of the flow. In locations where the flow is strongly rotational and has a positive strain rate along the rotation axis, fluid elements will be distorted into tubes regardless of the irrotational shear pattern. Results from numerical simulation show that this situation occupies at least 25 percent of the fluid volume (Ashurst et al. 1987), tipping the balance from one favoring disks (based on the irrotational shear component only) to that where tube shaped structures are expected to be most common.

Any investigation of bacterial clustering inevitably asks the question: How do bacteria find the phytoplankton? Experiments on the peritrichously flagellated bacteria *Escherichia coli* have shown that chemotactic bacteria move in a directed fashion towards higher concentrations of attracting compounds by regulating the switching rate between directions of flagellar rotation (Block et al. 1982). Counter-clockwise rotation (looking towards the cell) results in smooth straight runs, while clockwise rotation results in a tumbling reorientation of the cell with little net movement. Directed motion is accomplished by adjusting the length of runs depending on the temporal change in attractant sensed by the bacteria as it runs

through spatial gradients of attractant. While this description of chemotactic swimming pattern is based on experiments performed with enteric and photosynthetic bacteria (e.g., MacNab and Koshland 1972, Brown and Berg 1974, Armitage and MacNab 1987) these bacteria possess the same peritrichous or polar flagellation observed for many isolates of heterotrophic marine bacteria (e.g., Baumann and Baumann 1978). Furthermore, the small cell size of both marine and enteric bacteria prevents these bacteria from directly measuring spatial gradients of attractant (Berg and Purcell 1977). Considering the similarity in morphologies and the limits to the ways in which bacteria can respond to chemical cues, it seems reasonable to expect that marine bacteria have chemotactic swimming patterns similar to that already described for enteric or photosynthetic bacteria.

In an effort to better understand the balance between the physical and biological process involved in bacterial clustering, a theoretical analysis of clustering was conducted that is based on a simpler, deterministic description of the bacterial population response. Keller and Segel (1971) first proposed that the response of a chemotactic population can be modelled as the sum of an effective chemotactic velocity dependent on the spatial gradient of chemoattractant and a random diffusion coefficient. From this deterministic description of chemotactic behavior, predictions of the distribution of chemotactic bacteria have been made for chemotaxis in a uniform flow with plane source of attractant (Lapidus 1980), or for chemotaxis and bacterial growth in motionless fluid with a plane source of attractant (Lauffenburger et al. 1982). The deterministic description of chemotaxis has also been used in analyzing chemotaxis experiments that measure directly the bacteria population density (e.g., Dahlquist et al. 1972).

In Chapter 4 an analysis of published experiments on the pattern of chemotactic movement (Brown and Berg 1974, Dahlquist et al. 1976) is used to relate the deterministic and stochastic descriptions of chemotactic behavior. It is shown that

the model of run time regulation for *E. coli* (Brown and Berg 1974) results in an effective chemotactic velocity that is a hyperbolic function of the temporal change in chemoreceptor occupancy. Measurements of each of the parameters in the equation for effective chemotactic velocity are available in the literature, allowing for quantitative predictions of the bacterial population density for a given flux of chemoattracting compound.

Analytical solutions for the population density distribution are derived using the deterministic model of chemotaxis. The analytical solutions predict that the population density near the phytoplankton cell decreases exponentially with increasing distance at a rate related to an average run length for the bacteria. The bacterial population density approaches a uniform value at a distance directly related to a normalized exudation flux, but unrelated to the swimming speed of the bacteria. In motionless fluid these two results lead to the prediction that the maximum population density, which is achieved at the phytoplankton cell surface, decreases with increasing bacterial swimming speed.

A scaling analysis is used to predict the bacterial population density distribution in cases where the fluid surrounding the phytoplankton is in relative motion due to either sinking of the phytoplankton cell or through shearing of the fluid. Near the phytoplankton cell the population density decreases exponentially as in the motionless case, but it is shown that for cases with fluid motion the distance where population densities approach background levels depends on the exudation rate of the phytoplankton. Comparison of results from the simulation model of bacterial clustering with predictions that utilize the derived relationship for effective chemotactic velocity show that in moving fluids the density approaches background levels at a distance where the effective chemotaxis velocity towards the phytoplankton is equal to the fluid velocity away from the phytoplankton. This result leads to the conclusion that for moving fluids the peak population density

near the phytoplankton is maximized for an intermediate swimming speed that provides enough effective velocity to overcome fluid motions while minimizing the random component of bacterial motion.

In the final phase of the study the simulation model of bacterial motion around phytoplankton was utilized to address these questions regarding the ecological implications of bacterial clustering in the oceanic mixed layer:

1. How much of the chemotactic population is in a cluster at any given time? Is this fraction high enough so that phytoplankton grazers might also be important bacteria grazers?
2. How much of an advantage in terms of time-averaged exudate exposure does a population of chemotactic bacteria receive relative to a non-chemotactic population?
3. How much of the dissolved organic carbon released by the phytoplankton is taken up by the bacteria in a cluster?
4. Does the spatial distribution of chemotactic bacteria affect the spatial distribution of exudate surrounding the phytoplankton?
5. Assuming that bacteria and phytoplankton are competitors for inorganic nutrients, does the spatial distribution of chemotactic bacteria affect the flux of these nutrients to the phytoplankton?

The simulation model predicts that the bacterial population density near a phytoplankton cell may be orders of magnitude above background levels for the exudation rates, bacterial swimming speeds, and fluid motions expected in the mixed layer. Both the fraction of the bacteria population in a cluster and the time-averaged exudate exposure are found to vary with phytoplankton exudation rate, bacterial swimming speed and chemotactic sensitivity. However, these parameters do not depend directly on phytoplankton cell size as has been hypothesized in earlier modelling studies of marine bacterial chemotaxis (Jackson 1987). At turbulence intensities expected in the upper mixed layer of the oceans (shear intensity of 0.15 sec^{-1}) as much as twenty percent of the chemotactic bacteria population can be

clustered at any given time, even though individual encounters between phytoplankton and bacteria last only seconds. At these shear intensities the fraction clustered is found to increase for faster bacteria swimming speeds when the exudation rates and chemotaxis sensitivities are held constant. The fractions clustered do not appear high enough, however, to represent a significant link in the microbial food web between bacteria and phytoplankton grazers.

The time-averaged exudate exposure is found to be highest for the intermediate swimming speed of $40 \mu\text{m sec}^{-1}$, a finding that is consistent with the analysis of the run and tumble chemotaxis model described in Chapter 4. At this intermediate swimming speed the time-averaged exudate concentration experienced by the chemotactic population is as much as ten times higher than that experienced on average by non-chemotactic bacteria. The large differences in time-averaged exudate exposure between chemotactic and non-chemotactic populations occurs over the entire range of shear intensities simulated.

A simulation of unsteady shearing is accomplished by randomly selecting individual shear rates from a log-normal distribution, with mean and variance matched to oceanographic measurements of wind or convectively driven shearing in the upper mixed layer. The simulation predicts that bursts of intense shearing, with intensities more than five times the mean value, are strong enough to completely disperse clusters. However, between the bursts are periods where the shearing is below the mean value, and the simulation shows that these intervening calm periods last long enough for clusters to reform. By the end of the calm period the fraction clustered exceeds that expected for steady shearing at the mean value for both swimming speeds simulated ($V = 12$ and $40 \mu\text{m sec}^{-1}$). The reformation rate of the cluster and the time-averaged exudate exposure are higher for a swimming speed of $40 \mu\text{m sec}^{-1}$, as compared with a swimming speed of $12 \mu\text{m sec}^{-1}$. The unsteadiness

of the shearing results in a time-averaged exudate exposures that are twenty to seventy-five percent higher than the corresponding values for steady shearing.

The calculated bacterial population densities are used to estimate clustering effects on the exudate distribution surrounding a phytoplankton and on the competition for limiting nutrients between phytoplankton and bacteria. Small clustered fractions are found to be capable of a cumulative uptake that is a significant percentage of the phytoplankton exudation rate. Approximately thirty percent of the material released by the phytoplankton can be taken up by a bacterial cluster of only fifty cells when the bacteria's exudate uptake is assumed to be at the maximum diffusion limited rate. At the assumed bacterial population density of 10^6 cells ml^{-1} , fifty bacteria represents only five percent of the bacteria population. However, the simulation results indicate that the spatial distribution of bacteria does not significantly affect the uptake of limiting inorganic nutrient by the phytoplankton.

The simulation model indicates that for the range of conditions expected in the oceanic mixed layer, clustering can be important to the ecology of heterotrophic, free-living bacteria. Because of shearing motions and phytoplankton sinking, free-living bacteria spend a relatively small fraction of their lifetime in bacterial clusters, and individual encounters last only seconds, nonetheless chemotactic behavior significantly improves exposure to exuded organic carbon, as compared with the exudate exposure of non-chemotactic bacteria. Exudate uptake by the bacteria in a cluster can be a significant percentage of the phytoplankton exudation rate, and this uptake can modify the exudate concentrations experienced by non-chemotactic cells.

References

- Armitage, J.P., and R.M. MacNab. 1987. Unidirectional, intermittent rotation of the flagellum of *Rhodobacter sphaeroides*. *Journal of Bacteriology*. 169: 514-518.
- Ashurst, W.T., A.R. Kerstein, R.M. Kerr, and C.H. Gibson. 1987. Alignment of vorticity and scalar gradient with strain rate in simulated Navier-Stokes turbulence. *Phys. Fluids*. 30: 2343.
- Batchelor, G.K. 1979. Mass transfer from a particle suspended in fluid with a steady linear ambient velocity distribution. *Journal of Fluid Mechanics*. 95: 369-400.
- Batchelor, G.K. 1980. Mass transfer from small particles suspended in turbulent fluid. *Journal of Fluid Mechanics*. 98: 609-623.
- Baumann, P., and L. Baumann. 1978. The marine gram-negative eubacteria: Genera *Photobacterium*, *Beneckea*, *Alteromonas*, *Pseudomonas*, and *Alicagenes*. In: *Bergeys Manual of Systematic Bacteriology*, pp. 1301-1331. N.R. Krieg and J.G. Holt, eds. Williams and Wilkins.
- Bell, W.H., and R. Mitchell. 1972. Chemotactic and growth responses of marine bacterial to algal extracellular products. *Biological Bulletin*. 143: 265-277.
- Berg, H.C., and E.M. Purcell. 1977. Physics of chemoreception. *Biophysical Journal*. 20: 193-209.
- Block, S.M., J.E. Segall, and H.C. Berg. 1982. Impulse responses in bacterial chemotaxis. *Cell*. 31: 215-226.
- Brown, D.A., and H.C. Berg. 1974. Temporal stimulation of chemotaxis in *Escherichia coli*. *Proceedings of the National Academy of Sciences of the U.S.A.* 71: 1388-1392.
- Carlucci, A.F., D.B. Craven, and S.M. Henrichs. 1984. Diel production and microheterotrophic utilization of dissolved free amino acids in waters off southern California. *Applied and Environmental Microbiology*. 48: 165-170.
- Chet, I., and R. Mitchell, 1976, The relationship between chemical structure of attractants and chemotaxis by a marine bacterium. *Canadian Journal of Microbiology*. 22: 1206-1208.
- Csanady, G.T. 1966. *Turbulent Diffusion in the Environment*. D. Reidel.
- Dahlquist, F.W., P. Lovely, and D.E. Koshland, Jr. 1972. Quantitative analysis of bacterial migration in chemotaxis. *Nature, New Biology*. 236: 120.
- Dahlquist, F.W., R.A. Elwell, and P.S. Lovely. 1976. Studies of bacterial chemotaxis in defined concentration gradients: A model for chemotaxis toward L-Serine. *Journal of Supramolecular Structure*. 4: 329.
- Fenchel T. 1988. Marine plankton food chains. *Annual Review of Ecology and Systematics*. 19: 19-38.

- Foister, R.T., and T.G.M. Van de Ven. 1980. Diffusion of brownian particles in shear flows. *J. Fluid Mech.* **96**: 105.
- Frankel, N.A. and A. Acrivos. 1968. Heat and mass transfer from small spheres and cylinders freely suspended in shear flow. *Physics of Fluids.* **11**: 1913.
- Fuhrman, J.A., J. Ammerman, and F. Azam. 1980. Bacterioplankton in the coastal euphotic zone: Distribution, activity, and possible relationships with phytoplankton. *Marine Biology.* **66**: 109-120.
- Fuhrman, J. A., and F. Azam. 1980. Bacterioplankton secondary production estimates for coastal waters of British Columbia, Antarctica, and California. *Applied Environmental Microbiology.* **39**: 1085-1102.
- Gallucci, K.K., and H.W. Paerl, 1984. *Pseudomonas aeruginosa* chemotaxis associated with blooms of N₂-fixing blue-green algae (Cyanobacteria). *Applied and Environmental Microbiology.* **45**: 557-562.
- Geesey, G.G., and R.Y. Morita. 1979. Capture of arginine at low concentrations by a marine psychrophilic bacterium. *Applied and Environmental Microbiology.* **38**: 1092-1097.
- Hagstrom, A., U. Larsson, P. Horstedt, and S. Normark. 1979. Frequency of dividing cells: A new approach to the determination of bacterial growth rates in aquatic environments. *Applied and Environmental Microbiology.* **37**: 805.
- Hazen, T.C., R.F. Dimock Jr, G.W. Esch, A. Mansfield, and M.L. Raker. 1984. Chemotactic behavior of *Aeromonas hydrophila*. *Current Microbiology.* **10**: 13-18.
- Hellebust, J.A. 1965. Excretion of some organic compounds by marine phytoplankton. *Limnology and Oceanography.* **10**: 192-206.
- Jackson, G.A. 1987. Simulating chemotaxis by marine microorganisms. *Limnology and Oceanography.* **32**: 1253-1266.
- Jackson, G.A. 1989. Simulation of bacterial attraction and adhesion to falling particles in an aquatic environment. *Limnology and Oceanography.* **34**: 514-530.
- Jones, A.K., and Cannon, R.C. 1986. The release of micro-algal photosynthate and associated bacterial uptake and heterotrophic growth. *British Phycological Journal.* **21**: 341-358.
- Jumars, P.A., D.L Penry, J.A. Baross, M.J. Perry, and B.W. Frost. 1989. Closing the microbial loop: dissolved carbon pathway to heterotrophic bacteria from incomplete ingestion, digestion and absorption in animals, *Deep-Sea Research.* **36**: 483-495.
- Keller, E.F., and L.A. Segel. 1971. Model for chemotaxis. *J. Theor. Biol.* **30**: 225.
- Kerr, R.M. 1985. Higher-order derivative correlations and the alignment of small-scale structures in isotropic numerical turbulence. *J. Fluid Mech.* **153**: 31.

- Lampert, W. 1978. Release of dissolved organic carbon by grazing zooplankton. *Limnology and Oceanography*. **23**: 831-834.
- Lapidus, I.R. 1980. Microbial chemotaxis in flowing water in the vicinity of a source of attractant or repellent. *J. Theor. Biol.* **85**: 543.
- Lauffeburger, D., R. Aris, and K. Keller. 1982. Effects of cell motility and chemotaxis on microbial population growth. *Biophysical Journal*. **40**: 209.
- Liu, J.T.C. 1989. Coherent structures in transitional and turbulent free shear flows. *Annual Review of Fluid Mechanics*. **21**: 285-315.
- Lumley, J.L. 1972. On the solution of equations describing small scale deformation. In *Symposia Matematica: Convegno sulla Teoria della Turbolenza al Istituto Nazionale di Alta Matematica*, pp. 315-334, Academic Press.
- Macnab, R.M., and D.E. Koshland Jr. 1972. The gradient-sensing mechanism in bacterial chemotaxis. *Proceedings of the National Academy of Sciences of the U.S.A.* **69**: 2509-2512.
- Mopper, K., and P. Lindroth. 1982. Diel and depth variations in dissolved free amino acids and ammonium in the Baltic Sea determined by shipboard HPLC analysis. *Limnology and Oceanography*. **27**: 336-347.
- Okubo, A., and M. J. Karweit. 1969. Diffusion from a continuous source in a uniform shear flow. *Limnology and Oceanography*. **14**: 514.
- Scavia, D., G.A. Laird, and G.L. Hahnenstiel. 1986. Production of planktonic bacteria in Lake Michigan. *Limnology and Oceanography*. **31**: 612-626.
- Sharp, J.H. 1977. Excretion of organic matter by marine phytoplankton: Do healthy cells do it? *Limnology and Oceanography*. **22**: 381-399.
- Steele, H.H. 1974. *The Structure of Marine Ecosystems*. Harvard University Press.
- Stevenson, L.H. 1978. A case for bacterial dormancy in aquatic systems. *Microbial Ecology*. **4**: 127-133.
- Townsend, A.A. 1951. On the fine-scale structure of turbulence. *Proc. Roy. Soc. A*, **208**: 534.
- Williams, P.J.LeB. 1981. Incorporation of microheterotrophic processes into the classical paradigm of the planktonic food web, *Kieler Meeresforsch.* **5**: 1-28.
- Williams, P.J.LeB. 1984. Bacterial production in the marine food chain: The emperor's new suit of clothes? In *Flows of Energy and Materials in Marine Ecosystems*, pp 345-360. M.J.R. Fasham, Ed. Plenum.

Chapter 2.

Concentration Distributions Around Continuous Point Sources in a Fluid with a Steady Linear Velocity Distribution

Abstract

Concentration distributions resulting from continuous point sources in a fluid with a steady linear variation in velocity are distorted by the flow at distances greater than $\gamma/E_b^{1/2}$, where γ is the molecular diffusion coefficient and E_b is a characteristic shear rate. The distributions have two distinct shapes depending on the number of principal axes of fluid strain that are expansive and the relative magnitude of irrotational and rotational shears. For irrotational flows a single expansive principal axis of strain results in tube-like structures, while two expansive axes result in disk-like structures. Approximate analytical solutions, derived by neglecting diffusion along the expansive axes, agree well with concentrations calculated by numerically convolving the exact instantaneous source solution. The effect of fluid vorticity is generally to reorient the distributions away from the principal axes of strain and to reduce the asymmetry of the concentration distributions. The shape and structure of the concentration distribution varies little until the vorticity approaches a critical value defined by a kinematic condition for equilibrium orientation in the presence of rotation. For larger values of vorticity the concentration distributions gradually become axisymmetric around the axis of rotation. Application of these results to numerical simulations of isotropic turbulence suggests that tubes are more common than disks and that vorticity exceeds the critical value throughout a significant portion of the fluid. Fluid shearing motions may modulate the chemosensory association of aquatic microorganisms in a turbulent mixed layer of the ocean.

1. Introduction

In this article we consider the concentration distribution resulting from a continuous point source of soluble mass into an incompressible fluid with a steady velocity that is a homogeneous linear function of the distance from the point of input and which may be either irrotational or rotational. Of particular interest are the qualitative and quantitative features of the concentration distribution far enough from the source to be affected by the fluid motion but sufficiently close that the assumptions of steady homogeneous shear are valid for real flows. The analysis presented here will be applicable to mass transfer from a finite-sized particle as long as the Peclet number based on the particle diameter and the shear rate is small (Batchelor 1979).

In general we seek solutions to the advection-diffusion equation, given here in the steady-state form as

$$U_i \frac{\partial C}{\partial x_i} = \gamma \frac{\partial^2 C}{\partial x_i \partial x_i} \quad (1.1)$$

where C is the dissolved constituent concentration, \mathbf{x} is the position vector from the point of mass input, and γ is the molecular diffusion coefficient. The boundary conditions are

$$\begin{aligned} C &\rightarrow 0 \quad \text{as } r \rightarrow \infty \\ 4\pi r^2 \gamma \frac{dC}{dr} &= F \quad \text{as } r \rightarrow 0 \end{aligned} \quad (1.2)$$

where F is the steady mass input rate and $r = (\mathbf{x}_i \mathbf{x}_i)^{\frac{1}{2}}$ is the distance from the point source. The general linear form for the relative fluid velocity \mathbf{U} is

$$U_i = G_{ij} x_j = (E_{ij} + \Omega_{ij}) x_j \quad (1.3)$$

where the velocity gradient tensor \mathbf{G} is split into symmetric and anti-symmetric parts, \mathbf{E} and $\mathbf{\Omega}$ respectively, subject to the continuity constraint for an incompressible fluid $E_{ii} = G_{ii} = 0$. The elements of the velocity gradient tensor \mathbf{G} are assumed to be constant in time and space.

Little previous work has been done on the concentration distributions for continuous point sources in flows with general linear velocity distributions. Analytical solutions are available for a continuous point source in a uniform stream (Carslaw and Jaeger 1959) and numerical solutions for continuous sources in two-dimensional shear flows have been presented (Csanady 1966, Okubo and Karweit 1969). In contrast, the problem of diffusion of instantaneous sources in isotropic turbulence has a long theoretical and experimental history. The diffusion of heat spots in irrotational sheared flow was investigated by Townsend (1951a) whose equations for heat spot dispersal agreed well with experiments using hot wire anemometry. The problem of diffusion of instantaneous sources in simple sheared flows was solved first by Novikov (1958) and again by Elrick (1962). Lumley (1972) investigated the effects of vorticity on the dispersal of point sources in two dimensional shearing flow. The instantaneous source solution for a general linear flow was given by Batchelor (1979) and by Foister and Van de Ven (1980).

In the following sections we examine first solutions for both instantaneous and continuous point sources in flows with linear velocity distributions. A numerical solution for a continuous source based on a convolution of the exact instantaneous source solution is described. Next, the simple case of irrotational shearing is analyzed, for which analytical solutions exist for instantaneous pulses (Townsend 1951a) and approximate analytical solutions for continuous sources are also possible. We then analyze the effects of rotation by examining how the relative magnitude of the strain and vortical components affect the shape of a particular concentration contour. In the discussion section we consider the assumption that the velocity

gradient tensor is steady and homogeneous and give a qualitative picture of the shape of concentration contours from point sources in isotropic turbulence. We conclude with the application of our results to the problem of chemosensing by aquatic microorganisms.

2. General Solutions for Instantaneous and Steady Point Sources

For diffusion of continuous sources in general linear flows, a solution technique for the concentration field was presented by Batchelor (1979) as a convolution integral of the instantaneous source solution. These analytical solutions for instantaneous point sources can be integrated to yield concentration distributions for all linear flow fields described by Eq. 1.3. In some special cases the form of the instantaneous point source solutions can be used as a basis for approximate analytical results. In addition we will show that for any velocity gradient \mathbf{G} the instantaneous source solution has a simple form related to the dimensions and orientation of the instantaneous pulse. With this in mind we will first present in some detail the instantaneous point source solution.

Instantaneous Source Solution

The solution for an instantaneous point source can be given by the generalized Gaussian

$$C(\mathbf{x},t) = B(t) \exp\left[-\frac{1}{2}I_{pq}^{-1} x_p x_q\right] \quad (2.1)$$

where I is the second moment tensor of the concentration distribution defined as (Tennekes and Lumley 1972)

$$I_{pq}(t) = \iiint_{-\infty}^{\infty} x_p x_q C(\mathbf{x},t) dx_1 dx_2 dx_3 \quad (2.2)$$

The generalized Gaussian is a solution for the instantaneous point release provided that the second moment tensor satisfies the following ordinary differential equation.

$$\frac{dI_{pq}}{dt} - I_{pj}G_{qj} - I_{qj}G_{pj} = 2\gamma\delta_{pq} \quad (2.3)$$

The concentration term $B(t)$ is found using the instantaneous source boundary condition, which gives

$$B(t) = \frac{M}{(2\pi)^{3/2} I^{1/2}} \quad (2.4)$$

where M is the source strength for the instantaneous pulse and I is the determinant of the second moment tensor I .

Eq. (2.3) is invariant to an exchange of indexes for I_{pq} , therefore the second moment tensor will be symmetric for all time for any G since the boundary condition, given as $I_{pq} \sim 2\gamma\delta_{pq}t$ as $t \rightarrow 0$ is also symmetric (Batchelor 1979). All symmetric matrices have principal axes that are real and orthogonal, thus I can be transformed according to $\lambda_i = I_{pq}\zeta_p^{(i)}\zeta_q^{(i)}$ where $\zeta^{(i)}$ is the unit position vector in the original coordinate system for the i th eigenvector of I . The generalized Gaussian solution can now be more simply given as

$$C(\mathbf{x},t) = B(t) \exp\left[\frac{-\mathbf{x}_i\mathbf{x}_i}{2\lambda_i}\right] \quad (2.5)$$

with \mathbf{x} now defined as the position vector relative to point of mass release in the coordinate system formed by the principal axes for I . The concentration term $B(t)$ can now be specified with the following simple form.

$$B(t) = \frac{M}{(2\pi)^{3/2}(\lambda_1\lambda_2\lambda_3)^{1/2}} \quad (2.6)$$

The diffusing instantaneous pulse has an orientation defined by $\zeta^{(i)}$ and dimensions along each axes given by λ_i . The time evolution of λ is determined by

the solution to the ordinary differential equation (Eq. 2.3). This analysis is valid for all linear flow fields, although it will be shown that when the relative velocity includes a rotational component the principal axes of the pulse will be functions of time and will not coincide with the principal axes of strain.

Steady Concentration Distributions

The concentration for any location \mathbf{x} surrounding the point of input for a continuous source can be given by convolution of the instantaneous source solution (Eq. 2.1 and 2.4) as

$$C(\mathbf{x}) = \frac{F}{(2\pi)^{3/2}} \int_0^{\infty} I^{-\frac{1}{2}} \exp(-\frac{1}{2} I_{pq}^{-1} x_p x_q) dt \quad (2.7)$$

where the steady source strength F replaces the instantaneous source strength M . Concentration distributions for general velocity gradient tensors were calculated using a numerical integration of Eq. 2.7, obtained by summing the contributions of a finite number of instantaneous pulses. The time evolution of the second moment tensor I (Eq. 2.3) for each instantaneous pulse was solved with an explicit finite difference method. The time step of the finite difference approximation was limited to be no more than 0.5 per cent of the minimum time scale of the velocity gradient tensor G . Sensitivity analysis was conducted to determine the minimum number of pulses necessary for the numerical convolution and the evolution of the second moment tensor I was compared with the analytical solution for irrotational shear, Eq. 3.2 (Townsend 1951a). The concentration distribution was compared with the analytical solution for motionless diffusion $C=F/4\pi\gamma r$ (Carslaw and Jaeger 1959).

3. Point Sources in Steady Irrotational Shear

In the special case where the rotational, antisymmetric component of the rate of strain tensor is zero ($\Omega = 0$), the velocity gradient tensor given as $G = E$ will be symmetric. Rotating to the principal axes for the velocity gradient tensor we simplify G as

$$E_i = G_{pq} \xi_p^{(i)} \xi_q^{(i)} \quad (3.1)$$

where E_i is the extension rate along the symmetric tensor's i th principal axis, whose unit position vector is $\xi^{(i)}$. For irrotational shearing whose velocity gradients are steady in time, the second moment tensor of an instantaneous pulse, I , is given as (Townsend 1951)

$$I_{ij}(t) = \delta_{ij} \left[\frac{\gamma}{E_j} (\exp 2E_j t - 1) \right] \quad (3.2)$$

and the concentration distribution for the instantaneous pulse is given by Eq. 2.1. The transformation to the principal axis for G , defined by $\xi^{(i)}$, also diagonalizes $I(t)$, so that $\xi^{(i)} = \zeta^{(i)}$. The principal axes of strain are also the principal axes for the second moment tensor of the instantaneous pulse, thus the orientation of the pulse is constant in time. The dimensions of the pulse increase exponentially with time along expansive axes ($E_i > 0$) and approach a constant along compressive axis, that is $I_i = \frac{-\gamma}{E_i}$ for $t \gg \frac{1}{-E_i}$ and $E_i < 0$. The concentration distribution for a continuous release is then given by the convolution of the instantaneous source as

$$C(\mathbf{x}) = \frac{F(E_1 E_2 E_3)^{\frac{1}{2}}}{(2\pi\gamma)^{3/2}} \int_0^{\infty} \frac{1}{[\prod_{i=1}^3 (\exp 2E_i t - 1)]} \exp \left[\frac{-E_i x_i x_i}{2\gamma(\exp 2E_i t - 1)} \right] dt \quad (3.3)$$

The form of the solution to Eq. 3.3 depends on the signs and magnitudes of the shear components. To simplify the specification of these components we adopt the following conventions, noting that $\Sigma E_i = 0$ from continuity, and $(E_i E_i)^{\frac{1}{2}} \neq 0$ for sheared flows. Because of the flow field's symmetry about the origin we choose, with no loss of generality, the principal axes so that $E_1 > E_2 > E_3$, which requires that $E_1 > 0$ and $E_3 < 0$. The shear tensor can then be completely specified with two parameters, given as

$$\begin{aligned} E_b &= \frac{1}{2} \Sigma |E_i| \\ s &= \frac{2E_2}{E_b} \quad -1 < s < 1 \end{aligned} \quad (3.4)$$

where E_b specifies the strength of the shearing while s is a symmetry factor such that $s = 1$ gives an axisymmetric plane with expansive flow while $s = -1$ gives an axisymmetric plane with compressive flow.

Qualitative Features of the Continuous Point Source Solution

Two distinct concentration distributions result for continuous sources depending on the number of expansive axes. When the flow is compressive along two axes ($s < 0$) concentration gradients along these axes are steeper than along the single expansive axis, giving concentration contours distorted by the flow into tube-like structures (Figure 1a). A structure similar to the tube results when the flow is zero along x_2 ($s = 0$) and is referred to as a diffusive tube since the transport in the x_2 direction is diffusive. When the flow is expansive along x_1 and x_2 ($s > 1$) the distribution becomes flattened along the compressive x_3 axes giving disk-like concentration contours (Figure 1b). For both tubes and disks the concentration distributions are oriented along the principal axes of strain since these axes are also the principal axes of the instantaneous pulses. Near the source where the relative

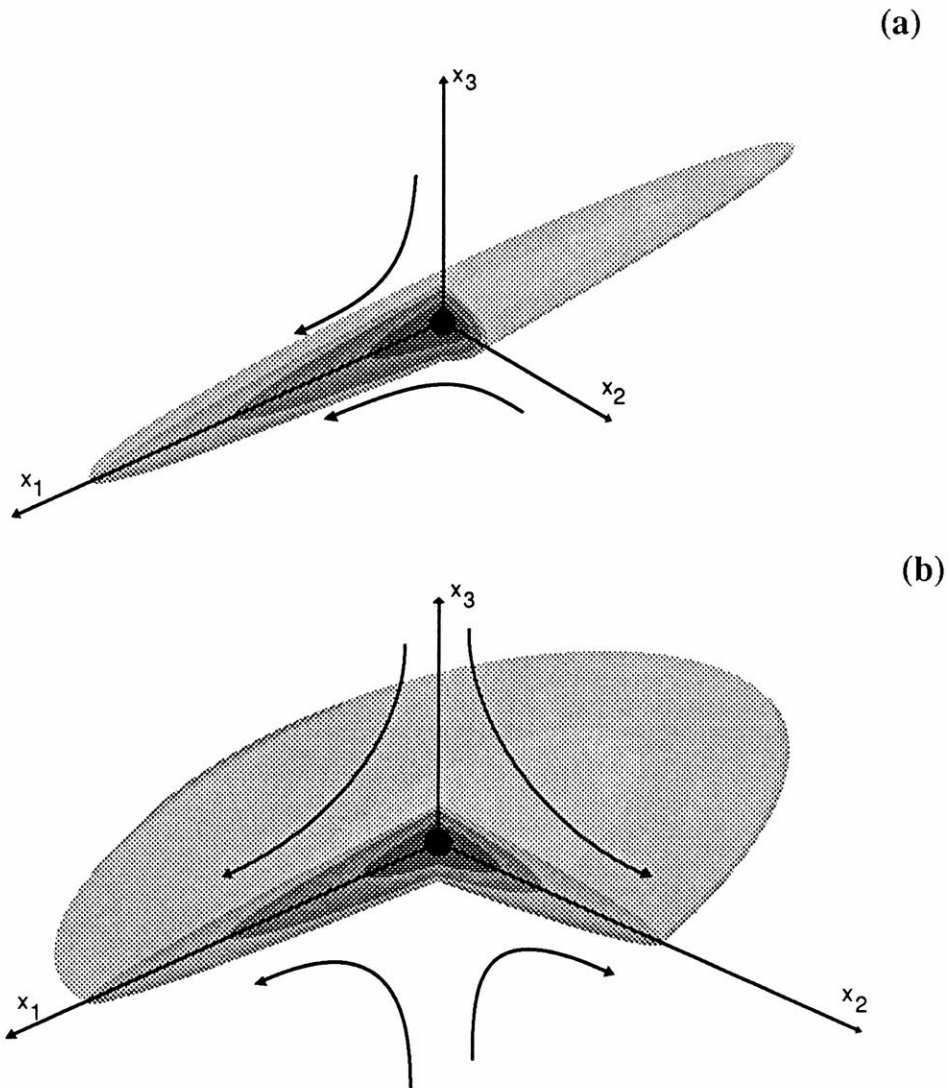


Figure 1. Qualitative features of concentration distributions for continuous point sources in steady homogeneous shear flows. The dark sphere at the origin has a radius of $(\gamma/E_b)^{1/2}$ that indicates the size of the diffusive region unaffected by the fluid motion. The lighter shading indicates concentration contours distorted by the shearing flow. The arrows indicate the fluid streamlines.

(a) Tube: $E_1 > 0$, E_2 and $E_3 < 0$.

(b) Disk: Principal strain rates E_1 and $E_2 > 0$, $E_3 < 0$.

fluid velocity is small, the concentration contours are spherical (Figure 1). The shape and orientation of concentration distributions for instantaneous point sources show a similar behavior (Townsend 1951). This similarity is not surprising because in shearing flows elements of the second moment tensor grow exponentially in time, thus only a narrow range of times contribute to the convolution integral giving the concentration distribution for a continuous source (Eq. 3.3).

Concentration Distributions

The importance of diffusive and advective transport in the region surrounding the point source can be compared by defining the characteristic quantities

$$\begin{aligned} x_0 &= \left[\frac{\gamma}{E_b} \right]^{\frac{1}{2}} \\ C_0 &= \frac{F E_b^{\frac{1}{2}}}{4\pi\gamma^{3/2}} \end{aligned} \tag{3.5}$$

where the length x_0 is the distance from the source where diffusive and advective dispersal are of the same magnitude, and the concentration C_0 is the concentration that would result at $r = x_0$ in the complete absence of motion.

For distances from the source small relative to the characteristic length x_0 the transport from the source is purely diffusive. In this region the dimensionless concentration is inversely proportional to the dimensionless distance from the source (Carslaw and Jaeger 1959).

$$C = C_0 \left[\frac{r}{x_0} \right]^{-1} \tag{3.6}$$

This limiting behavior is observed in the exact solutions for $r < x_0$ (Figure 1(a), 2.2(b)).

Beyond the diffusive region ($r > x_0$), the effects of anisotropic shearing distort the concentration into tube and disk like structures. Along the expansive x_1 axis for tubes ($-1 \leq s < 0$) the concentrations decrease as $(x_1/x_0)^{-1}$ (Figure 2(a)); for an axisymmetric disk the concentrations decrease along either expansive axis as $(r/x_0)^{-2}$ (Figure 2(a), (b)). For non-axisymmetric disks and diffusive tubes ($0 \leq s < 1$) the concentrations decrease along expansive axes at rates between the two bounding functions (Figure 2(a), (b)). For both tubes and disks concentrations along compressive axes fall off sharply in the region where the mass transport is primarily advective ($r > x_0$) (Figure 2(b), (c)).

(a)

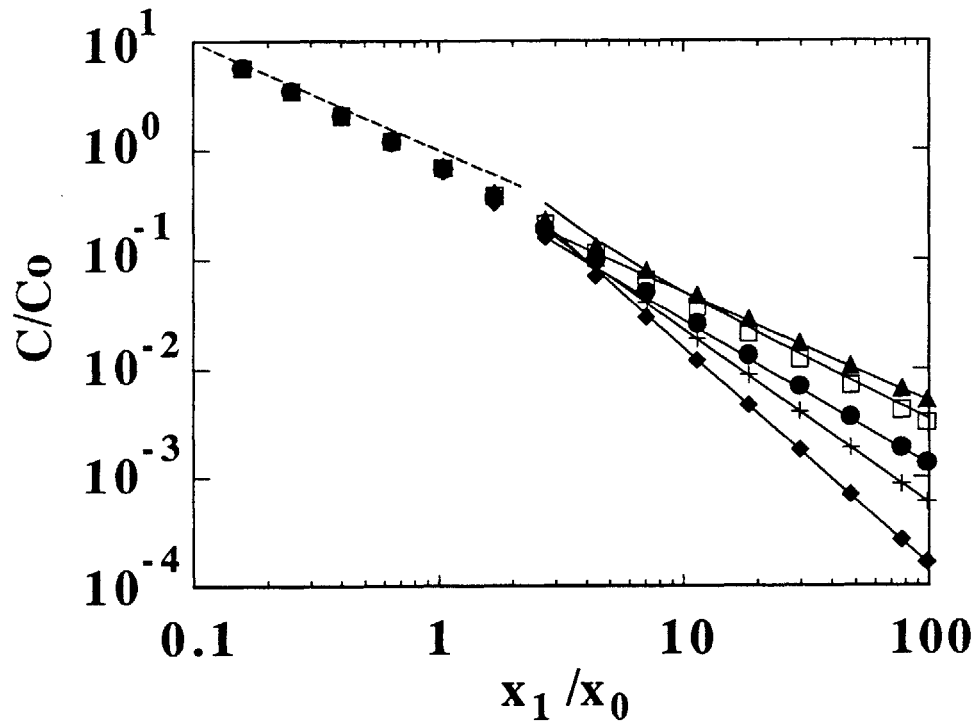


Figure 2. Normalized concentration C/C_0 vs. normalized position x/x_0 (see Eq. 3.5 for characteristic scales x_0 and C_0). Symbols give numerical solution of convolution integral (Eq. 2.4), while the solid lines give the approximate analytical solutions (Sec 4.). The dashed line gives the motionless diffusion analytical solution.

(a) Distributions along the line $(x_1/x_0, 0, 0)$ for (left to right): $s=1.0$ (\blacklozenge), $s=0.75$ (\times), $s=0.5$ (\bullet), $s=0.0$ (\square), $s=-1.0$ (\blacktriangle).

(b)

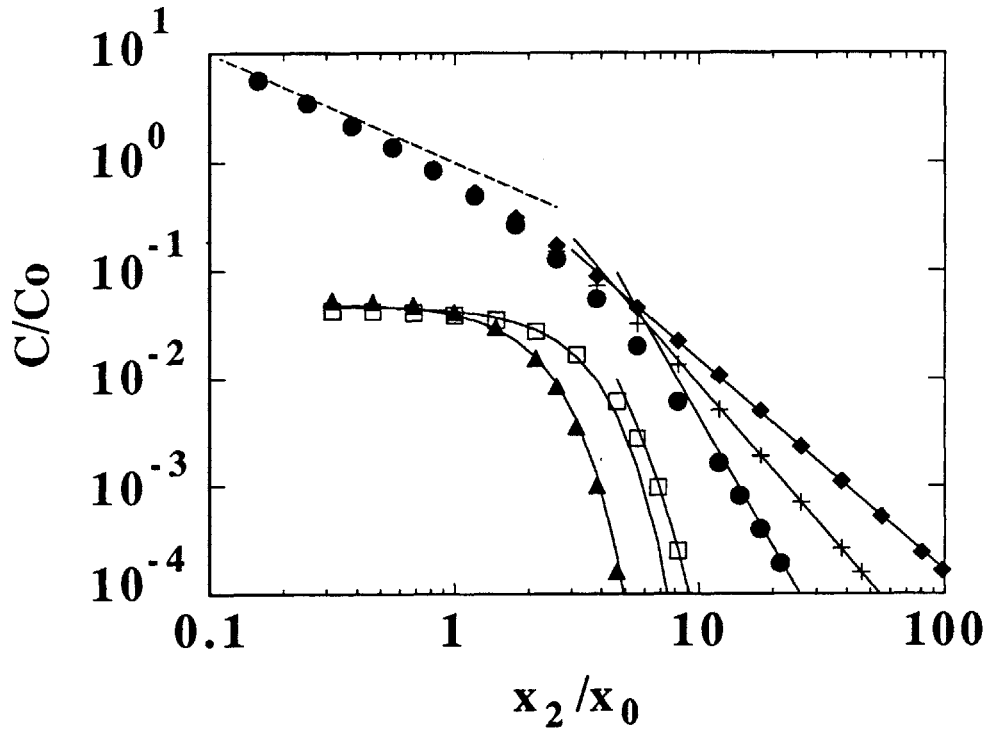


Figure 2. Normalized concentration C/C_0 vs. normalized position x/x_0 (see Eq. 3.5 for characteristic scales x_0 and C_0). Symbols give numerical solution of convolution integral (Eq. 2.4), while the solid lines give the approximate analytical solutions (Sec 4.). The dashed line gives the motionless diffusion analytical solution.

(b) Distributions along the line $(10, x_2/x_0, 0)$ for (left to right): $s = -1.0$ (▲), $s = 0.0$ (□) (solid line on right gives approximate analytical solution for $x_2 > x_1$); and along the line $(0, x_2/x_0, 0)$ for (left to right): $s = 0.5$ (●), $s = 0.75$ (×), $s = 1.0$ (◆).

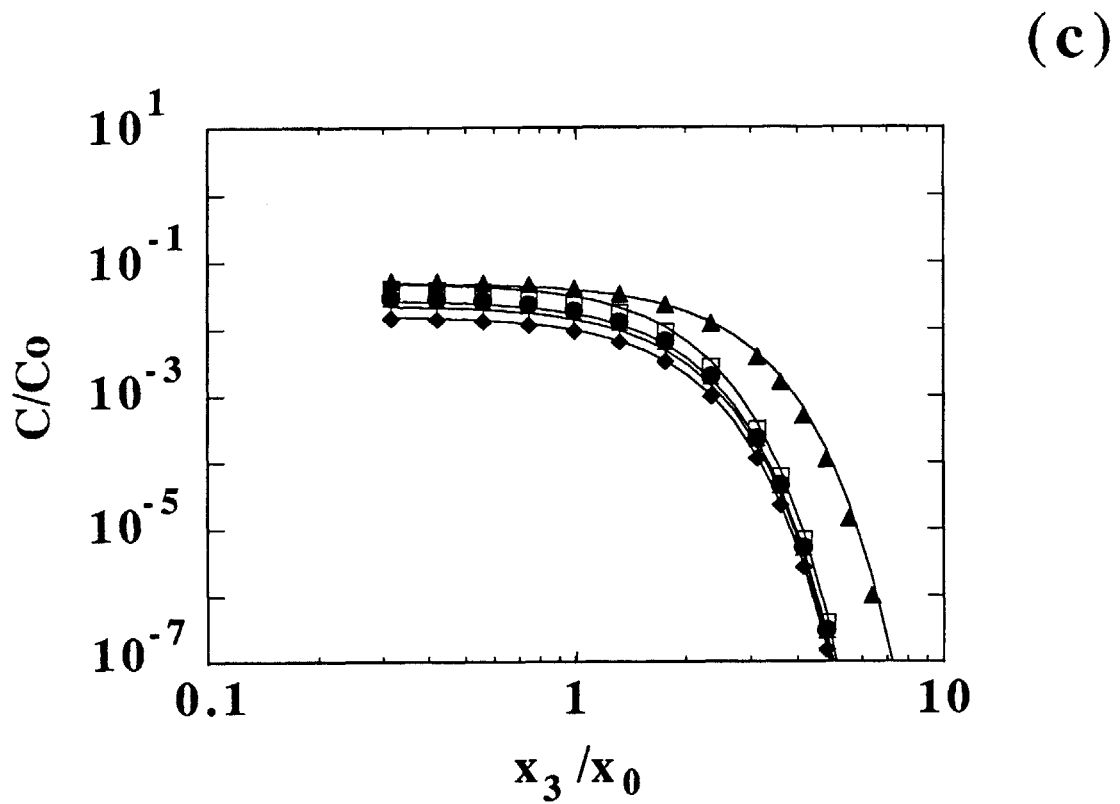


Figure 2. Normalized concentration C/C_0 vs. normalized position x/x_0 (see Eq. 3.5 for characteristic scales x_0 and C_0). Symbols give numerical solution of convolution integral (Eq. 2.4), while the solid lines give the approximate analytical solutions (Sec 4.). The dashed line gives the motionless diffusion analytical solution.

(c) Distributions along the line $(10, 0, x_3/x_0)$ for (left to right): $s = -1.0$ (▲), $s = 0.0$ (□), $s = 0.5$ (●), $s = 0.75$ (×), $s = 1.0$ (◆).

4. Approximate Analytical Solutions in the Sheared Region

The qualitative and quantitative features of the concentration distributions and the convolution integral from which they arise suggest that approximate analytical equations can be developed for the sheared region ($r > x_0$). We assume that in this region the flux of material away from the source is due entirely to advection along the expansive axes. Along compressive axes, no net flux from the source occurs as the advective flux towards the source is balanced by the diffusive flux. In the sheared region we expect that the times contributing to the convolution integral will be greater than $1/E_i$, where E_i is the strain rate along compressive axes. Examination of Eq 3.3 with this assumption suggests that concentrations along a compressive axis will be approximately Gaussian with a variance of E_i/γ . Approximate analytical solutions for the concentration distributions can then be found for each of the shear patterns described earlier by writing a flux equation using the assumed form of the concentration distribution.

Tube

For a tube $E_1=E_b$, $E_2, E_3 < 0$. The assumed concentration distribution is

$$C(\mathbf{x}) = C_c \exp \left[\frac{E_2 x_2^2}{2\gamma} + \frac{E_3 x_3^2}{2\gamma} \right] \quad (4.1)$$

where C_c is the concentration along the expansive x_1 axis. The flux equation is given as

$$F = 2 \int_{-\infty}^{\infty} \int_{-\infty}^{\infty} u_1(x_1) C(\mathbf{x}) dx_2 dx_3 = 2E_1 x_1 C_c(x_1) \int_{-\infty}^{\infty} \int_{-\infty}^{\infty} \exp \left[\frac{E_2 x_2^2}{2\gamma} + \frac{E_3 x_3^2}{2\gamma} \right] dx_2 dx_3 \quad (4.2)$$

which after integration gives the tube centerline concentration as

$$C_c(x_1) = \frac{1}{2} C_0 \frac{-x_0 s (s+2)}{|x_1|} \quad (4.3)$$

The centerline concentration is independent of the rate of strain but is dependent on the symmetry factor s . For an axisymmetric tube ($s = -1$) the centerline concentration is equal to one half the corresponding concentration for a continuous point source in a motionless fluid. Comparison with the numerically derived solution for an axisymmetric tube shows that the concentration distribution given by Eqs. 4.1 and 4.3 agrees well with this approximate analytical solution in the region where advective effects are dominant (Figure 2).

Diffusive Tube

In the two-dimensional pure shear flow, $E_i = (E_b, 0, -E_b)$, instantaneous pulses elongate exponentially along x_1 and diffusively along x_2 . The continuous source solution should have a similar character for which, unlike the tube, the length scale in the x_2 direction should grow diffusively as x_1 increases. With moments for instantaneous pulses growing exponentially along x_1 , we expect a logarithmic increase along x_1 for the length scale in the x_2 direction. Applying this instantaneous source analysis to the continuous source concentration distribution gives the following equation for the concentration $C(\mathbf{x})$

$$C(\mathbf{x}) = C_c(x_1) \exp \left[\frac{-E_b x_2^2}{2\gamma \ln \left[\frac{E_b x_1^2}{\gamma} \right]} - \frac{E_b x_2^2}{2\gamma} \right] \quad (4.4)$$

where again C_c gives the concentration along the x_1 axis. Equating the integral of the concentration distribution over x_2 and x_3 with the flux from the continuous

source as in Eq. 4.2 gives the following equation for the centerline concentration of a diffusive tube distribution.

$$C_c(x_1) = C_0 \frac{x_0}{|x_1|} \frac{1}{\left[\ln \left[\frac{E_b x_1^2}{\gamma} \right] \right]^{\frac{1}{2}}} \quad (4.5)$$

The approximate analytical solution agrees well with the concentration distribution along the diffusive tube centerline (Figure 2(a)). In the x_2 direction the concentration distribution deviates from that predicted by Eq. 4.4 in the region $x_2 > x_1$ (Figure 2(b)), but the deviation is insignificant to the flux analysis since the concentration in this region is several orders of magnitude below the centerline value. By assuming that $x_2 \gg x_1$ and $x_3 = 0$ the convolution integral (Eq. 3.3) can be integrated directly to give

$$C = C_0 \exp(-x_2/x_0) \quad (4.6)$$

which agrees well with the exact numerical solution in the region where $x_2 > x_1$ (Figure 2(b)).

Disk

An analogous flux analysis for a disk requires that the flow be axisymmetric in the x_1 - x_2 plane, that is $E_1 = E_2 = -\frac{1}{2}E_3 = \frac{1}{2}E_b$ and $s = 1$. In this case the flux equation can be written as

$$F = \frac{1}{2}E_b l \int_{-\infty}^{\infty} C_d(l) \exp \left[\frac{E_3 x_3^2}{2\gamma} \right] dx_3 \quad (4.7)$$

where C_d is the concentration in the axisymmetric x_1 - x_2 plane and $l = (x_1^2 + x_2^2)^{\frac{1}{2}}$ is the distance from the source in the x_1 - x_2 plane. Integrating across x_3 gives the following equation for the concentration distribution.

$$C(\mathbf{x}) = 2\left(\frac{2}{\pi}\right)^{\frac{1}{2}} C_0 \left[\frac{x_0}{l}\right]^2 \exp\left[\frac{E_3 x_3^2}{2\gamma}\right] \quad (4.8)$$

For non-axisymmetric disks ($0 < s < 1$) our flux analysis is indeterminate because we are unable to state *a priori* the shape of concentration contours in the x_1 - x_2 plane. We can, however, find the concentration distribution along either expansive axes by direct integration of Eq. 3.3 with $x_1 = 0$ or $x_2 = 0$ to give the following equation.

$$C(x_1, 0, 0) = \left(\frac{2}{\pi}\right)^{\frac{1}{2}} C_0 \frac{\frac{1}{2}(E_2/E_1)^{\frac{1}{2}} \Gamma(\frac{1}{2}E_b/E_1)}{\left[\frac{E_1 x_1^2}{2\gamma}\right]^{\frac{1}{2}} E_b/E_1} \quad (4.9)$$

Exchange of indices gives the equation for x_2 , the second expansive axis. This approximate analytical solution also agrees well with the concentration distributions derived numerically for several axisymmetric and non-axisymmetric disks (Figure 2) in the region where advective transport dominates diffusive transport. Comparison with the previous equations shows that in the sheared region for both tubes and disks the concentration decreases along an expansive axis i as $x_i^{-E_i/E_b}$.

Although the shape of a concentration contour in the x_1 - x_2 plane can not be written *a priori* for a non-axisymmetric disk, by assuming that the transport from the source is purely advective we can write a general relation for the outward flux across the contour in the x_1, x_2 plane ($C = C_z$) as

$$\text{Flux} = F_{x_1} + F_{x_2} = C_z \left[\frac{2\pi\gamma}{-E_3} \right]^{\frac{1}{2}} \left[\int_{x_2(\min)}^{x_2(\max)} E_1 f^{-1}(x_2) dx_2 + \int_{x_1(\min)}^{x_1(\max)} E_2 f(x_1) dx_1 \right] \quad (4.10)$$

with the integration limits given by the particular concentration contour according to Eq. 4.9. The unknown function f and its inverse f^{-1} give the shape of the contour in the x_1 - x_2 plane such that $C(x_1, f(x_1), 0) = C_z$. The flux equation 4.10 has already been integrated in the x_3 direction using the assumed concentration distribution for disks given earlier for axisymmetric disks. Eq. 4.10 can be integrated, noting that $E_b = E_1 + E_2 = -E_3$, to give the following relation for the area of the concentration contour in the x_1 - x_2 plane.

$$\text{Area} \Big|_{\substack{C \geq C_z \\ x_3=0}} = \frac{F}{(2\pi\gamma E_b)^{\frac{1}{2}} C_z} = 2 \left(\frac{2}{\pi} \right)^{\frac{1}{2}} \frac{C_0}{C_z} \quad (4.11)$$

For a given intensity of shear E_b and a flux rate F , the area of a contour is independent of the asymmetry of the shearing, though the shape of the contour will be affected by changes in the symmetry factors. The volume of a contour is also approximately independent of the symmetry factors since the concentration distributions are flattened along the compressive x_3 direction and the strength of the shearing in this direction is unaffected by changes in the symmetry factor.

5. Continuous Point Sources in Steady Rotational Shear Flows

In this section we describe the shape and orientation of the concentration distributions when the flow includes both rotational and irrotational components. As in the irrotational case we expect that the convolution of the instantaneous source solution receives contributions from only a narrow range of times, since the linear increase in velocity with distance from the source leads to length scales for a pulse that increase exponentially with time. We therefore use the behavior of instantaneous pulses in rotational shear to gain insight into the continuous point source solution.

To examine the deformation of instantaneous pulses we use a kinematic model justified by the earlier observation that the eigenvalues of a pulse in any linear flow field are always real and orthogonal. The deformation of the pulse can be seen as the superposition of an extensional motion that changes the length scales of the pulse together with an angular motion that reorients the pulse. The extensional motion depends only on the components of the rate of strain tensor along the principal axes of the pulse and increases pulse dimensions along expansive principal axes. The angular motion changes the orientation of the pulse and has contributions from both the irrotational and rotational components of the flow (see Appendix A), but the shear contribution is zero when the pulse is aligned with the principal axes of strain.

The presence of rotation turns the pulse away from the principal axes of strain so the extension rates along the principal axes of the pulse vary in time. Using the example of two-dimensional shear Lumley (1972) showed that for rotation rates weak relative to the shearing, instantaneous pulses rotate to an equilibrium orientation where the angular motion is zero. Extension rates along the equilibrium orientation axes are equal to a weighted average of the extension rates along the principal axes of strain. The difference between the extension rates along the two

equilibrium orientation axes perpendicular to the vorticity vector decreases as the rotation rate increases (Lumley 1972), and approaches zero as the rotation rate approaches a critical value for the existence of the equilibrium orientation.

Batchelor (1979) also investigated the effects of rotation on mass dispersal in shear flows, but looked at the other extreme where the rotation rate is strong relative to the shear component. For strongly rotational flows the concentration distribution is the same as that resulting from an axisymmetric, irrotational flow with an axis of symmetry along the rotation axes. The extension rate along the axis of symmetry for the equivalent irrotational flow is the component of the rate of strain tensor in the direction of the rotation vector for the strongly rotational flow.

These two bounding cases for instantaneous sources indicate qualitatively how the rotation affects the concentration distribution around continuous point sources. Vorticity rotates the concentration distribution away from the principal axes and towards the rotation axes, approaching an axisymmetric distribution as the rotation rate becomes strong relative to the shear component. For weak rotation, the continuous source concentration distribution should be aligned with the equilibrium orientation of an instantaneous pulse, and from this perspective the shape of the distribution should be similar to those described for irrotational shearing with extension rates given in the equilibrium orientation.

To analyze the effects of rotation we examine how changing the strength of the rotation component changes the dimensions of a concentration contour when viewed from the equilibrium orientation. This analysis is done initially with a simple specification of rotation, where the rotation axis is aligned with a principal axis of strain. The criteria for weak rotation, which requires that an equilibrium orientation exists, is given for this simple rotational case and later for a general velocity gradient tensor. We then look at a more general rotational shearing flow where the rotation axes is not aligned with the principal axes of strain. In both

examples we look at the shape of the distributions for rotation rates beyond the critical value for the existence of the equilibrium orientation and compare the results with the theory given by Batchelor (1979) for strong rotation.

Concentration Distributions with Rotation along a Principal Axis of Strain

The effects of rotation were examined by determining how the size and shape of a particular concentration contour varies with increasing rotation rate.

Concentrations distributions were calculated using the convolution integral for a series of velocity gradient tensors, each with an identical shear component, and with rotation components that varied in intensity but not in orientation. In this first case the rotation axis is aligned with a principal axis of strain so that it is possible to give simple equations giving the angular location of the equilibrium orientation relative to the principal axes of strain and the extension rates along the equilibrium orientation.

The rotational shearing flows analyzed have a fixed shear component ($s = -0.6$) and a vorticity component of varying intensity ω that is aligned with x_2 such that $\omega_i = -\epsilon_{ijk}\Omega_{jk} = \omega\delta_{i2}$. With rotation only around the x_2 axes the equilibrium orientation can be found by determining the directions in which the angular component of the motion is zero (see Appendix A). The equilibrium orientation turns from the principal axes around the x_2 axes by an angle α given by

$$\alpha = \frac{1}{2} \sin^{-1} \left[\frac{\omega}{E_1 - E_3} \right] \quad (5.1)$$

giving the following condition for weak rotation

$$-1 < \frac{\omega}{E_1 - E_3} < 1 \quad (5.2)$$

By substituting the terms describing the irrotational shear (E_b and s) into Eq. 5.2, the vorticity can be normalized to the critical value for the existence of an equilibrium orientation as

$$\omega_* = \omega_2/\omega_{\text{crit}} = \frac{\omega}{E_b(2 - \frac{1}{2}|s|)} \quad (5.3)$$

The extension rates along the two rotated axes of the equilibrium orientation, x'_1 and x'_3 , are given as functions of the normalized rotation rate and the irrotational strain component assuming that the rotation is weak ($\omega_* \leq 1$).

$$E'_1/E_b = -\frac{s}{4} + (1 - \frac{|s|}{4})(1 - \omega_*^2)^{\frac{1}{2}} \quad (5.4)$$

$$E'_3/E_b = -\frac{s}{4} - (1 - \frac{|s|}{4})(1 - \omega_*^2)^{\frac{1}{2}} \quad (5.5)$$

The difference between the extension rates E'_1 and E'_3 decreases with increasing vorticity although the effect is not pronounced until the normalized rotation rate approaches unity (Figure 3). Above the critical rotation rate ($\omega_* > 1$) the extension rates are calculated for $\alpha = 45^\circ$ giving $E'_1 = E'_3$. The extension rate along x'_2 (E'_2) is unaffected by vorticity since the rotation axis is aligned with x_2 (Batchelor 1979). The irrotational shear component ($s = -0.6$) gives a concentration distribution that is a non-axisymmetric tube with the tube centerline aligned with x_1 . In the limit of strong rotation the concentration distribution is an axisymmetric disk ($s = 1.0$) with an axis of symmetry along x_2 . The characteristic shear rate for the strong rotation limit (E'_b), calculated according to Eq. 3.5 using the extension rates along the rotated axes (E'_i), is less than the characteristic shear rate for the irrotational shear case ($E'_b/E_b = 0.3$).

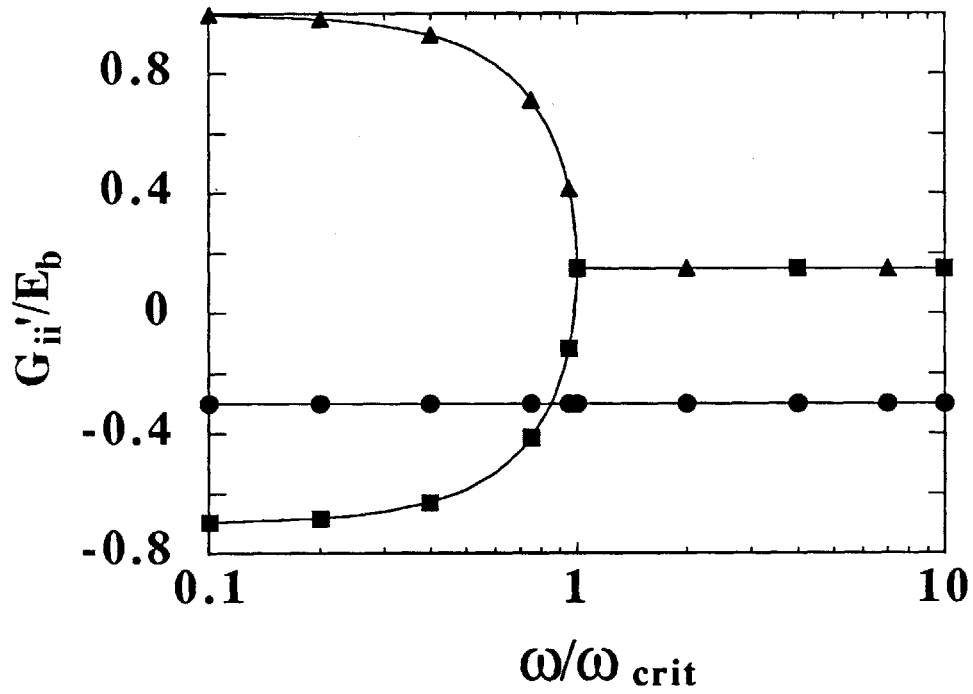


Figure 3. Extension rates along each rotated coordinates axis G'_{ii} normalized by the irrotational strain intensity E_b vs. the normalized vorticity ω/ω_{crit} for the vorticity vector $(0, \omega, 0)$: ▲ G'_{11} ; ● G'_{22} ; ■ G'_{33} .

Concentration distributions were calculated along the equilibrium orientation using Eq. 5.1 to determine its location relative to the principal axes of strain. The rotation angle α varies from 0.0 to 45.0 degrees as the normalized vorticity approached 1.0. For rotation rates above the critical value ($\omega_* > 1$) the concentrations were calculated at $\alpha = 45^\circ$. Normalized concentrations and distances were calculated using Eq. 3.5 based on the constant irrotational shear component. The distance to a constant concentration level in the sheared region ($C/C_0 = 0.01$) was then calculated along each equilibrium orientation axes for various values of normalized vorticity.

The shape of the concentration distributions approaches the expected axisymmetric pattern as the rotation rate becomes strong relative to the shear rate ($\omega_* \gg 1$), but the effect of the rotation on the distributions is small for most of the weak rotation region ($\omega_* < 1$). For normalized rotation rates, ω_* , below approximately 0.95, the dimensions of the concentration contour ($C/C_0 = 0.01$) change little from the irrotational pattern (Figure 4), with the length scale for the long axis of the distribution being more than ten times the other two dimensions. The orientation of concentration distribution does change significantly since the equilibrium orientation axes x'_1 and x'_3 rotate around x_2 by 33.2° at $\omega_* = 0.9$. As the vorticity intensity is increased past the critical value, the dimensions of the concentration contour change quickly and by $\omega_* = 2.0$ the long axis of the contour is only twice the length for the other axes in the plane perpendicular to the rotation vector. At higher rotation rates the distribution approaches the limiting axisymmetric distribution predicted by Batchelor (1979).

As anticipated the effect of rotation is to turn the concentration distribution away from the principal axes of strain while reducing the asymmetry of the distributions. At high rotation rates the distribution approaches an axisymmetric distribution with the axis of symmetry along the rotation axes. The critical

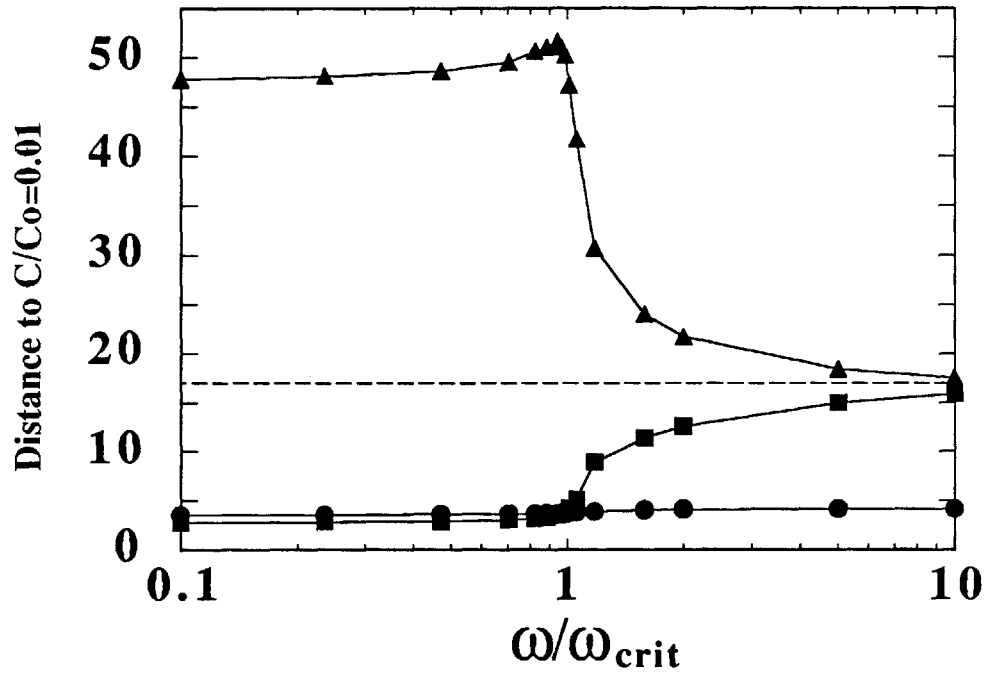


Figure 4. Normalized distances from the source to the concentration level $C/C_0=0.01$ along each rotated coordinate axis vs. the normalized vorticity ω/ω_{crit} for the vorticity vector $(0, \omega, 0)$:
 ▲ Normalized distance along x_1' ; ● Normalized distance along x_2' ; ■ Normalized distance along x_3' ;
 The dashed line represents the normalized distance to $C/C_0=0.01$ along expansive axes for the strong rotation limit that is the axisymmetric irrotational shear with principal strain rates $E_1 = E_2 = 0.3E_b$, $E_3 = -0.6E_b$

rotation rate for the existence of an equilibrium orientation is the key parameter in describing the shape of the distributions. The shape of the distribution changes little for rotation rates much below this critical value, but changes rapidly as the rotation is increased above the critical value. In the next section we give the criteria for this critical rotation rate for a general velocity gradient tensor.

The General Condition for Weak Rotation

In the previous section the placement of the rotation vector along a principal axis of strain allowed us to calculate the equilibrium orientation of an instantaneous pulse and the critical rotation rate using the simple kinematic model of the pulse's behavior in rotational shear. For a general vorticity vector, however, no simple geometrically based relationship for the critical rotation is possible. Nonetheless we can use information on the velocity gradient tensor to determine the critical rotation rate.

As shown by Lumley (1972) for weak rotation, the equilibrium orientation axes and the eigenvectors of the velocity gradient tensor form a set of right and left eigenvector pairs. For an equilibrium orientation to exist we know that it must be real, since the principal axes of the pulse must always be real. This in turn requires that the extension rates along the equilibrium orientation be real, since our solution must have no imaginary part. Because the equilibrium orientation and the eigenvectors of the velocity gradient tensor form an eigenvector pair, then the eigenvalues of the velocity gradient tensor must be real if the extension rates along the equilibrium orientation are real. For an equilibrium orientation to exist we must therefore require that the velocity gradient tensor have three real eigenvalues. It is this condition that we will use to give the specification of the critical rotation rate for the existence of an equilibrium orientation.

The characteristic polynomial giving the eigenvalues of \mathbf{G} is $y^3 + ay + b = 0$, where $a = R^2 - \frac{1}{2}E^2$, $b = -(E_1E_2E_3 + E_i\omega_i\omega_i/4)$, $E^2 = E_iE_i$, and $R^2 = (\omega_i\omega_i)/4$. The roots of the polynomial are the eigenvalues of the velocity gradient tensor \mathbf{G} . The condition that all the roots of the polynomial are real can then be used to give the following condition for weak rotation

$$E^2 - 2R^2 > 3 \cdot 2^{1/3} \left[E_1E_2E_3 + \frac{E_i\omega_i\omega_i}{4} \right]^{2/3} \quad (5.6)$$

For rotation rates less than that indicated by Eq. 5.6, an instantaneous pulse will rotate to a stable orientation and subsequent deformation of the pulse will be determined by the components of the rate of strain tensor in the equilibrium orientation. At rotation rates above the critical value, the velocity gradient tensor will have one real eigenvalue with two imaginary eigenvalues that are complex conjugates, giving an oscillatory behavior to the solution for an instantaneous pulse. The orientation of the pulse will oscillate around an orientation given by the eigenvectors corresponding to the real part of the velocity gradient's eigenvalues at a frequency equal to the rotation rate. At high rotation rates ($\omega_* \gg 1$) the behavior of the pulse will be independent of the rotation rate and the pulse will deform in an axisymmetrically fashion with an axis of symmetry aligned with the vorticity vector.

Concentration Distributions for a General Rotation Vector

With specification of the critical rotation rate for a general velocity gradient tensor, we can now analyze rotational effects on continuous sources for any combination of shear and rotation components. As in the simple example we examine the changes in the shape of a concentration contour ($C/C_0 = 0.01$) as rotation intensity is increased. The shear component is fixed ($s = -0.6$) with a

vorticity vector of constant direction, given as $(0, \omega, \omega)$, and a variable intensity ω . Vorticity is normalized to the critical value which is calculated using Eq. 5.6 for $s = -0.6$ so that $\omega_{\text{crit}} = 0.73E_b$. The irrotational limit is the same as in the earlier case giving a tube-like distribution for irrotational strain, but the strong rotation is now an axisymmetric disk ($s = 1.0$) with $E'_b/E_b = 0.5$. An analysis of the velocity gradient tensor in the coordinate system formed by the equilibrium orientation is used to calculate the extension rates along the equilibrium orientation (Appendix B). The concentration distribution is expected to change from a non-axisymmetric tube to an axisymmetric disk as the vorticity becomes strong relative to the critical value for the existence of the equilibrium orientation.

The extension rates along the equilibrium orientation and the shape of the distribution with varying rotation intensity follow the anticipated pattern. The difference between extension rates decreases with increasing rotation rate, but the effect of rotation is minor until the rotation intensity approaches the critical value (Figure 5). The asymmetry of the distribution remains nearly unchanged until the vorticity intensity approaches the critical value (Figure 6). Increases in vorticity from this point change dramatically the shape of the distribution and the ratio of length scales is reduced to below 2.0 by the time the vorticity is twice the critical value. As in the previous example, further increases in vorticity give distributions that approach the limiting strong rotation case as predicted by Batchelor (1979). The limiting length scale in this case is slightly larger than the first case because the strength of the axisymmetric shearing is stronger ($E'_b/E_b = 0.5$ vs. 0.3).

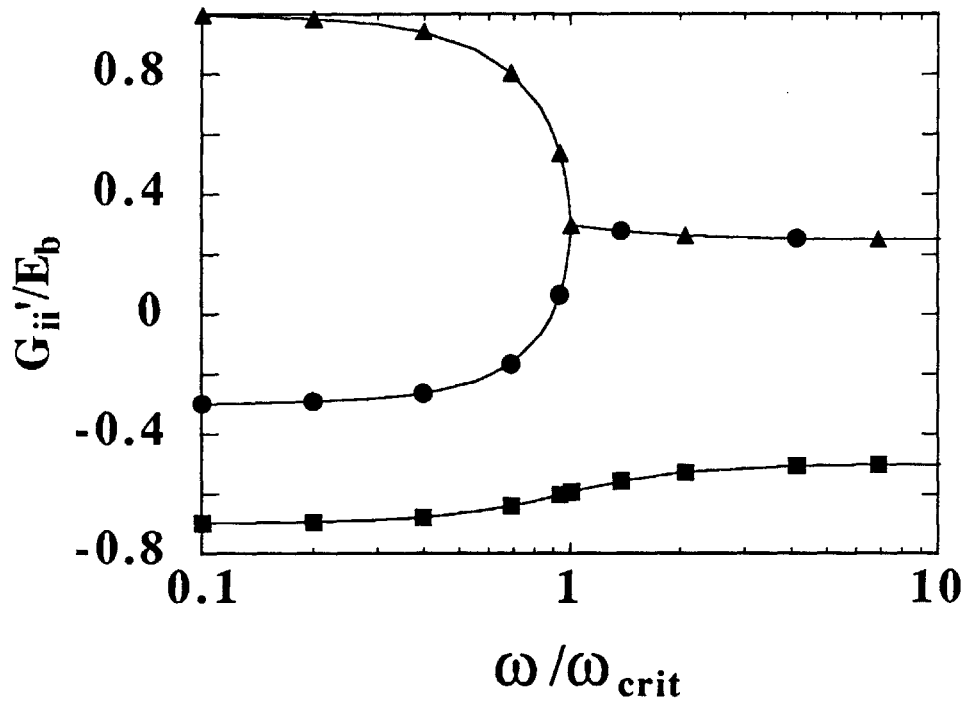


Figure 5. Extension rates along each rotated coordinates axis G'_{ii} normalized by the irrotational strain intensity E_b vs. the normalized vorticity $\omega / \omega_{\text{crit}}$ for the vorticity vector $(0, \omega, \omega)$: ▲ G'_{11} ; ● G'_{22} ; ■ G'_{33} .

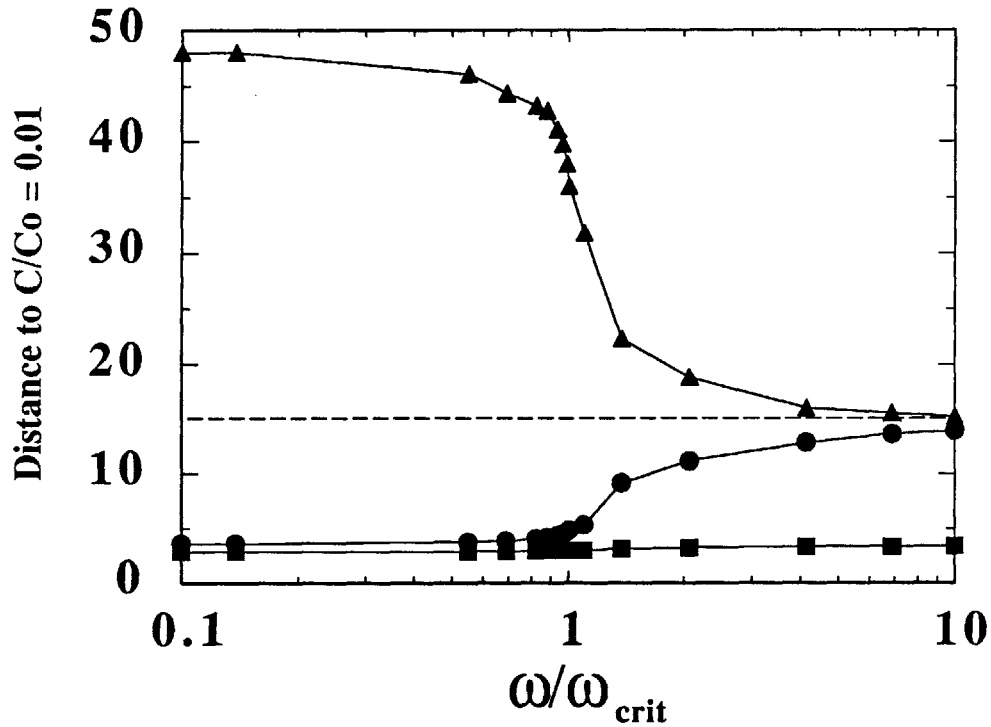


Figure 6. Normalized distances from the source to the concentration level $C/Co = 0.01$ along each rotated coordinate axis vs. the normalized vorticity ω/ω_{crit} for the vorticity vector $(\omega, \omega, 0)$.
 ▲ Normalized distance along x_1 . ● Normalized distance along x_2 .
 ■ Normalized distance along x_3 .
 The dashed line represents the normalized distance to $C/Co = 0.01$ along expansive axes for the strong rotation limit that is the axisymmetric irrotational shear with principal strain rates $E_1 = E_2 = .5E_b$, $E_3 = -1.0E_b$

6. Discussion

We have found that beyond a diffusive zone extending a distance $x_0 = \gamma/E_b^{\frac{1}{2}}$ from a source of continuous mass input flows with linear velocity distributions have two characteristic concentration distributions depending on the number of expansive principal axes and the relative magnitudes of the shear and vorticity components. For irrotational shears expansive flow along a single axis gives tube-like structures while two expansive axes gives disk-like structures, with both of these distributions oriented along the principal axes of strain. Concentrations in the sheared region ($r > x_0$) for all irrotational shearing flows decrease along expansive axes as $x_i^{-E_i/E_b}$ where E_i is the shear rate along the i th principal axis of strain; along compressive axes the concentration distributions are Gaussian with a variance of γ/E_i . The analytical solutions for the sheared region of irrotational flows, derived for all cases except non-axisymmetric disks by neglecting diffusive transport along the expansive axes and assuming zero transport along compressive axes, agree well with the concentrations distributions determined numerically by convolving exact instantaneous source solutions.

The effect of rotation on the concentration distributions in shearing flows is generally to reorient the distribution away from the principal axes of strain and to reduce the asymmetry of the distribution. Rotational shearing flows can be divided into weak and strong rotation cases by comparing the rotation rate to a critical value defined by a kinematic condition for the existence of an equilibrium orientation for an instantaneous pulse. Weakly rotating flows have concentration distributions similar to that predicted by the irrotational component of the flow, and are aligned with the equilibrium orientation of an instantaneous pulse, which moves away from the principal axes and towards the rotation axis as the rotation rate increases. The concentration distributions for strongly rotating flows approach a limiting axisymmetric pattern with an axis of symmetry along the rotation vector

and a shear rate along the rotation vector given by the irrotational component of the flow in that direction. The transition between these two limiting cases occurs rapidly as the rotation rate increases beyond the critical rotation value.

The general features of the concentration distributions along expansive axes for shearing flows are similar to the concentration distributions downstream from the source for either simple streaming flows or streaming flows with simple shear. For all tube-like distributions ($1 \leq s < 0$) in irrotational shear the concentration decreases along the single expansive axis as x_1^{-1} . Similarly, the concentration distribution downstream of a continuous source in a simple uniform flow decreases as x_1^{-1} (Carslaw and Jaeger 1959). For flows with both a uniform flow and a simple shear component Okubo and Karweit (1969) calculated concentration distributions for a continuous point source by numerically convolving an exact instantaneous source solution. Near the source where diffusive transport dominates, the concentration decreases as x_1^{-1} , and far downstream from the source ($x_1 \gg U_0/G_{12}$) where shear effects are important, the concentration again decreases as x_1^{-1} . As would be predicted by our analysis of a simple shearing flow ($\omega/\omega_c = 1.0$) the concentration distribution in the sheared region is oriented 45 degrees from the principal axes of strain.

Continuous Sources in Homogeneous Turbulence

Our analysis of concentration distributions in flows with linear velocity distributions assumes that the velocity gradient tensor is both homogeneous in space and steady in time. In turbulent flows the assumption that the velocity gradient tensor is homogeneous is satisfied if the region of interest is smaller than the smallest scale of the turbulent motion, the Kolmogorov microscale $(\nu^3/\epsilon)^{1/4}$. Since the shear rate E_b is of order $(\epsilon/\nu)^{1/2}$, the Kolmogorov time scale, the requirement that the distance from the mass source be less than the Kolmogorov length scale

yields the following limitation on the dimensionless distance from the source, $(E_b x_i x_i / \gamma)^{\frac{1}{2}} < (\nu / \gamma)^{\frac{1}{2}}$. For small molecular weight dissolved compounds in water the Schmidt number (ν / γ) is of order 1000 which limits the range of interest to dimensionless distances of approximately 30. For typical organic compounds with larger molecular weights (1500 g/mole) the region of interest may be as much as three times higher.

A second assumption in our analysis is that the velocity gradient tensor is steady in time. The time scale for establishment of a steady state concentration distribution is $1/E_b \sim (\nu / \epsilon)^{\frac{1}{2}}$. Our steady state analysis is therefore appropriate if the time scale of variation in the shear rate is long relative to the Kolmogorov time scale. Lumley (1972) has hypothesized that the shearing lasts for a time equal to the Lagrangian integral time scale. The ratio of the Lagrangian integral time scale to the Kolmogorov time scale has been estimated to be of order $R_\lambda^{\frac{1}{2}}$ (Corrsin 1963) where R_λ is the Reynolds number calculated using the Taylor microscale λ . There is, however, some doubt about this hypothesis (Monin and Yaglom 1975), though recent particle tracking experiments show Lagrangian integral time scales in excess of Kolmogorov time scales (Sato and Yamamoto 1987). Unfortunately the Reynolds numbers of these experiments are not high enough to be a true test. Nonetheless, numerical models of turbulent processes in large Reynolds number flows have used the assumption that the shearing lasts at least as long as the Kolmogorov time scale (Pearson et al. 1984) and we believe the hypothesis is a reasonable one.

Recent numerical simulations of homogeneous turbulence examining correlations between shear and vorticity (Kerr 1985) and alignment between components of shear and vorticity (Ashurst et al. 1987) can be used in conjunction with our analysis to give a qualitative description of the shape of continuous point source concentration distributions in isotropic turbulence. Ashurst et al. (1987) examined the velocity gradient tensor at 16,384 uniformly distributed points in space for

isotropic turbulence with $R_\lambda = 82.9$. To characterize the strain component they define a normalized principal strain rate nearly equivalent to our symmetry factor s (Eq. 3.4) as $\beta = E_2\sqrt{6}/(E_1E_3)^{\frac{1}{2}} \approx s$.

In locations with viscous dissipation below the median rate they found that positive and negative values for β are equally likely and 75% of the β values are between $\beta = 0.5$ and $\beta = -0.5$. The flow is strongly rotational (average $\omega/\omega_{\text{crit}} = 7$) when there are two positive principal strain rates ($\beta > 0$) and the viscous dissipation is below the median value. For the majority of these locations ($\approx 20\%$ of total) the vorticity is aligned with the axes of the intermediate principal strain rate (E_2), resulting in concentration distributions for point sources that are axisymmetric tubes aligned with the vorticity vector. Extension rates along the vorticity vector are significantly below the average shear rate because of the relatively weak dissipation and the particular alignment of vorticity vector. In locations with weak dissipation and two compressive axes ($\beta < 0$) the rotation is not aligned with either compressive axes, thus these locations also have tube-like concentration distributions.

Ashurst et al. report that locations with viscous dissipations above the median value have two positive principal axes ($\beta > 0$). The high viscous dissipation regions have an average vorticity level near the average for the entire fluid, thus we expect some concentration distributions shaped as non-axisymmetric disks in weakly rotating locations ($\beta > 0, \omega < \omega_{\text{crit}}$). However, Kerr (1985) discovered regions of high vorticity in vortex tubes associated with regions of strong shear and with the single compressive strain axis perpendicular to the vortex tube axes. Neither Kerr nor Ashurst et al. give the relative magnitude of the shear and vorticity components in the vortex tubes so we cannot determine whether the flow is strongly or weakly rotational. With the observed alignment of strain and vortical components, however, a strongly rotational vortex tube results in tube-like concentration

distributions aligned with the vorticity vector while weakly rotational flow results in disk-like concentration distributions.

Summarizing the results for the entire turbulent fluid, we expect that tube-like concentration distributions are more common than disks even though regions with $\beta > 0$ occupy a majority of the fluid (Ashurst et al. report 75%). The preponderance of locations with two positive principal strain rates is consistent with a similar analysis by Townsend (1951b). Of interest, however, is the relative strength of the vorticity and its alignment with a positive principal strain rate, which results in axisymmetric tube-like concentration distributions for strong rotation even though the irrotational shear alone would result in disk-like distributions. Strongly rotational axisymmetric tubes occupy at least half of the locations with viscous dissipation below the median rate ($\approx 20\%$ of total volume). Axisymmetric tube-like concentration distributions are also expected in strongly rotational vortex tubes with strain rates significantly above the median level. Disk-like concentration distributions are found only in locations where viscous dissipation is above the median value and the rotation is weak relative to the shear ($< 50\%$ of total volume). Flatness factors for shear and vorticity are significantly above uncorrelated levels (Kerr 1985), so that median levels of fluid motion, and consequently the distortion of concentration distributions by fluid motion, are below estimates based on average conditions.

Ashurst et al. (1987) explain the tendency toward positive β values and the alignment of vorticity with the intermediate principal strain as a result of interaction between strain and vorticity in an axially stretching vortex tube. They analyze coupled equations for \mathbf{E} and $\mathbf{\Omega}$ developed from the Euler equation neglecting transport terms in the vorticity equation and transport and pressure terms in the shear equation (Vieillefosse 1982). Numerical solutions to these equations for various strongly rotating shear flows ($\omega_* > 1.7$) show β values approaching 1.0

within the characteristic time scale $1/E_b$ (Ashurst et al. 1987). This behavior is attributed to coupling between shear and rotational motions. However it may be shown using the same equations with $\omega = 0$ that β approaches positive values even in irrotational shear, though the rate of increase in β does depend on the strength of the vorticity. Vorticity aligned with the strongest principal strain increases monotonically, but the relative magnitudes of the principal strain rates adjust so that the vorticity is aligned with an intermediate principal strain. The applicability of this analysis may be limited, however, since the equations for vorticity and shear neglect viscous and transport effects. In addition the shear equation neglects pressure terms which are known to redistribute turbulent energy between the velocity terms (Tennekes and Lumley 1972).

Applications to Chemosensing

We now consider the application of our results to the problem of chemosensing by aquatic organisms in turbulent fluids. Azam and Ammerman (1984) hypothesized that concentration distributions of organic compounds exuded by marine single-celled algae (10^{-5} m diameter) (Jackson 1987) are detected by motile bacteria (10^{-6} m diameter) that actively cluster around the algae to improve their access to the food source. Such a non-random interaction between algae and bacteria may also have important consequences to the cycling of carbon in the microbial food web and is a controversial topic in marine ecology (Williams 1984, Williams and Druffel 1988).

Estimates of the importance of bacterial clustering require information on the expected turbulent motions and the relevant biological rate processes such as the rate of algal exudation, the chemical detection threshold of the motile bacteria, and the swimming speed of the motile bacteria. The mixing intensity varies both temporally and spatially in the marine upper mixed layer, with a maximum near the

surface and a minimum at the thermocline. An upper limit on E_b is approximately 1.0 sec^{-1} based on measurements of viscous dissipation rates in the marine upper mixed layer (Dillon and Caldwell 1980, Oakey and Elliot 1980, Shay and Gregg 1984). Using experimental measurements of velocity flatness factors (van Atta and Antonia 1980) to account for intermittency effects, we estimate a median value for E_b of approximately 0.2 sec^{-1} , significantly lower than the maximum value.

Estimates of the rate of algal exudation are problematic because of the difficulty in quantifying the exuded fraction of the algal photosynthesis rate and the composition of the exuded material. Based on assumed typical values for algal photosynthesis rate, fraction of photosynthate exuded, and molecular weight of exuded compound, an exudation rate of approximately $10^{-17} \text{ mole cell}^{-1}\text{sec}^{-1}$ has been estimated (Mitchell et al. 1985). The minimum concentration of exudate that can be detected by bacteria is in the micromolar to nanomolar range depending on the particular compound (Chet and Mitchell 1976), and typical bacterial swimming speeds are $0.4\text{-}1.0 \times 10^{-4} \text{ m} \cdot \text{sec}^{-1}$ (Azam and Ammerman 1984). The separation distance between phytoplankton cells is approximately 10^{-3} m and the estimated time between algae encounters by bacteria through either bacterial swimming or fluid shearing is approximately 50-500 seconds. The Peclet number, defined with the algal cell diameter d as $P = E_b d^2 / \gamma$ will be small, thus the algae can be considered point sources of exudate.

Mitchell et al. (1985) combined physical scaling arguments with estimates of the biological rates processes to estimate the ability of marine bacteria in the upper mixed layer to cluster around algal cells. Based on the estimate of exudation rate given above they estimated that in a motionless fluid the spherical zone surrounding an algal cell with concentrations above the detection threshold ($10^{-8} \text{ mole liter}^{-1}$) is approximately $1000 \mu\text{m}$ in diameter and establishment of this zone by motionless diffusion ($\gamma = 1.5 \times 10^{-9} \text{ m}^2\text{sec}^{-1}$) takes approximately 100 seconds. They stated

that clustering is favored only if the characteristic time for the turbulent shearing motion, the Kolmogorov time scale, is greater than 100 seconds. Estimates of the Kolmogorov time scale were based on the measurements for the marine mixed layer referenced earlier and range from 1-10 seconds in the upper mixed layer to 100 seconds at the thermocline, values which are consistent with our estimates of characteristic shear rates. Mitchell et al. conclude that the intensity of fluid motions in the upper mixed layer prevent bacteria from clustering around algal cells.

Our analysis shows that turbulent fluid motions reduce but do not eliminate the region around algal cells where bacteria can detect the exuding organic compounds. At even the highest shear rates ($E_b = 1.0 \text{ sec}^{-1}$) the concentration contours are approximately spherical within $3 \times 10^{-5} \text{ m}$ of the source. Beyond this distance the fluid motions distort the concentration contours into disk and tube-like distributions, with tubes more common than disks. In addition to the spatial variability in viscous dissipation recognized by Mitchell et al., the temporal intermittency of dissipation results in periods when the intensity of fluid shearing is significantly below maximum or time average values. During these periods of relative calm, the size of the region where concentration distributions are unaffected by fluid motion will be larger than predicted by average conditions ($x_0 = 7 \times 10^{-5} \text{ m}$ for $E_b = 0.2 \text{ sec}^{-1}$) and the relative fluid motion between bacteria and algae will be reduced. Bacteria are able to find and cluster around algae in these calm periods since the encounter time for bacteria is less than the duration of the calm periods and bacteria swimming speeds ($5 \times 10^{-5} \text{ m sec}^{-1}$) are large relative to fluid velocities when $r < x_0$. The quantitative results of our analysis of concentration distributions can provide the basis for estimates of successful chemosensing by aquatic microorganisms.

This research was supported by the National Science Foundation under Grant Nos. OCE-8614488 and CES-8801767. J.D.B. acknowledges the support of a Hugh Hampton Young Fellowship. The authors would like to thank S. W. Chisholm, J. B. Waterbury, and P. M. Gschwend for their assistance and comments.

Appendix A. Kinematic analysis of the behavior of point sources in shearing fluids

In this appendix we examine the extensional and angular fluid motions in shearing fluid motion by writing the general linear velocity distribution given by Eq. 1.3 in spherical polar coordinates (r, θ, ϕ) . The principal axes of strain are used as the fixed coordinate system with E_1 , E_2 , and E_3 the principal strain rates, and with $\phi = 0$ along the x_3 axis and $\phi = \frac{1}{2}\pi$, $\theta = 0$ along the x_1 axis. With this specification the three velocity components are

$$u_r = r \left[\sin^2\phi(E_1\cos^2\theta + E_2\sin^2\theta) + E_3\cos^2\phi \right] \quad (\text{A } 1)$$

$$u_\theta = \frac{1}{2}r \sin\phi \left[\sin 2\theta(E_2 - E_1) + \omega_3 \right] - \frac{1}{2}r \cos\phi \left[\omega_1\cos\theta + \omega_2\sin\theta \right] \quad (\text{A } 2)$$

$$u_\phi = \frac{1}{2}r \sin 2\phi(E_1\cos^2\theta + E_2\sin^2\theta - E_3) + \frac{1}{2}r (\omega_2\cos\theta - \omega_1\sin\theta) \quad (\text{A } 3)$$

with ω the vorticity vector relative to the principal axes of strain.

The velocity term u_r gives the extensional component of the flow, while the terms u_θ and u_ϕ give angular components of the flow. Since ω does not appear in the equation for u_r the extensional motion depends only on the irrotational component of the flow. The angular velocities u_θ and u_ϕ depend on both ω and the principal strain rates E_1 , E_2 , and E_3 , but in irrotational flow ($\omega = 0$) the angular velocities are zero along the three principal axes of strain that form the coordinate system. The extension rate along each coordinate axis is given by the corresponding principal strain rate.

In rotational shear the angular motion of point sources will depend on the balance between the irrotational and rotational components of the flow. For vorticity aligned with the coordinate axes, the equilibrium orientation can be found by finding the directions in which the angular velocities are zero. For example we take the vorticity vector $\omega_i = \omega\delta_{i2}$ and find the position vector for the equilibrium

orientation axis x_1' ($\theta = 0$, $\phi = \frac{1}{2}\pi + \alpha$) where α is the rotation angle that results from the presence of vorticity. The angular velocity u_θ is identically zero but setting the angular velocity u_ϕ to zero, $u_\phi = -\frac{1}{2}r \sin 2\alpha(E_1 - E_3) + \frac{1}{2}r\omega = 0$, determines the position of x_1' relative to the principal axes of strain as

$$\alpha = \frac{1}{2} \sin^{-1} \left[\frac{\omega}{E_1 - E_3} \right] \quad (\text{A } 4)$$

The equilibrium orientation axis x_3' rotates around x_2 by the same angle ($\theta = 0$, $\phi = \alpha$). For vorticity along x_2 , the direction of the third equilibrium orientation axes (x_2') is unchanged from its direction in irrotational shear ($\theta = \frac{1}{2}\pi$, $\phi = \frac{1}{2}\pi$). The condition for weak rotation, $\text{abs} \left[\frac{\omega}{E_1 - E_3} \right] < 1$ (Eq. 5.2), is the maximum vorticity intensity that gives zero angular velocity for a real vector. For vorticity along a principal axis of strain at the critical rate the equilibrium orientation axes rotate around the vorticity vector by an angle of 45° . The extension rate along each equilibrium orientation axis (E_i') is given by Eq. A 1 as u_r/r where θ and ϕ specify the direction of each equilibrium orientation axis relative to the principal axes of strain. Vorticity along the x_2 axis gives $E_1' = E_1 \cos^2 \alpha + E_3 \sin^2 \alpha$ and $E_3' = E_1 \sin^2 \alpha + E_3 \cos^2 \alpha$ where α is given by Eq. A 4. Substituting A 4 into the equations for the extension rates gives

$$E_1' = \frac{E_1 + E_3}{2} + \frac{E_1 - E_3}{2} \sqrt{1 - [\omega / (E_1 - E_3)]^2} \quad (\text{A } 5)$$

$$E_3' = \frac{E_1 + E_3}{2} - \frac{E_1 - E_3}{2} \sqrt{1 - [\omega / (E_1 - E_3)]^2} \quad (\text{A } 6)$$

Vorticity at the critical rate gives equal extension rates along x_1' and x_3' .

Appendix B. The velocity gradient tensor in the equilibrium orientation

In this appendix we give the form of the velocity gradient tensor when the coordinate system is defined by the equilibrium orientation of an instantaneous pulse. This specification allows us to calculate how the extension rates along the equilibrium orientation vary with the intensity of a general rotation vector, without requiring that we know the orientation of the principal axes of strain relative to the equilibrium orientation. This is consistent with the emphasis placed on the shape rather than the absolute orientation of concentration distributions in shearing flow. To find the form of the velocity gradient tensor we first use the definition of an equilibrium orientation to give a condition on the evolution of the second moment tensor of an instantaneous pulse, I . Using the governing equations for the deformation of an instantaneous pulse (Eq. 2.3) together with an assumed form of the velocity gradient tensor G we then prove that the condition on I is satisfied.

An equilibrium orientation is the set of three asymptotic, orthogonal, and real eigenvectors for the second moment tensor I of an instantaneous pulse, eigenvectors that will exist for weakly rotating flows (criteria given by Eq. 5.6). This definition requires that I defined relative to the equilibrium orientation have the following evolution in time

$$\frac{I_{pq}}{I_{pp}-I_{qq}} \rightarrow 0 \quad \text{as } t \rightarrow \infty \quad (\text{B } 1)$$

This condition comes from requiring that the angle between the eigenvectors of I and the corresponding position vectors of the equilibrium orientation approach zero as time increases.

Since the trace of the velocity gradient tensor is zero, the criteria for an equilibrium orientation need only be specified for two distinct forms of G . As in the

irrotational case we require that $G_{11} > G_{22} > G_{33}$. Concentration distributions in flows with $G_{11} > G_{22} > 0$ are disks, distributions in flows with $G_{22} = 0$ are diffusive tubes, and distributions in flows with $0 > G_{22} > G_{33}$ are tubes. Generalization of the irrotational case is based on the kinematic analysis giving the deformation of the pulse as dependent on the extension rates along the axes of the pulse, which are equal to G_{ii} if the velocity gradient tensor is defined in the principal axes of the pulse. If the velocity gradient tensor is defined relative to the equilibrium orientation which is the asymptotic orientation of the pulse, then G_{ii} gives the asymptotic extension rates of the instantaneous pulse. Seen from the equilibrium orientation, the asymptotic behavior of a pulse in weakly rotating flows is analogous to the behavior of a pulse in irrotational shear seen from the principal axes of strain. The forms of the velocity gradient tensors in the equilibrium orientation for disks, diffusive tubes, and tubes are given below.

Disk

To determine the velocity gradient tensor in the equilibrium orientation for a disk, we assume that the pulse is sufficiently distorted by the rotational shear so that $I_{11} > I_{22} > I_{33}$. The condition given by Eq. B 1 requires that the tensor I relative to the equilibrium orientation have the following asymptotic form.

$$\begin{bmatrix} I_{11} & \llcorner I_{11} & \llcorner I_{11} \\ \llcorner I_{11} & I_{22} & \llcorner I_{22} \\ \llcorner I_{11} & \llcorner I_{22} & I_{33} \end{bmatrix} \quad (B 2)$$

We will show that this condition will be met if the velocity gradient tensor in the equilibrium orientation is upper triangular, as

$$\begin{bmatrix} E_1 & -\omega_3 & \omega_2 \\ 0 & E_2 & -\omega_1 \\ 0 & 0 & E_3 \end{bmatrix} \quad (\text{B } 3)$$

where E_1 , E_2 and E_3 are the extension rates along the equilibrium orientation axes. Note that since the velocity gradient tensor is upper triangular, E_1 , E_2 and E_3 are the eigenvalues of the velocity gradient tensor \mathbf{G}

With the assumed upper triangular form of the velocity gradient tensor \mathbf{G} we can then solve solve the ordinary differential equation for the moment tensor \mathbf{I} which is given as

$$\frac{dI_{pq}}{dt} - G_{pj}I_{qj} - G_{qj}I_{pj} = 2\gamma\delta_{pq} \quad (\text{B } 4)$$

Integrating the differential equations for the diagonal elements of \mathbf{I} gives

$$I_{ii} = \delta_{ij} \frac{\gamma}{E_i} [\exp(2E_j t) - 1] \quad (\text{B } 5)$$

The differential equations for the off-diagonal elements are

$$\begin{aligned} \frac{dI_{23}}{dt} - (E_2 + E_3)I_{23} + \omega_1 I_{33} &= 0 \\ \frac{dI_{13}}{dt} - (E_1 + E_3)I_{13} + \omega_3 I_{23} - \omega_2 I_{33} &= 0 \\ \frac{dI_{12}}{dt} - (E_1 + E_2)I_{12} + \omega_3 I_{22} - \omega_2 I_{23} + \omega_1 I_{13} &= 0 \end{aligned} \quad (\text{B } 6)$$

where the symmetry of the tensor gives only three independent equations. Substituting the solutions for the diagonal elements gives solutions for the off-diagonal elements that are sums of exponentials with leading terms of

$$\begin{aligned}
I_{23} &\sim A \exp(E_2+E_3)t \\
I_{13} &\sim B \exp(E_1+E_3)t \\
I_{12} &\sim C \exp(E_1+E_2)t
\end{aligned}
\tag{B 7}$$

where the constants A, B, and C are constants of order $[\gamma/(G_{ij}G_{ij})^{\frac{1}{2}}]$. Examination of Eq. B 7 and B 5, with the specification that $E_1 > E_2 > E_3$ and $E_2 > 0$ shows that the elements of I satisfy the condition given by Eq. B 2 in the limit of large times. An orthogonal coordinate system with an upper triangular velocity gradient tensor G gives the asymptotic orientation of an instantaneous pulse in a weakly rotating shear flow.

Diffusive Tube

When $G_{22}=0$ the diagonal element of the second moment tensor I_{22} will not increase exponentially as was found for the case when $G_{22}>0$. Nonetheless the condition for an equilibrium orientation will be satisfied if the velocity gradient tensor G is upper triangular as

$$\begin{bmatrix} E_1 & -\omega & \omega_2 \\ 0 & 0 & -\omega_1 \\ 0 & 0 & E_3 \end{bmatrix}
\tag{B 8}$$

where $E_1 = -E_3$ from continuity of an incompressible fluid.

With the above form of the velocity gradient tensor the differential equation for I_{pq} can be integrated. The diagonal elements I_{11} and I_{33} are unchanged from the disk (Eq. B 5). Likewise, the off-diagonal elements I_{12} , I_{23} , and I_{13} evolve in time as in the previous case (Eq. B 7) with the specification $E_2=0$. The asymptotic evolution of the I_{22} can be found using the asymptotic value for I_{23} ($I_{23} \rightarrow \Omega_1\gamma/E_3^2$ as $t \rightarrow \infty$) which gives

$$I_{22} \propto 2\gamma t [1 + (\Omega_1/-E_3)^2] \quad (\text{B } 9)$$

Examination of Eqs. B 6, B 7, and B 9 with the specification that $E_1 > 0$ and $E_3 < 0$ shows that the elements of the second moment tensor I meet the criteria for an equilibrium orientation in the limit of large times. Diffusive tube concentration distributions will deform asymptotically according to the upper triangular velocity gradient tensor given by Eq. B 8.

Tube

If the diagonal elements of the velocity gradient tensor G_{22} and G_{33} are negative, then the moments I_{22} and I_{33} will asymptotically approach a constant value. The condition for an equilibrium orientation (Eq. B 1) therefore requires that I have the following asymptotic form

$$\begin{bmatrix} I_{11} & \ll I_{11} & \ll I_{11} \\ \ll I_{11} & I_{22} & 0 \\ \ll I_{11} & 0 & I_{33} \end{bmatrix} \quad (\text{B } 10)$$

As in the analysis for the disk we solve the ordinary differential equation for I using a proposed form of the velocity gradient tensor, which can be given as

$$\begin{bmatrix} E_1 & -\omega_3 & \omega_2 \\ 0 & E_2 & \frac{-\omega_1}{E_2+E_3} \\ 0 & \frac{\omega_1}{E_2+E_3} & E_3 \end{bmatrix} \quad (\text{B } 11)$$

Comparison of the velocity gradient tensors (Eqs. B 11 and B 4) shows that the elements of the tensor I will evolve in time as in the previous case, except for I_{23} , which evolves according to the differential equation

$$\frac{dI_{23}}{dt} - (E_2 + E_3)I_{23} + \frac{\omega_1}{E_2 + E_3}(E_3I_{33} - E_2I_{22}) = 0 \quad (\text{B } 12)$$

Substituting the asymptotic values for I_{33} and I_{22} in B 12 with the specification that $E_2 < E_3 < 0$ gives

$$I_{23} \sim \exp(E_2 + E_3)t \rightarrow 0 \quad \text{as} \quad t \rightarrow \infty \quad (\text{B } 13)$$

The elements of the tensor I have the form required by Eq. B 10. Velocity gradient tensors of the form given by Eq. B 11 give instantaneous pulses with an asymptotic orientation aligned with the coordinate axes. The asymptotic extension rate of these pulses will be given by the diagonal components of the velocity gradient tensor as defined by Eq. B 11.

REFERENCES

- Ashurst, W.T., Kerstein, A.R., Kerr, R.M., and Gibson, C.H., 1987, Alignment of vorticity and scalar gradient with strain rate in simulated Navier-Stokes turbulence, *Phys. Fluids*, **30**, 2343.
- Azam, F., and Ammerman, J.W., 1984, Cycling of organic matter by bacterioplankton in pelagic marine ecosystems: microenvironmental considerations, In *Flows of Energy and Materials in Marine Ecosystems* (ed. M.J.R. Fasham), pp. 345-360, Plenum.
- Batchelor, G.K., 1979, Mass transfer from a particle suspended in fluid with a steady linear ambient velocity distribution, *J. Fluid Mech.*, **95**, 369.
- Carslaw, H.S., and Jaeger, J.C., 1959, *Conduction of Heat in Solids*, Oxford University Press.
- Chet, I., and Mitchell, R., 1976, The relationship between chemical structure of attractants and chemotaxis by a marine bacterium, *Canadian Journal of Microbiology*, **22**, 1206.
- Corrsin, S., 1963, Estimates of the relation between Eulerian and Lagrangian scale in large Reynolds number turbulence, *J. Atmos. Sci.*, **20**, 115.
- Csanady, G.T., 1973, *Turbulent Diffusion in the Environment*, D. Reidel Publishing Company.
- Dillon, T.M., and Caldwell, D.R., 1980, The Batchelor spectrum and dissipation in the upper ocean, *Journal of Geophysical Research*, **85**, 1910.
- Elrick, D.E., 1962, Source functions for diffusion in uniform shear flow, *Australian J. Phys.*, **15**, 283.
- Foister, R.T., and Van de Ven, T.G.M., 1980, Diffusion of brownian particles in shear flows, *J. Fluid Mech.*, **96**, 105.
- Jackson, G.A., 1987, Physical and chemical properties of aquatic environments, In *Ecology of Microbial Communities* (eds. M. Fletcher, T.R.G. Gray and J.G. Jones), pp. 213-233, Cambridge University Press.
- Kerr, R.M., 1985, Higher-order derivative correlations and the alignment of small-scale structures in isotropic numerical turbulence, *J. Fluid Mech.*, **153**, 31.
- Lumley, J.L., 1972, On the solution of equations describing small scale deformation, In *Symposia Matematica: Convegno sulla Teoria della Turbolenza al Istituto Nazionale di Alta Matematica*, pp. 315-334, Academic Press.
- Mitchell, J.G., Okubo, A., and Fuhrman, J.A., 1985, Microzones surrounding phytoplankton form the basis for a stratified microbial ecosystem, *Nature*, **316**, 58.

- Monin, A.S., and Yaglom A.M., 1975, *Statistical Fluid Mechanics*, Vol. 2, MIT Press.
- Novikov, E.A., 1958, Concerning turbulent diffusion in a stream with a transverse gradient of velocity, *Appl. Math. Mech. (P.M.M.)* **22**, 412.
- Oakey, N.S., and Elliott, J.A., 1980, Dissipation in the mixed layer near Emerald Basin, In *Marine Turbulence* (ed. J.C. Nihoul), pp. 123-133, Elsevier.
- Okubo, A., and Karweit, M.J., 1969, Diffusion from a continuous source in a uniform shear flow, *Limnology and Oceanography*, **14**, 514.
- Pearson, H.J., Valioulis, I.A., and List, E.J., 1984, Monte Carlo simulation of coagulation in discrete particle-size distributions. Part 1. Brownian motion and fluid shearing, *J. Fluid Mech.*, **143**, 367.
- Sato, Y., and Yamamoto, K, 1987, Lagrangian measurement of fluid-particle motion in an isotropic turbulent field, *J. Fluid Mech.*, **175**, 183.
- Shay, T.J., and Gregg, M.C., 1984, Turbulence in the oceanic convective mixed layer, *Nature*, **310**, 282.
- Tennekes, H., and Lumley, J.L., 1972, *A First Course in Turbulence*, MIT Press.
- Townsend, A.A., 1951a, On the fine-scale structure of turbulence, *Proc. Roy. Soc. A*, **208**, 534.
- Townsend, A.A., 1951b, The diffusion of heat spots in isotropic turbulence, *Proc. Roy. Soc. A*, **209**, 418.
- Van Atta, C.W., and Antonia, R.A., 1980, Reynolds number dependence of skewness and flatness factors of turbulent velocity derivatives, *Phys. Fluids*, **23**, 252.
- Vieillefosse, P., 1982, Local interaction between vorticity and shear in a perfect incompressible fluid, *J. Physique*, **43**, 837.
- Williams, P.J. LeB., 1984, Bacterial production in the marine food chain: the emperor's new suit of clothes?, In *Flows of Energy and Materials in Marine Ecosystems* (ed. M.J.R. Fasham), pp. 271-299, Plenum.
- Williams, P.M., and Druffel, E.R.M., 1988, Dissolved organic matter in the the ocean: Comments on a controversy, *Oceanography*, **1**, 14.

Chapter 3.

Strong Rotation Produces Vortex Tubes in Homogeneous, Isotropic Turbulence

Abstract

Regions of concentrated vorticity have been observed to be primarily in tube-shaped structures in contrast to predictions based on measurements of the irrotational shearing component of turbulent flows. Rotational effects can modify the deformation of fluid elements to produce tube-shaped structures whenever the rotation is above a critical value and the extension rate along the rotation axis is positive. An analysis of numerical turbulence results indicates that these conditions are satisfied throughout a significant fraction of the fluid, lending support to the observation that vortex tubes are more common than vortex sheets.

Recent results from numerical simulations of turbulence (Siggia 1981, Kerr 1985, Rogers and Moin 1987, Ashurst et al. 1987) show areas of intense vorticity concentrated in vortex tubes, in contrast to earlier predictions that vortex sheets should be more common. Townsend (1951) showed that an irrotational shearing motion having two positive principal strain rates imposed on a vorticity distribution weak relative to the shear would concentrate the vorticity into sheets of finite thickness. Skewness measurements indicated that locations having two positive principal strain rates were more frequent than those with a single positive principal strain (Batchelor and Townsend 1947), thus Townsend predicted that vortex sheets were more common than vortex tubes. In this note we show how the effects of strong rotation can modify the deformation of fluid elements. Tube-shaped structures are produced, even in locations with two positive principal strain rates, if the rotational component of the motion is above a critical intensity and if the extension rate along the rotation axis is positive. The critical rotation intensity has been identified as that necessary to produce imaginary eigenvectors for the velocity gradient tensor (Bowen and Stolzenbach 1989). An analysis of the results of numerical turbulence simulations shows that in a significant fraction of the fluid the rotation rate is indeed above the critical value and extension rates along the rotation axes are positive. The frequency of these strongly rotational locations is high enough so that vortex tubes rather than vortex sheets are expected to predominate.

The deformation of a fluid element in a linear flow fields can be analyzed by following the temporal variation in a moment of inertia tensor, $J_{ij}(t)$ that specifies the size and shape of the element. For an initially spherical element of radius r , the initial condition for the moment tensor is $J_{ij}(0) = r^2 I_{ij}$, where I is the identity matrix. The components of the moment tensor J_{ij} vary in time for a linear flow

field according to (Vieillefosse 1984)

$$\frac{dJ_{ij}}{dt} = G_{il} J_{jl} + G_{jl} J_{il} \quad (1)$$

where G_{ij} is the velocity gradient tensor $G_{ij} = \partial u_i / \partial x_j$ which we assume is homogeneous in space and steady in time. Linear velocity distributions deform fluid elements into ellipsoids whose dimensions change in time according to the rates of strain along each axis of the ellipsoid. In flows that are essentially irrotational each dimension of the ellipsoid changes exponentially according to the corresponding principal strain rate (Eq. 1, $G_{ij} = 0$, $i \neq j$). Therefore, tube-shaped fluid elements result only when two principal strain rates are negative. Because of the conservation of angular momentum in the fluid element vorticity increases along the tube's axis as its cross-sectional area decreases, while vorticity decreases in the other two directions. Townsend (1951) showed that a stationary solution representing a vortex tube could result in which the production of vorticity from axial stretching is balanced by diffusion of vorticity away from the tube axis.

Strong rotation spins the fluid element around the vorticity axis, averaging the ellipsoid's extension rate in the plane perpendicular to the rotation axis, but not affecting the extension parallel to the axis. Batchelor (1979) showed that mass transfer in the limit of strong rotation is equivalent to that for an irrotational, axisymmetric shear with a principal strain rate along the symmetry axis equal to the extension rate along the rotation axis. Concentration distributions surrounding continuous point sources in the region where the mass transfer is advection dominated also show this behavior in the limit of strong rotation (Bowen and Stolzenbach 1989). Since the deformation of a fluid element is equivalent to the advection dominated dispersal of an instantaneous source, we expect that the results

for mass transfer and concentration distribution in shear flows with strong rotation can be applied to our analysis of fluid element deformation.

The assertion that tubes are produced by strongly rotational flows with positive extension rates along the rotation axis can be proven with a perturbation analysis presented by Batchelor (1979) for mass transfer in linear flows, with the additional constraint that transport by molecular diffusion coefficient is small relative to advection. Following Batchelor we choose a coordinate system with x_3 aligned with the vorticity vector. The shear component, which may have one or two positive principal strain rates, is split into two parts, so that the velocity gradient tensor is given as $\mathbf{G} = \mathbf{E}^{(0)} + \mathbf{E}^{(1)} + \mathbf{\Omega}$, with the following individual elements.

$$\mathbf{E}^{(0)} = \begin{bmatrix} -\frac{1}{2}E_{33} & 0 & 0 \\ 0 & -\frac{1}{2}E_{33} & 0 \\ 0 & 0 & E_{33} \end{bmatrix} \quad \mathbf{E}^{(1)} = \begin{bmatrix} 0 & E_{12} & E_{13} \\ E_{21} & 0 & E_{23} \\ E_{31} & E_{32} & 0 \end{bmatrix} \quad \mathbf{\Omega} = \begin{bmatrix} 0 & -\Omega & 0 \\ \Omega & 0 & 0 \\ 0 & 0 & 0 \end{bmatrix} \quad (2)$$

$\mathbf{E}^{(0)}$ defines an irrotational shearing that is axisymmetric about the vorticity axis x_3 . Assuming that the rotation component $\mathbf{\Omega}$ is strong relative to the shearing component $\mathbf{E}^{(1)}$, the moment tensor can be solved with the following perturbation scheme (Batchelor 1979)

$$\mathbf{J}_{ij}(t) = t \left\{ \mathbf{J}_{ij}^{(0)}(t) + \frac{E'}{\Omega} \mathbf{J}_{ij}^{(1)}(T) + O\left[\frac{E'^2}{\Omega^2}\right] \right\} \quad (3)$$

where $T = \Omega t$, $E' = (E_{12}^2 + E_{23}^2 + E_{13}^2)^{\frac{1}{2}}$ and E' is assumed to be small relative to Ω .

The term $t\mathbf{J}_{ij}^{(0)}(t)$ represents the moment tensor for the irrotational, axisymmetric flow that produces a tube-shaped element elongated along x_3 when $E_3 > 0$. In the strongly rotational case the fluid element will deform into a tube along x_3 if each of the elements of the perturbation matrix $\mathbf{J}^{(1)}$ in the x_1 - x_2 plane approach zero as

time increases. Because of the symmetry of the perturbation tensor $J^{(1)}$ and the antisymmetry of the vorticity tensor (see Eq. 2.37, Batchelor 1979) this condition is satisfied if $J_{12}^{(1)} \rightarrow 0$ and $J_{11}^{(1)} \rightarrow 0$ as $T \rightarrow \infty$. The equations for these components read

$$\frac{dJ_{12}^{(1)}}{dT} = - \left[\frac{1}{T} + \frac{E_{33}}{\Omega} \right] J_{12}^{(1)} + \frac{2E_{12}^{(1)}}{E} J_{11}^{(0)}, \quad (4a)$$

$$\frac{dJ_{11}^{(1)}}{dT} = - \left[\frac{1}{T} + \frac{E_{33}}{\Omega} \right] J_{11}^{(1)} + 2J_{12}^{(1)} \quad (4b)$$

Since T and E_{33} are always greater than zero and $J_{11}^{(0)}$ approaches zero, Eq. 4a shows that $J_{12}^{(1)}$ approaches zero as time increases which in turn ensures that $J_{11}^{(0)}$ approaches zero (Eq. 4b). Thus spherical fluid elements deform into tubes when the extension rate along the rotation axis is positive and the rotation is strong, even if two principal rates of strain are positive.

While the preceding analysis gives the behavior of fluid elements in the limit of strong rotation, we still need an estimate of the level of rotation that is required to modify deformations from that of irrotational flow. Bowen and Stolzenbach (1989) analyzed the effects of rotation on concentration distributions around continuous point sources by systematically varying the strength of rotation for a fixed irrotational shear component. Their findings can be applied to the deformation of fluid elements because they examined the shape of concentration distributions over distances from the source where the mass transport was advection dominated. The shape of distributions for an instantaneous source will be qualitatively similar to that described for a continuous source since the convolution of the instantaneous source selects only a narrow range of times in advectively dominated regions (Bowen

and Stolzenbach 1989). Rotation effects on concentrations distributions were found to be minor until the rotation rate approaches a critical value shown to be equal to the rotation rate required to give imaginary eigenvectors for the velocity gradient tensor (Bowen and Stolzenbach 1989). Concentration distributions quickly approach an axisymmetric configuration when the rotation exceeds the critical value, and are essentially axisymmetric whenever the vorticity is more than twice the critical value. For a general velocity gradient tensor the critical vorticity is specified as

$$\omega_i \omega_i = 2E_i E_i - 3^{*2^{4/3}} \left[E_1 E_2 E_3 + \frac{E_i \omega_i \omega_i}{4} \right]^{2/3} \quad (5)$$

where E_1 , E_2 and E_3 are the principal strain rates and ω_i specifies the vortical component as $\omega_i = -\epsilon_{ijk} G_{jk}$. In the special case where the vorticity vector lies along a principal axes of strain, the critical vorticity is the difference in the two principal strain rates perpendicular to the vorticity axes.

In addition to the strength of vorticity, we must also determine the extension rate along the vorticity axis to predict the deformation of fluid elements in rotational shearing. Batchelor (1980) has shown that the average extension rate along the vorticity axis is related to the velocity gradient skewness so that flows with a preponderance of locations having two positive principal strain rates also have positive extension rates along the vorticity axis. Betchov (1956) showed that shearing flows which are characterized by a negative velocity derivative skewness produce vorticity through stretching of fluid elements, and he hypothesized that vorticity production is confined to the locations having two positive principal strains.. Using coupled equations for shear and rotation developed from the Euler equation, Vieillefosse (1984) predicted that in an isolated element of fluid the velocity

gradient tensor evolves towards higher shear and rotation rates. The shear component evolves to a pattern having two positive principal strain rates and the vorticity vector becomes aligned with one of the positive principal strains. Each of these analyses provide theoretical support for the view that strong rotation is localized and is associated with a shearing pattern having two positive principal strain rates and a vortex axis aligned with a positive principal axes of strain. We now examine the results of numerical simulations of turbulence to compare vorticity intensities to the critical value given earlier to see if vortex tubes or sheets are produced through the combined effects of shear and rotation.

Ashurst et al. (1977) examined alignment of the vortex vector to the principal axes of strain for numerical simulations of isotropic free shear and turbulent shear from an imposed large scale shearing. For both flows they found that vorticity is most often oriented along the principal axes having a strain rate of intermediate magnitude. Approximately 75 percent of all locations have two positive principal strain rates, which is consistent with measurements of velocity gradient skewness for these cases (Kerr 1985). In regions containing relatively strong shearing motions there are always two positive principal strain rates. These regions also have high levels of vorticity, based on correlations between shear and vorticity intensity (Kerr 1985). For the shear flow case, more than 40 percent of the locations characterized by the highest levels of shear (locations constituting the top 1/64th of the dissipation rate distribution) have a vorticity axes within 18 degrees of the intermediate strain, which is always positive. Although Ashurst et al. do not give the relative magnitude of shear and rotation for these high shear locations, the maximum vorticity is more than three times the critical vorticity (Eq. 5) as estimated from the maximum dissipation rate (Ashurst, personal communication). High vorticity in these regions produces vortex tubes because of the alignment between shear and rotation, even though there are two positive strain rates.

In the isotropic flow case approximately 25 percent of all locations have the vorticity vector within 18 degrees of the intermediate strain, which is positive (Ashurst et al. 1987). The average vorticity for this fraction of the fluid is nearly seven times the critical rotation rate estimated from Eq. 5. Strongly rotational flow, with expansive shear along the rotation axis, therefore occupies at least 25 percent of the total fluid volume, and rotational effects produce vortex tubes in these locations. Vortex tubes are also expected in all locations having a single positive principal strain rate (25 percent of all locations), since the vorticity axes is always oriented along the single positive principal strain (Ashurst et al. 1987).

In summary, because of rotational effects, vortex tubes are expected in at least half the fluid, even though a majority of the fluid has an irrotational shear component with two expansive axes. High shear locations have strong vorticity which is aligned with the smaller positive strain to produce vortex tubes. These predictions are consistent with the graphical displays of concentrated vorticity, showing primarily vortex tubes with a positive strain rate along the vortex tube and a second positive strain rate perpendicular to the tube axis (Kerr 1985, Ashurst et al. 1987).

REFERENCES

- Ashurst, W.T., Kerstein, A.R., Kerr, R.M., and Gibson, C.H., 1987, Alignment of vorticity and scalar gradient with strain rate in simulated Navier-Stokes turbulence, *Phys. Fluids*, **30**, 2343.
- Batchelor, G.K., and Townsend, A.A., 1947, *Proc. Roy Soc. A*, **190**, 534.
- Batchelor, G.K., 1979, Mass transfer from a particle suspended in fluid with a steady linear ambient velocity distribution, *J. Fluid Mech.*, **95**, 369.
- Batchelor, G.K., 1980, Mass transfer from small particles suspended in a turbulent fluid, *J. Fluid Mech.*, **98**, 609.
- Betchov, R., 1956, An inequality concerning the production of vorticity in isotropic turbulence, *J. Fluid Mech.*, **1**, 497.
- Bowen, J.D., and Stolzenbach, K.D., 1989, Concentration distributions around continuous point sources in a fluid with a steady linear velocity distribution, submitted to the *J. Fluid Mechanics*.
- Kerr, R.M., 1985, Higher-order derivative correlations and the alignment of small-scale structures in isotropic numerical turbulence, *J. Fluid Mech.*, **153**, 31.
- Rogers, M.M., and Moin, P., 1987, The structure of the vorticity field in homogeneous turbulent flows, *J. Fluid Mech.*, **176**, 33.
- Siggia, E.D., 1981, Numerical study of small-scale intermittency in three-dimensional turbulence, *J. Fluid Mech.*, **107**, 375.
- Townsend, A.A., 1951, On the fine-scale structure of turbulence, *Proc. Roy. Soc. A*, **208**, 534.
- Viellefosse, P., 1984, Internal motion of a small element of fluid in an inviscid flow, *Physica*, **125A**, 150.

Chapter 4.

Microbial Chemotaxis Towards a Continuous Point Source of Attractant

An analysis of published experiments on the pattern of bacterial chemotactic swimming shows that the approach velocity to a continuous point source of attractant can be described with a hyperbolic function of the temporal change in chemoreceptor occupancy experienced by the bacterium. In a motionless fluid, the population density of chemotactic bacteria surrounding the point source shows a characteristic form reflecting the balance between random and directed chemotactic motions. Near the source, the population density decreases exponentially with distance at a rate dependent on the bacterial swimming speed and a characteristic time scale. The population density approaches a uniform value at a distance dependent on the mass flux of chemoattractant and bacterial chemotaxis sensitivity, but independent of the bacterial swimming speed. In a moving fluid bacterial densities approach background levels at a distance where effective chemotactic motion towards the source balances fluid motion away from the source. Near the source, where the concentration gradients saturate the bacteria's effective chemotactic response, bacteria population densities decrease exponentially with increasing distance. Results from a Monte-Carlo simulation of a chemotactic population indicate that the decrease in population density near the source is related to the minimum bacterial run length.

1. Introduction

Descriptions of bacterial motion in the presence of spatial gradients of attracting chemicals can be divided into two groups: 1) stochastic descriptions of an individual bacterium's swimming pattern, and 2) deterministic descriptions of the chemotactic bacteria's population response. The deterministic descriptions of population response are useful because of their simplicity. Analytical relations can be derived that balance random and directed components of bacterial swimming with physical processes such as fluid motion. Analyses of this sort have been found to be good predictors of population response (Keller 1971, Dahlquist et al. 1976). The analytical relationships can then be used predictively by relating the deterministic description of chemotactic behavior to measurable quantities describing the stochastic swimming pattern.

In this paper we use a deterministic description of chemotaxis first proposed by Keller and Segel (1971) to develop analytical solutions for the population density distribution of chemotactic bacteria surrounding a continuous point source of attractant. Parameters in the deterministic description are related to the behavior of individual bacteria as described by Brown and Berg (1974) in order to understand how differences in swimming characteristics such as swimming speed or chemotactic sensitivity affect the population distribution around the source. Analytical solutions are developed initially for a motionless fluid, but the effects of fluid motion through movement of the source or shearing of the fluid are also analyzed with scaling estimates. The problem considered has applications to the clustering of chemotactic bacteria around individual phytoplankton cells that are exuding dissolved organic carbon. Non-random interactions between phytoplankton and bacteria resulting from chemotactic behavior may have important consequences to the ecology of marine systems (Bowen et al. 1989).

Keller and Segel (1971) first proposed that the response of a chemotactic population can be modelled as the sum of an effective chemotactic velocity dependent on the spatial gradient of chemoattractant and a random diffusion coefficient. The derived average response arose from a one-dimensional version of the "run and tumble" swimming pattern as observed for the enteric bacteria *Salmonella typhimurium* and *Escherichia coli* (e.g. MacNab and Koshland 1972, Berg and Brown 1972). Bacterial motion is seen as a succession of straight, constant velocity runs separated by short tumbles that alter the direction of the succeeding run. Directed motion is accomplished by adjusting the length of each run depending on the gradients of chemoattractant experienced by the moving bacteria.

Keller (1971) used the deterministic description of chemotaxis to analyze the movement of bacteria placed at the end of a capillary tube containing an attracting organic compound. Consumption of the attracting chemical by the bacteria produced spatial gradients of the attractant that in turn resulted in directed chemotactic movement away from the initial bacteria position. A band of bacteria was observed to move along the capillary at a constant speed. The deterministic description of the population response predicted this behavior and the predicted band speed agreed satisfactorily with observations. The width of the band was found to be related to the relative strengths of the chemotactic and random components of bacterial motion.

Dahlquist et al. (1976) used the deterministic description of bacterial chemotaxis to analyze the movement of bacteria placed in a capillary tube with prescribed spatial gradients of attractant. The population average velocity was calculated by measuring the flux of bacteria of known population density across a fixed location along the capillary. By using equations that related the population average velocity to the bacteria's swimming speed and run duration (Lovely and Dahlquist 1975),

Dahlquist et al. (1976) were able to predict that the duration of a run is linearly related to the spatial gradient of attractant in the direction of the run. They also showed that gradients sensed by the bacteria are related to changes in the number of attractant molecules bound to bacterial chemoreceptors. These predictions agree well with models of individual behavior based on microscopic observations of individual bacteria in temporal gradients of chemoattractant (Brown and Berg 1974).

Other chemotactic systems analyzed with a deterministic description of behavior include the chemotactic motion in a uniform flow with a plane source of attractant (Lapidus 1980), or chemotaxis and bacterial growth in motionless fluid with a plane source of attractant (Lauffenburger et al. 1982). Lauffenburger et al. (1982) showed that populations with superior motility properties can outgrow bacteria that would dominate through superior growth kinetics if there were no motility effects. Lapidus (1980) showed that the population density distribution near a source in a uniform flow could also be affected by bacterial chemotaxis given a sufficiently strong chemotactic response.

Studies of bacterial clustering around phytoplankton cells that are exuding organic carbon have been based on Monte-Carlo simulations utilizing the stochastic description of chemotactic swimming (Jackson 1987, 1989, Bowen et al. 1989). These Monte-Carlo simulations can easily incorporate additional characteristics of the run and tumble chemotactic pattern that have been observed from more recent observations of individual chemotactic bacteria. Experiments have shown that bacteria temporally average concentration signals over several seconds (Segall et al. 1986) and are limited in how quickly they can respond to sudden changes in chemoattractant concentration (Segall et al. 1982).

In this paper we will utilize the analytical relationships derived from the deterministic description of chemotaxis to

interpret the results of our own Monte-Carlo simulation of bacterial chemotaxis around individual phytoplankton cells (Bowen et al. 1989). The simulation model results indicate that the bacterial population density near the source decreases at a rate related to the minimum run length of the bacteria. The simulation also indicates that the size of the region where chemotactic behavior concentrates bacteria can be predicted from the deterministic description of chemotaxis. Population densities approach background levels at a distance where effective chemotactic velocities balance fluid motions.

2. Effective Chemotactic Velocity in Motionless Fluid

Bacteria cluster around point sources by adjusting the duration of runs depending on the concentration gradients experienced as they move through the fluid. For a motionless fluid, a continuous addition of mass results in the following concentration distribution around the point source

$$C(r) - C_{\infty} = \frac{F}{4\pi Dr} \quad (2.1)$$

where C is the chemoattractant concentration, r is the distance from the source, C_{∞} is the background concentration, F is the steady mass input rate, and D is the molecular diffusion coefficient for the chemoattractant compound (Carslaw and Jaeger 1959). The bacteria's effect on concentration distributions through consumption are assumed to be negligible. The description of chemotactic swimming pattern is based on observations of *E. coli* in temporal gradients of attractant (Brown and Berg 1974). The duration of a run is related to the temporal gradient in chemoreceptor occupancy according to

$$T = T_0 \exp \left[\alpha \frac{K_d}{(K_d + C)^2} \frac{dC}{dt} \right] \quad (2.2)$$

where T is the run duration, T_0 is the average run duration when there is no chemotactic signal, α is a sensitivity factor, K_d is the chemoreceptor affinity, and the overbar indicates temporal averaging of the derivative. If the temporal averaging effects can be considered negligible, then the temporal gradient term in Eq. 2.2 can be specified according to the speed and direction of the bacteria and the spatial derivative of the chemoattractant concentration as

$$\frac{T}{T_0} = \exp \left[\frac{\alpha K_d}{(K_d + C)^2} \frac{dC}{dr} \frac{dr}{dt} \right] = \exp \left[\frac{\alpha K_d}{(K_d + C)^2} \frac{F}{4\pi D r^2} V \cos \phi \right] \quad (2.3)$$

where V is the bacterial swimming speed and ϕ is the angle between the bacterial heading and the direction to the source. The effective chemotactic velocity of a bacteria population can be related to the description of individual behavior by integrating the effective motion of the bacteria over all possible swimming paths, as

$$V_e = V \frac{\int_{-1}^1 T(u) u du}{\int_{-1}^1 T(u) du} \quad (2.4)$$

where $u = \cos \phi$ (Lovely and Dahlquist 1975). In relating the run length and the effective chemotactic velocity in this way we have assumed that tumbles are instantaneous and that the choice of direction after tumbling is independent of the direction travelled (Lovely and Dahlquist 1975). Eq. 2.3 can be simplified by assuming that the concentration experienced by the bacterial is significantly less than the chemoreceptor affinity K_d , a reasonable assumption for the fluxes expected from phytoplankton cells and the range of chemoreceptor affinities measured for chemotactic bacteria (Bowen et al. 1989). Performing the integration of Eq. 2.4 with the description of run duration (Eq. 2.3) results in the following equation for

the effective chemotactic velocity V_e

$$\frac{V_e}{V} = \coth \left[\frac{r_0}{r} \right]^2 - \left[\frac{r}{r_0} \right]^2 \quad (2.5)$$

where r_0 is a "chemotactic length" defined as

$$r_0 = \left[\frac{FV\alpha}{4\pi DK_d} \right]^{\frac{1}{2}} \quad (2.6)$$

Of interest is the fact that the chemotactic length depends not only on the concentration signal and the chemotaxis sensitivity but on the bacterial swimming speed V .

The normalized effective velocity described by Eq. 2.5 has a hyperbolic character that varies linearly with the argument $(r_0/r)^2$ in the region where $r \gg r_0$ and approaches a uniform value when $r \ll r_0$. A similar hyperbolic relationship has been derived by Dahlquist et al. (1976) based on experiments on the chemotactic bacteria *Salmonella typhimurium* in spatial gradients of chemoattractant. Their description of chemotaxis assumes that the run duration varies linearly rather than exponentially with the attractant gradient. In fact, the strengths of the attractant signal are small enough in the experiments of Brown and Berg (1974) that it is impossible to distinguish between the exponential (Eq. 2.2) and linear relationships; later models of *E. coli* have adopted the assumption that the run time varies linearly with the strength of the gradient (Block, Segall, and Berg 1982). A linear variation in run duration leads to the following equation for the effective velocity

$$\frac{V_e}{V} = \left[\frac{r_0^2}{r_0^2 + 3r^2} \right] \quad (2.7)$$

Because of its simplicity and its relevance to recent observations of chemotactic bacteria, this relationship for effective velocity will be used to predict the population density distribution around the continuous point source.

3. Population Density Distributions in Motionless Fluid

The steady state distribution of bacteria around a continuous point source in motionless fluid results from a balance between the diffusive and effective chemotactic components of the bacterial motion according to

$$D_b \frac{dn}{dr} = -V_e n \quad (3.1)$$

where n is the bacterial population density and D_b is the diffusion constant describing the random motion of the bacteria as (Dahlquist and Lovely 1975)

$$D_b = \frac{V^2 T_c}{3(1-\gamma)} \quad (3.2)$$

where γ is the cosine of the angle between successive bacterial headings, and T_c is a characteristic time scale. These equations lead to the following differential equation for the population density.

$$\frac{dn}{n} = \frac{3(1-\gamma)}{VT_c} \left[\frac{r^2}{r_0^2 + 3r^2} \right] dr \quad (3.3)$$

Integrating this equation results in the following equation for the bacterial population density surrounding the continuous point source.

$$n(r) = n_0 \left\{ \exp \left[-\tan^{-1} \left[\frac{r}{r_0} \right] \right] \right\}^{\frac{3r_0}{VT_c}} \quad (3.4)$$

where n_0 is the background population density and T_c' is the characteristic time scale that includes the term dependent on the angle between successive run directions (Eq. 3.2). This complicated function has simple, asymptotic forms in the regions both near and far from the source. Near the source ($r \ll r_0$) the population density decreases exponentially according to

$$n(r) = n_0 \exp \left[-\frac{r}{l} \right] \quad (3.5)$$

whereas far from the source ($r \gg r_0$) the population density approaches the uniform background value n_0 as

$$n(r) = n_0 \exp \left[\frac{r_c}{r} \right] \quad (3.6)$$

The “inner length scale” l defines the balance between random and chemotactic motion near the source where the chemotactic response is maximized, while the length scale r_c gives the distance where chemotactic behavior begins to elevate bacterial population densities. These two scales are related to the concentration field and the characteristics of the bacteria swimming pattern in the following way

$$l = \frac{VT_0}{3(1-\gamma)} \quad r_c = \frac{F \alpha}{4\pi DK_d T_c'} \quad (3.7)$$

Notice that although the relationship for effective velocity did depend on the swimming speed, the distance where chemotaxis begins to influence population densities, the “cluster size” r_c , does not depend on the swimming speed, reflecting the balance between effective chemotactic and random motion at the edge of the cluster. In the region where the effective velocity relationship is unsaturated ($r \gg r_0$)

(Eq. 2.7), the hyperbolic function for effective chemotactic velocity varies linearly in the signal strength according to

$$V_e = \frac{V^2 F \alpha}{12 \pi D K_d r^2} \quad (3.8)$$

In a motionless fluid, the effective chemotactic motion is balanced by the diffusive component of the bacteria's swimming motion. A characteristic diffusion velocity can be scaled as $V_d = D_b/r$, (see Eq. 3.2). Equating the diffusive velocity V_d and the chemotactic velocity V_e , both of which depend on V^2 (Eq. 3.2 and 3.8), leads to the conclusion that the cluster size r_c does not depend on the bacterial swimming speed V .

4. Simulation Model Results - The Cluster Size in Moving Fluids

A Monte-Carlo simulation model of bacterial chemotaxis was developed to predict bacterial population densities surrounding continuous sources in fluids with relative motions due to sinking of the source or shearing of the fluid (Bowen et al. 1989). The steady-state density distribution of a chemotactic bacteria population was determined by time-averaging instantaneous distributions for a variety of exudation fluxes, chemotaxis sensitivities, swimming speeds, and fluid motion conditions. Bacteria moving out of the simulation region by random swimming or fluid motion were reflected back in at random positions on the region's boundary so that steady population densities could be simulated. The model simulated the effects of shearing or uniform fluid motions on both the concentration distributions surrounding the source and the movement of the bacteria. A more thorough description of the simulation model has been provided elsewhere (Bowen et al. 1989).

The steady-state population distributions for chemotaxis in moving fluids were qualitatively similar to the analytical relations presented earlier for motionless fluids. Near the source the population density decreased exponentially at a rate dependent on the bacterial swimming speed (Fig. 1). The population density approached a uniform value as the distance from the source increased (Fig. 1). However, the distance where the density approached background levels, the cluster size r_c , varied with the bacterial swimming speed (Fig. 1), in contrast to the prediction for motionless fluids (Eq. 3.7).

The increase in the cluster size with increasing swimming speed for both sinking and shearing motions suggests that at the edge of the cluster there exists a balance between fluid motions and effective chemotactic swimming. For the uniform flow case, the characteristic velocity for the fluid motion is simply the phytoplankton fall velocity w_s . If we assume that at the edge of the cluster the concentration gradients are approximately those expected for the motionless case, then the effective chemotactic velocity can be specified with Eq. 3.8. Equating the phytoplankton fall velocity with the effective chemotactic velocity results in the following prediction for the cluster size r_c .

$$r_c = \left[\frac{V^2 F \alpha}{12\pi DK_d w_s} \right]^{1/2} \quad (4.1)$$

In a shearing fluid the velocity opposing chemotactic motion increases linearly with the distance from the source as $V_f = E_b r$, where V_f is the fluid velocity and E_b is a characteristic shear intensity. Equating this velocity with the effective chemotactic velocity provides the following estimate of the cluster size in a

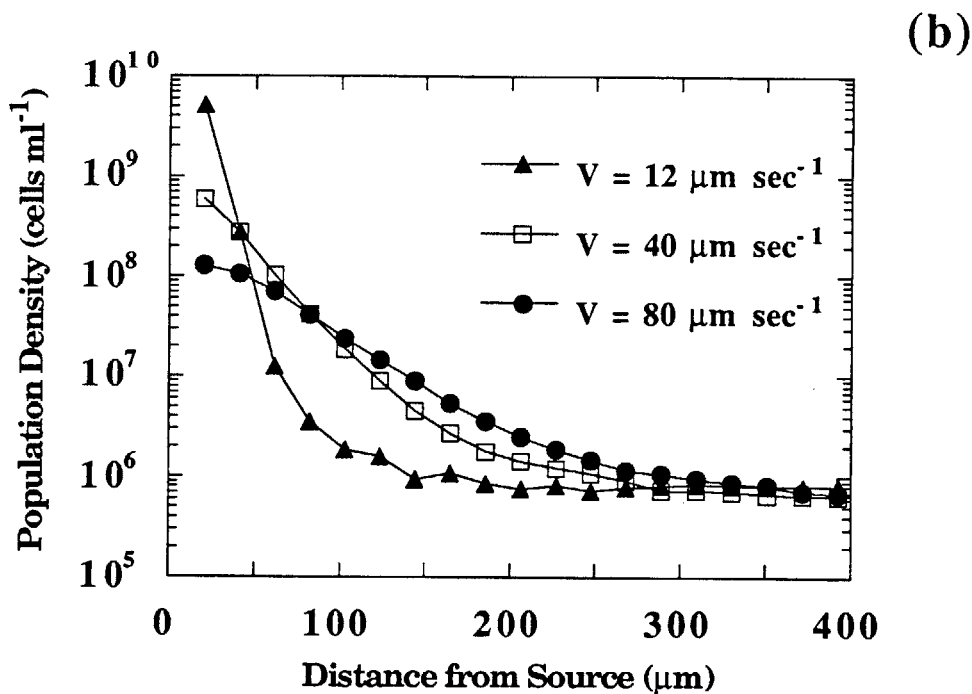
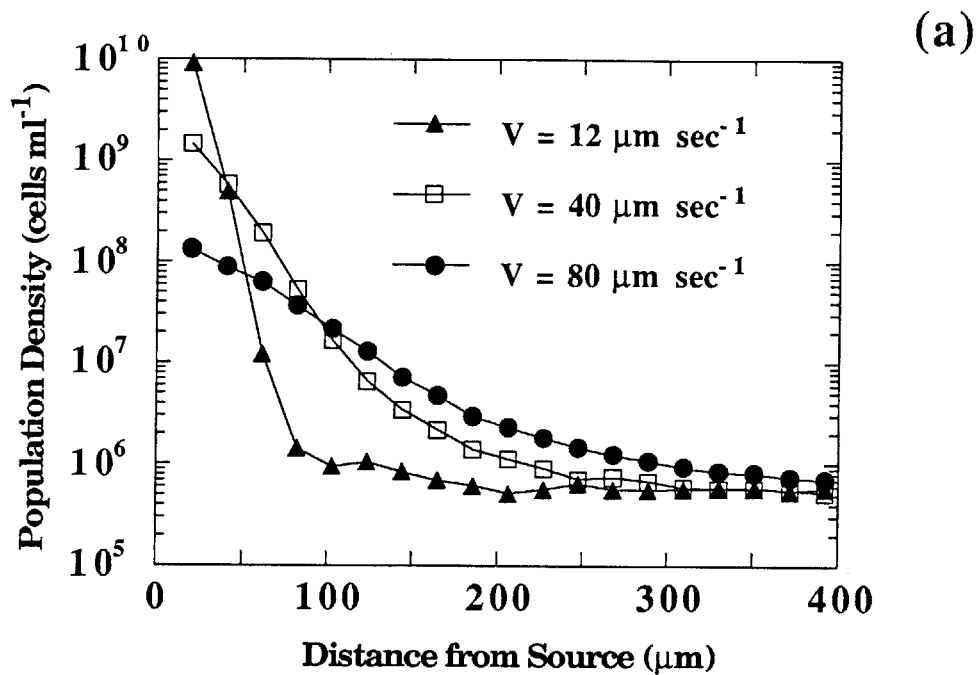


Figure 1. Simulated bacterial population densities versus the distance from the continuous point source

- (a) Weak shearing motion ($E_b = 0.05 \text{ sec}^{-1}$), at the maximum normalized exudation rate ($F/4\pi DK_d = 1140 \mu\text{m sec}$), for a range of swimming speeds.
- (b) Uniform motion from a sinking source ($w_s = 10 \mu\text{m sec}^{-1}$), at the maximum normalized exudation rate ($F/4\pi DK_d = 1140 \mu\text{m sec}$), for a range of swimming speeds.

shearing fluid

$$r_c = \left[\frac{V^2 F \alpha}{12\pi DK_d E_b} \right]^{1/3} \quad (4.2)$$

Both relationships predict the overall trend in the cluster size, with increased cluster sizes for stronger exudation, faster bacterial swimming, and weaker fluid motion. Calculations of cluster sizes for simulations of chemotaxis in a uniform flow showed that the cluster size did not increase as quickly as predicted by Eq. 4.1 (Figure 2a), although the scaling analysis did predict the cluster size to an order of magnitude. Variations in the cluster size for the shear case more closely followed the scaling relationship given by Eq. 4.2 (Fig. 2b), but the scaling relationship underestimated the cluster size for the slowest swimming speed. In this case the cluster was probably too small to be affected by fluid motion, so the bacteria's random motion rather than fluid motions balanced effective chemotactic motion at the edge of the cluster. Cluster sizes were overpredicted for the highest levels of the scaling parameters in both the shear flow and uniform flow cases (Fig 2). This effect may be due to the assumption that the concentration distribution was described by motionless fluid equation (Eq. 2.1). Cluster sizes smaller than predicted by the scaling estimates could result if the concentrations decreased more rapidly than estimated through the effects of uniform streaming or fluid shearing.

5. Simulation Model Results - Distributions near the Source

Differences in the density distributions near the phytoplankton for differing swimming speed suggest that population densities in this region are determined solely by the bacteria's random motion. In the motionless case the decrease in population density near the source was related to a characteristic time scale T_c .

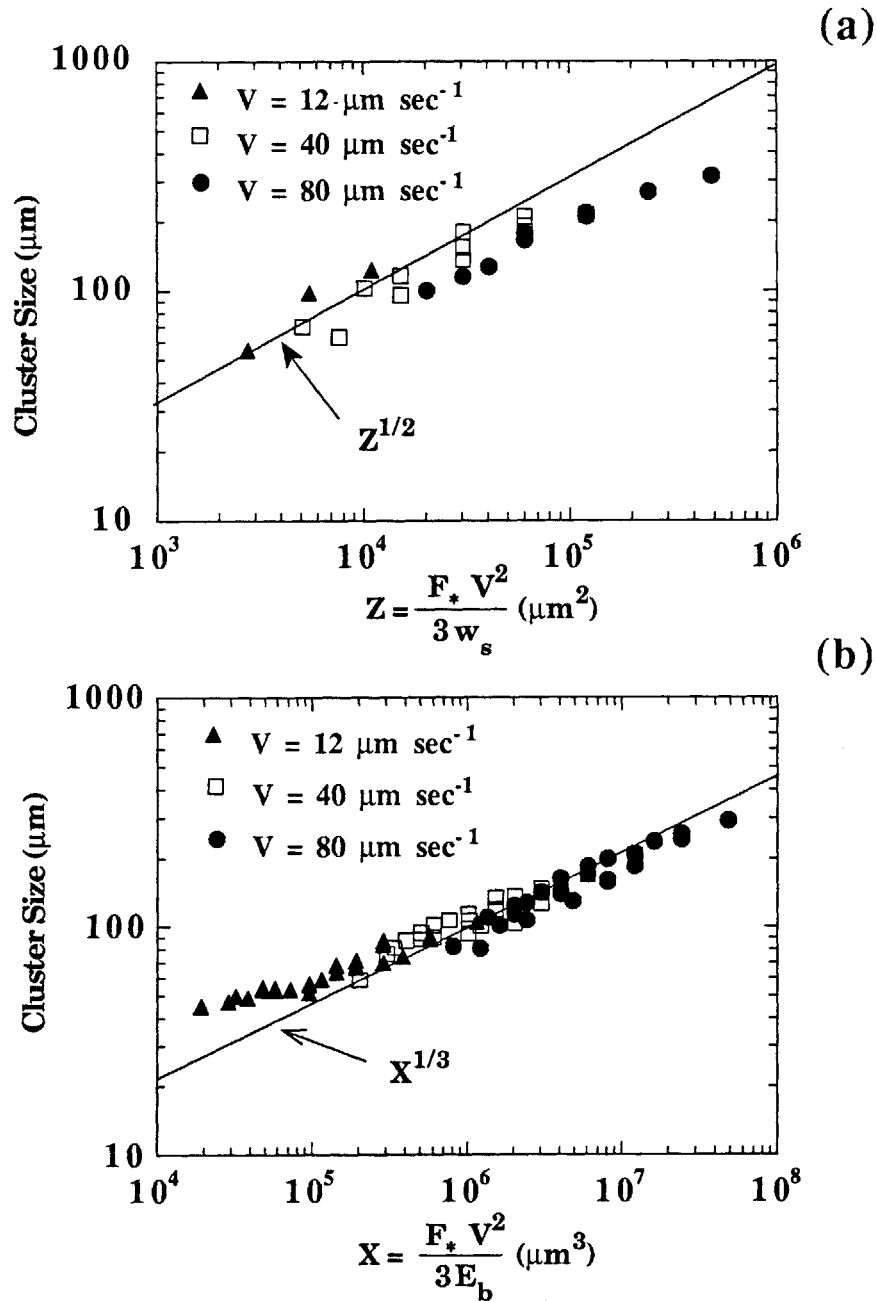


Figure 2. Cluster size vs. the scaling parameters $Z = F_* V^2 (3w_s)^{-1}$ for fluid motions from a sinking source (a) and $X = F_* V^2 (3E_b)^{-1}$ for fluid motions from shearing (b). F_* is the normalized exudation rate $F/4\pi DK_d$, V is the bacterial swimming speed, E_b is the characteristic shear rate, and w_s is the sinking speed of the source. The cluster size is determined from the population density distributions. The solid lines represent $Z^{1/2}$ and $X^{1/3}$, which are the predicted cluster sizes (Eq. 4.1 and 4.2).

(Eq. 3.7). When there are no concentration gradients of attractant, the appropriate time scale in quantifying a bacterium's random motion is its average run time, T_0 , i.e., $T_c = T_0$ (Lovely and Dahlquist 1975). In the general case, however, where chemotactic behavior may result in runs either much shorter or much longer than T_0 (Eq. 2.2), we must consider other time scales that quantify the chemotactic swimming pattern. Bacteria are known to average concentration signals over a few seconds (Segall et al. 1986), represented here in the simplest way by a single averaging time scale T_m . In addition, bacteria are limited in how quickly they can respond to sudden changes in concentration (Segall et al. 1982), represented by the response latency time T_{min} . A sensitivity analysis of the three time scales T_0 , T_m and T_{min} was performed to determine which parameter best characterizes the bacteria's random motion near the source.

The simulation model of bacterial chemotaxis was utilized to perform the sensitivity analysis of the three time scales T_0 , T_m and T_{min} . The model of run time regulation was based on Eq. 2.2. The response latency T_{min} was incorporated into the chemotaxis model by restricting the minimum run time to be no shorter than T_{min} . Temporal concentration gradients were calculated by comparing the current concentration to a concentration time-averaged over a time T_m . Bacterial population densities were simulated for a range of swimming speeds and characteristic time scales T_0 , T_m , and T_{min} .

The sensitivity analysis of the average run time T_0 , the averaging time scale T_m and the response latency time T_{min} indicates that the chemotactic motion near a continuous source is dependent on the minimum run length of the bacteria. In all cases the population density near the source decreased exponentially as $n = n_p \exp(-r/l)$. The inner length scale l was determined from a linear regression of the logarithm of population density versus distance for the distribution near the source.

The inner length scale l increased with increasing swimming speed in all cases (Fig. 3) but there were marked differences in the inner length scale's variation with changing time scales. Changes in the average run time T_0 had little effect on the calculated inner length scale (Fig. 3a), and changes in the averaging time T_m had only a minor effect (Fig. 3b). Changes in the response latency had the largest effect on the inner length scale, and results from the different swimming speeds showed a consistent linear relationship between the length scale $V \cdot T_{\min}$ and the inner length scale (Fig. 3c). However, the response latency clearly does not explain all the variation in the inner length scale. Variations in the length scale over a factor of two were observed for identical values of swimming speed V and response latency T_{\min} (Fig. 3c). Nonetheless, the random motion of the bacteria near the source can best be parameterized with the length scale $V \cdot T_{\min}$, which represents the minimum run length of the chemotactic bacteria.

6. Discussion

We have found that the population densities of chemotactic bacteria surrounding a continuous point source reflect balances between three transport processes: 1) random bacterial swimming, 2) directed chemotactic swimming, and 3) relative fluid motion. Fluid motions affect chemotactic clustering by limiting the size of the bacterial cluster. At the edge of the cluster directed chemotactic motions begin to overcome fluid motions and population densities exceed background levels. The cluster size is maximized when the fluid is motionless, and in this case the bacterial swimming speed does not influence the size of the cluster. Fluid motions do not influence the variation in population density near the source, where characteristic velocities for chemotaxis and random motion are maximized. The random motion of bacteria near the source is related to both the swimming speed and the response latency time of the bacteria.

(a)

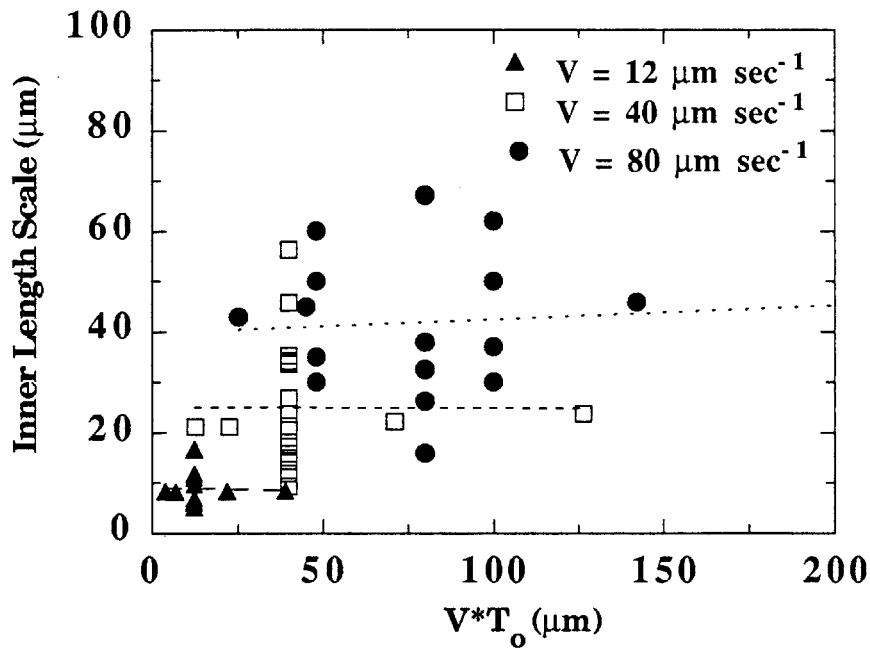


Figure 3. Sensitivity analysis for the time constants in the model of bacterial chemotaxis.

The average run time T_0 , the concentration averaging time scale T_m , and the response latency time T_{\min} were independently varied over a factor of ten around the standard conditions used by Bowen et al. (1989), $T_0 = 1.0$ sec, $T_m = 0.6$ sec, $T_{\min} = 0.2$ sec. The inner length scale is determined from a linear regression of the logarithm of the bacterial population density versus distance for the distribution near the phytoplankton. The bacterial swimming speed V varies from 12 to $80 \mu\text{m sec}^{-1}$, the shear strength E_b varies from 0.05 to 0.20 sec^{-1} , and the exudation strength $F^* = F/4\pi DK_d$ varies from $F^* = 1140 \mu\text{m sec}$ to $F^* = 300 \mu\text{m sec}$. In each plot the dashed lines show best fit lines when the data from each swimming speed is analyzed separately.

(a) Inner length scale l versus the length scale VT_0 .

(b)

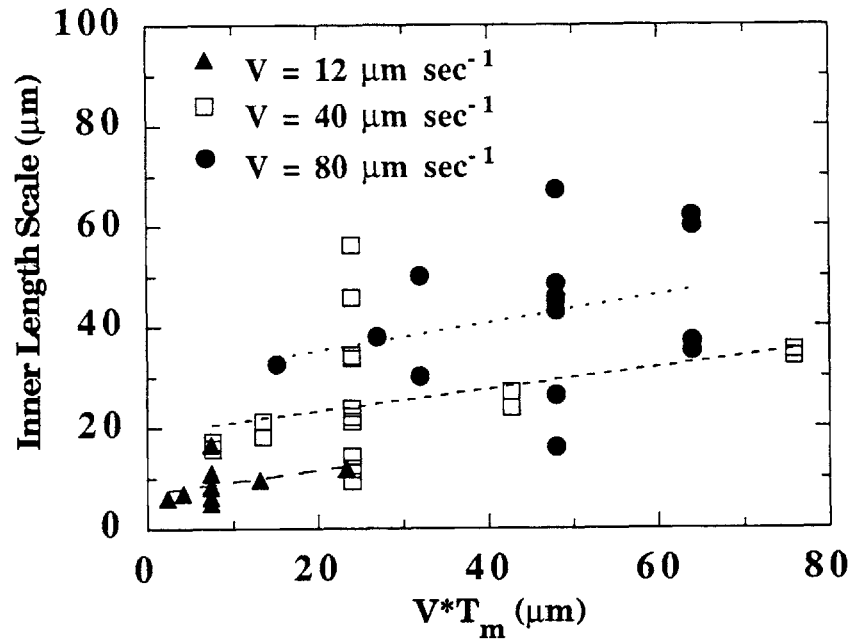
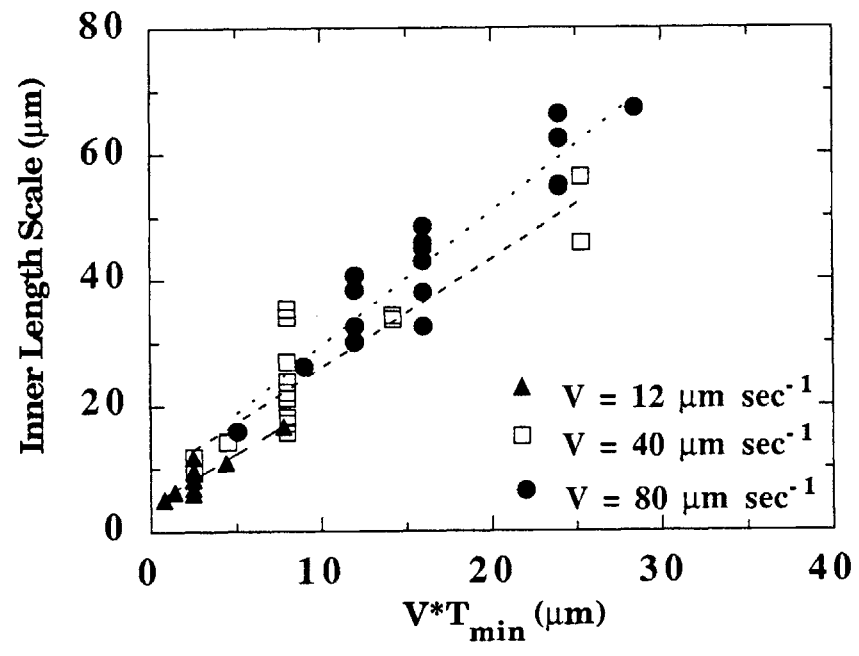


Figure 3b. Sensitivity analysis for the time constants in the model of bacterial chemotaxis.

(b) Inner length l versus the length scale $V T_m$.

(c)



The simulation model results reveal the importance of the response latency time T_{\min} in determining the population density of the chemotactic bacteria. The response latency used in the simulation model (0.2 sec) was taken directly from data on enteric bacteria, although Segall et al. (1982) have pointed out that the measured value seems large considering the small time necessary to transmit signals across a 1 μm bacterial cell. Segall et al. (1982) speculated that the response latency could be a result of the time-averaging of concentration signals. They also speculated that there may be no adaptive pressure for shorter adaptive times. This is clearly not the case for clustering around point sources. Shorter response latencies improve the ability of the bacteria to stay near the source without compromising its ability to overcome fluid motions, since the effective chemotactic velocity is not related to a characteristic time scale (see Eq. 2.7). There would seem to be a strong selective pressure for marine bacteria to minimize their response latency time. Therefore, the response latencies of marine bacteria may be shorter than those of enteric bacteria.

The analytical results presented can be applied to analyze how differences in bacterial swimming speeds might affect the clustering of bacteria in aquatic environments. Enteric bacteria swimming speeds range from 12–30 $\mu\text{m sec}^{-1}$ (e.g. Berg and Brown 1972, MacNab and Koshland 1972), while marine bacteria swimming speeds range from 30–80 $\mu\text{m sec}^{-1}$ (Azam and Ammerman 1984, Armitage and MacNab 1987). Our results suggest that the higher swimming speeds of marine bacteria may reflect differences in the fluid environment. In the ocean's upper mixed layer convective and wind-induced mixing result in shearing motions of an intensity favoring swimming speeds above that for enterics (Bowen et al. 1989), as revealed by simulations of time-averaged nutrient exposures. The results of this study provide the explanation for this finding; faster swimming speeds provide more effective chemotactic motion enabling chemotactic bacteria to overcome the fluid motions that limit bacterial clustering.

REFERENCES

- Armitage, J.P., and R.M. MacNab. (1987). *Journal of Bacteriology*. 169: 514-518.
- Azam, F., and J.W. Ammerman. (1984). in: M.J.R. Fasham [ed.], "Flows of energy and materials in marine ecosystems," Plenum, pp. 345-360.
- Berg, H.C., and D.A. Brown. (1972). *Nature*. 239: 500-504.
- Bowen, J.D., K.D. Stolzenbach, and S.W. Chisholm. (1989). to be submitted to *Limnology and Oceanography*.
- Brown, D.A., and H.C. Berg. (1974). *Proceedings of the National Academy of Sciences of the U.S.A.* 71: 1388-1392.
- Carslaw, H.S., and J.C. Jaeger. (1959). *Conduction of Heat in Solids*. Oxford University Press.
- Dahlquist, F.W., Lovely, P., and Koshland, D.E. Jr. (1972). *Nature, New Biology*. 236, 120.
- Dahlquist, F.W., Elwell, R.A., and Lovely, P.S. (1976). *Journal of Supramolecular Structure*. 4, 329.
- Keller, E.F., and L.A. Segel. (1971). *J. Theor. Biol.* 30, 225.
- Keller, E.F. (1971). *J Theor. Biol.* 30: 235.
- Jackson, G.A. (1987). *Limnology and Oceanography*. 32: 1253-1266.
- Jackson, G.A. (1989). *Limnology and Oceanography*. 34: 514-530.
- Lapidus, I.R. (1980). *J. Theor. Biol.* 85, 543.
- Lauffenburger, D., R. Aris, and K. Keller. (1982). *Biophysical Journal*. 40, 209.
- Lovely, P.S., and Dahlquist, F.W. (1975). *J. Theor. Biol.* 50, 477.
- MacNab, R.M., and D.E. Koshland Jr. (1972). *Proceedings of the National Academy of Sciences of the U.S.A.* 69: 2509-2512.
- Segall, J.E., M.D. Manson, and H.C. Berg. (1982). *Nature*. 296: 855-857.
- Segall, J.E., S.M. Block, and H.C. Berg. (1986). *Proc. Natl. Acad. Sci. USA*. 83: 8987-8991.

Chapter 5.

Simulating Bacterial Clustering Around Phytoplankton Cells in a Turbulent Ocean

Abstract

Simulations of bacterial chemotaxis towards a phytoplankton cell that is exuding dissolved organic carbon indicate that it is possible for bacteria to attain population densities orders of magnitude above background levels in microzones that occupy less than 0.1 percent of the total fluid volume separating each phytoplankton cell. The degree of clustering was found to vary with the intensity of fluid motions, the bacterial swimming speed and chemotactic sensitivity, and the phytoplankton exudation rate, but it did not depend directly on phytoplankton cell size. The simulation results indicate that at turbulence intensities expected in the upper mixed layer of the oceans (shear rates of approximately 0.15 sec^{-1}) as much as twenty percent of the chemotactic bacteria population could be clustered around exuding phytoplankton cells at any given time, even though individual bacteria stay in a cluster less than a minute. In turbulent shearing, a bacterium's ability to stay near a phytoplankton cell depends on both the random and directed chemotactic components of bacterial motion, such that intermediate bacterial swimming speeds of approximately $40 \mu\text{m sec}^{-1}$ maximize the bacteria population's time-averaged exudate exposure, which could be as much as ten times higher than for a non-chemotactic bacteria population. According to our simulations, unsteady turbulent mixing in the oceanic surface layer should disperse clusters during bursts of mixing, but intervening calm periods are long enough to allow clusters to reform. Bacteria in a cluster could take up as much as seventy percent of the exuded photosynthate if bacterial uptake is assumed to be diffusion limited, but the spatial distribution of bacteria does not significantly affect phytoplankton and bacteria competition for inorganic nutrients.

Introduction

The observation that most marine bacterial isolates are motile (Baumann et al. 1978) has led to speculation regarding the microscale spatial distribution of bacteria and the ecological implications of non-random interactions between phytoplankton and motile bacteria. Upon the discovery that some marine bacteria exhibit chemotactic behavior when exposed to algal exudate, Bell and Mitchell (1972) hypothesized that chemotactic bacteria actively congregate around phytoplankton cells to improve their exposure to the organic carbon exuded by phytoplankton. Chemotactic behavior has been observed repeatedly for marine and freshwater bacteria (Chet and Mitchell 1976, Geesey and Morita 1979, Gallucci and Paerl 1984, Hazen et al. 1984, Azam, personal communication), indicating that some bacteria have the capability of clustering around phytoplankton cells in motionless fluid. Azam and Hodson (1981) observed that glucose uptake by marine bacteria remains unsaturated even when glucose concentrations are orders of magnitude above background levels. This capacity was attributed to a multiphasic uptake system which would be of little value to the bacteria unless higher than ambient concentrations of substrate are actually experienced *in situ*. Furthermore, Azam and Ammerman (1984) showed that the bacterial turnover of dissolved organic carbon excreted by phytoplankton is more rapid than that for organic carbon added to the medium in a dispersed form. This accelerated turnover of phytoplankton exudate was attributed to the clustering of bacteria in microzones where exuded carbon concentrations are significantly above bulk average values, and provides strong, indirect evidence that bacterial clustering can increase the dissolved organic carbon exposure of a chemotactic bacteria population.

The clustering of bacteria may have ecological implications in addition to enhancing the chemotactic bacteria's exudate exposure. Since bacteria and phytoplankton are generally considered to be competitors for inorganic nutrients in

oligotrophic marine systems (Bratbak and Thingstad 1985, Lancelot and Billen 1985, Wheeler and Kirchmann 1986), clustered bacteria may actually depress the growth rate of exuding phytoplankton cells. High bacterial population densities near a phytoplankton may locally reduce nutrient concentrations, and therefore reduce the phytoplankton's uptake of limiting nutrients. This competition for limiting nutrients has been given as evidence that phytoplankton do not exude a significant fraction of their productivity (Jumars et al. 1989), although the function and significance of phytoplankton exudation continues to be an area of active debate (e.g., Bjornsen 1989, Wood and Van Valen 1989, Sharp 1984, Fogg 1983).

Carbon flow through the microbial food web might also be affected by clustering. Clustered bacteria may take up a significant fraction of the carbon exuded by phytoplankton, decreasing the average exudate concentration experienced by non-chemotactic bacteria, and further increasing the competitive advantage to the chemotactic population. While the relative importance of various sources of bacterial secondary production are still a matter of debate, in part because of the recent measurements of elevated dissolved organic concentrations in the ocean (Sugimura and Suzuki 1988), it is generally recognized that the release of DOC from phytoplankton is a major source of bacterial nutrition (Fenchel 1988). Therefore, uptake of exudate by clustered bacteria may be a significant fraction of total bacterial secondary production.

Bacterial clustering may also affect the fate of bacterial production. Water column enclosure experiments indicate that in certain instances a majority of bacterial production is lost to respiration and is not passed to the metazoans (Ducklow et al. 1986), but in general the fate of bacterial production, the "link versus sink" question (Banse 1984), may depend on the fraction of the bacteria population that is in a cluster. Dense clusters of bacteria surrounding a phytoplankton may be grazed with the phytoplankton by metazoans (microbial food

web as a link) while the production of non-clustered bacteria is passed first to microflagellates, then to ciliates, and then finally to metazoans (Williams 1984). In this longer food web much of the original bacterial production is lost to respiration (microbial food web as a sink).

Because of the difficulty in observing bacterial clusters *in situ*, our current understanding of the degree of bacterial clustering in the oceans relies primarily on order of magnitude estimates (Mitchell et al. 1985) and numerical simulations of chemotaxis (Jackson 1987, Jackson 1989). Using estimates of algal exudation rates and bacterial chemotaxis capabilities, and scaling arguments for the effects of turbulent motion on concentration distributions, Mitchell et al. (1985) predicted that clustering is possible only at the thermocline where sinking speeds and turbulence intensities are minimized. According to their scaling arguments, shearing fluid motions in the mixed layer prevent the formation of significant microzones of elevated exudate concentration where bacteria might congregate. They also hypothesized that directed bacterial swimming speeds ($1 - 2 \mu\text{m sec}^{-1}$) are too slow to follow phytoplankton sinking at more than $10 \mu\text{m sec}^{-1}$, thus preventing cluster formation. They did not consider, however, the case in which a bacterium uses directed, chemotactic motion to lengthen its stay near a phytoplankton cell, even though fluid motions from phytoplankton movement or turbulent mixing eventually transport the bacterium to other phytoplankton cells.

Using numerical simulations, Jackson (1987, 1989) predicted the short term (< 100 seconds) response of individual bacteria placed within $100 \mu\text{m}$ of either a motionless or a sinking phytoplankton cell. He found that chemotactic bacterial populations could not swim toward a phytoplankton smaller than approximately $2 \mu\text{m}$ and that increases in bacterial swimming speed above that measured for enteric bacteria ($12 \mu\text{m sec}^{-1}$) did not appreciably improve the approach towards a sinking phytoplankter. Jackson (1989) did find, however, that chemotactic behavior

in marine bacteria could lengthen the cells' exposure to elevated concentrations of phytoplankton exudate, even if their limited swimming speed prevents them from following the sinking phytoplankton cell.

None of the studies discussed above considered the effects of shearing fluid motion expected in the oceanic mixed layer. We expect that shearing motions in the ocean's mixed layer have a profound effect on bacterial clustering by altering both the exudate concentration distribution surrounding a phytoplankter and the motion of chemotactic bacteria relative to the phytoplankton cell. In addition, analyzing the short-term behavior of bacteria does not allow for predictions of the bacteria population density distribution or time-averaged exudate exposure. Assessing the full potential for bacterial clustering to exist in the ocean, and the ecological implications of bacterial clustering requires prediction of these parameters for the fluid motions expected in the mixed layer.

As suggested above, clusters could exist and be important even if a bacterium spends only a few seconds with each phytoplankter before fluid motion and random swimming move it away. Fluid motion associated with turbulent shear or phytoplankton sinking or swimming continually sweeps bacteria past phytoplankton cells where exudate concentrations are highest. Chemotactic bacteria would respond to the concentration gradients with a directed motion that temporarily counteracts the unsteady fluid and random swimming motions moving bacteria away from the phytoplankton. Elevated bacterial densities occur whenever the fraction of time spent by a bacterium in microzones surrounding phytoplankton exceeds the volume fraction of the microzones, regardless of the duration of an individual visit. With this conceptual model of bacterial behavior we can identify three distinct processes that must be quantified to estimate the importance of bacterial clustering: the exudation flux of individual phytoplankton cells, the response of motile marine

bacteria to concentration gradients of phytoplankton exudate, and the effects of fluid motions on the concentration distributions of exudate.

We have used a Monte-Carlo model to simulate bacterial clustering. Phytoplankton exudation rates, bacterial chemotaxis abilities, and fluid motions motion parameters were extracted from the literature and used to establish a matrix of possible conditions in the oceanic mixed layer. Bacterial population density distributions and time-averaged exudate exposures were then estimated by simulating multiple encounters between phytoplankton and bacteria for the shearing fluid motions characterizing the oceanic mixed layer. The model was also used to examine the effects of time-varying shear intensity characteristic of the turbulent ocean. The advantage of chemotactic behavior was examined by comparing time-averaged exudate exposures for chemotactic and non-chemotactic bacteria. Bacterial population density distributions were then used to estimate clustering effects on the exudate spatial distributions, inorganic nutrient flux to phytoplankton, and carbon flow through the microbial food web. The simulation model indicates that although shear mixing and phytoplankton sinking limit the time a bacterium spends near each phytoplankter, chemotaxis in the turbulently mixed upper layer may nonetheless increase the time-average exudate concentration experienced by a bacterium by more than an order of magnitude.

Components of the Model

Phytoplankton Exudation of Organic Carbon - Although considerable effort has been expended to measure phytoplankton exudation of organic carbon (see Fig. 1), only a few measurements include the necessary information to calculate an exudate flux per phytoplankton cell. This parameter together with a description of the fluid motion is necessary to model the exudate concentration distributions surrounding the phytoplankter, which constitutes the chemotactic signal to the bacteria. Measurements of carbon release by phytoplankton *in situ* are often presented only as an exudation rate per unit volume of water or as the percentage of an unspecified carbon fixation rate. Exudation measured on cells from laboratory cultures usually include the necessary cell number information, but the specific activities of added inorganic carbon, which are needed to calculate carbon fixation rates, are rarely reported. Exceptions include Nalewajko et al. (1976) and Blaauboer et al. (1982); they measured exudation rates for freshwater phytoplankton and found them to vary from 10^{-15} g C cell⁻¹ sec⁻¹ for an *in situ* measurement in a eutrophic lake to 10^{-18} g C cell⁻¹ sec⁻¹ for a log-phase population in culture (Table 1).

Measurements of exudation by marine phytoplankton in culture show that a relatively small fraction of fixed carbon is exuded, with most measurements under 15 percent (Fig. 1a). Higher exudate fractions come from stationary phase cells (Mague et al. 1980), cells in the dark (Sharp 1977, Zlotnik and Dubinsky 1989), or cells exposed to varying light intensity (Wood et al. 1989) or extreme temperatures (Zlotnik and Dubinsky 1989). *In situ* measurements, which contain cells of varying light and nutrient histories, are generally higher than culture values and show a broader range. Exudation percentages calculated by averaging the measurements for each location range from 0 to 50 percent, with a majority of the values in the 10 to 30 percent range (Fig. 1b). Exudate flux per cell can be estimated from these values by combining them with estimates of phytoplankton carbon content and

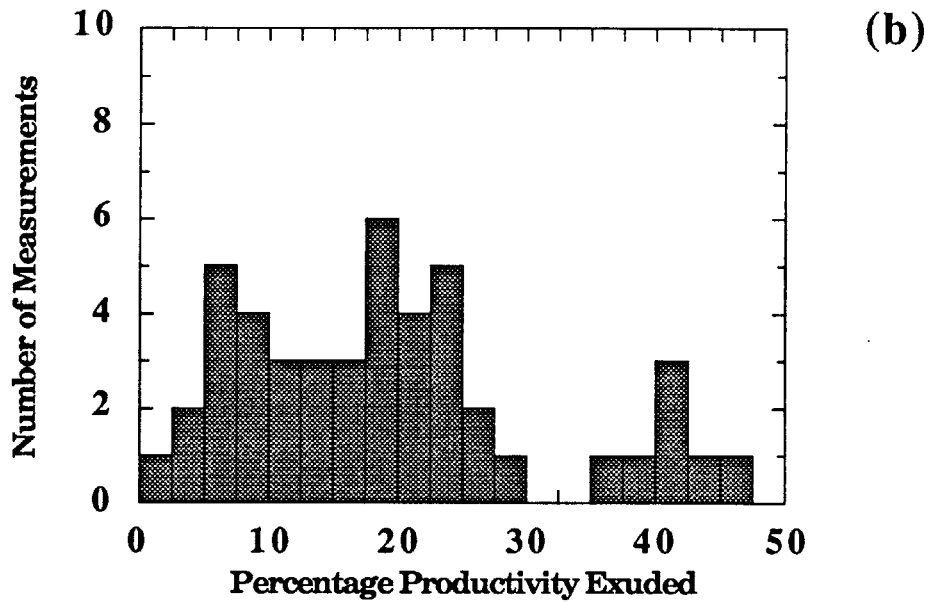
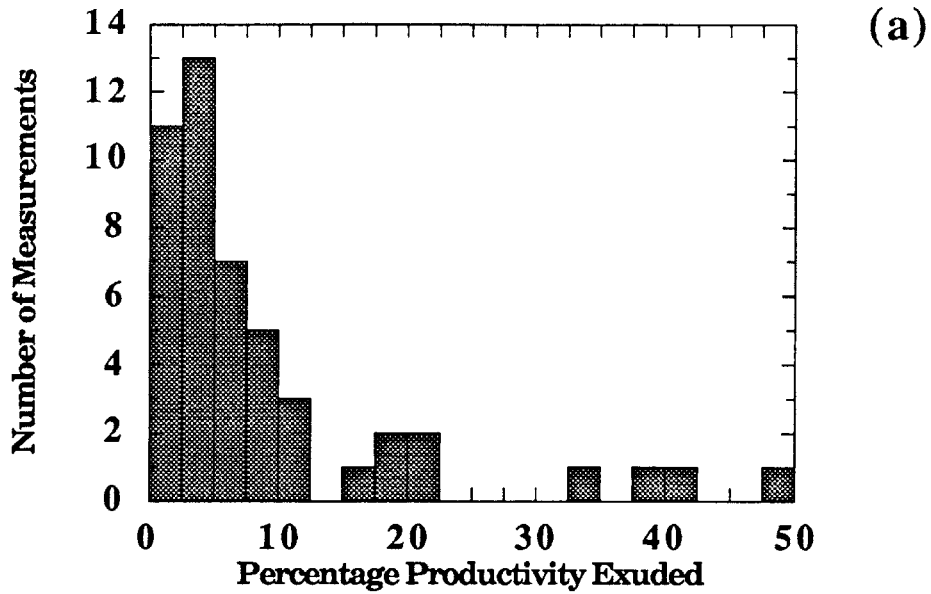


Figure 1. Histograms of the published measurements of exudation by marine phytoplankton. Each data point represents the fraction of primary productivity exuded from: a) a single-species laboratory culture, or b) an *in situ* measurement of marine phytoplankton exudation. For measurements having a range of values, the average of the maximum and minimum exudation percentage is plotted. Measurements taken from: Nalewajko et al. 1976, Sharp 1977, Mague et al. 1980, Blaauboer et al. 1982, Wolter 1982, Fogg 1983, Lancelot and Billen 1985, Sondergaard et al. 1985, Jones and Cannon 1986, Wood et al. 1989, Zlotnik and Dubinsky 1989.

Table 1. Phytoplankton Exudation Measurements

Exudation Rate Measured on a Per Cell Basis				
Species	Conditions ¹	PER ²	Exudation (g C/cell /sec)	Reference
<i>Mallomonas caudata</i>	Fr/IS	50	1.4x10 ⁻¹⁵	Blaauboer et al. 1982
<i>Dinobryon divergens</i>	Fr/IS	20-25	1.9x10 ⁻¹⁵	Blaauboer et al. 1982
<i>Anabaena flos-aquae</i>	Fr/Cu	8.2	1.8x10 ⁻¹⁸	Nalewajko et al. 1976
<i>Chlorella pyrenoidosa</i>	Fr/Cu	3.4	4.1x10 ⁻¹⁸	Nalewajko et al. 1976
Exudation Rate Normalized by Cell Carbon				
Exudation (day ⁻¹)				
microflagellates	Ma/IS	45	0.73	Wolter 1982
nannoflagellates	Ma/IS	40	0.36	Wolter 1982
nannoflagellates yr 2	Ma/IS	10	0.25	Wolter 1982
<i>Chaetoceros sp.</i>	Ma/IS	28	0.60	Wolter 1982
<i>Skeletonema costatum</i>	Ma/IS	10	0.36	Wolter 1982
<i>Detonula sp.</i>	Ma/IS	6	0.10	Wolter 1982

1 Fr -Freshwater, Ma - Marine, Cu - Culture Measurement, IS - *In Situ* Measurement

2 Exudate Release as a Percentage of Primary Production

growth rate. While this method sacrifices the detail of direct measurements of carbon fixation rate, it seems reasonable considering the variability in measurements of the percentage of fixed carbon that is exuded (Fig. 1).

Carbon content per cell was estimated using an allometric relationship between carbon content and cell radius (Mullin 1966),

$$F = \frac{b a_p^{2.28} \mu f}{m} \quad (1)$$

where F is the exudate flux ($\text{mol cell}^{-1} \text{sec}^{-1}$) b is an empirical constant, a_p is the phytoplankton radius, μ is the growth rate, f is the fraction of productivity exuded, and m is the exudate's molecular weight. The product of the growth rate and fraction exuded, μf , can be compared with measurements of exudation rate normalized by cell carbon, which were found to vary between 0.1 and 0.7 day^{-1} (Table 1). For phytoplankton cells ranging from 1-10 μm radius, and specific exudation rates ranging from 0.05 to 0.7 day^{-1} , we estimate the exudate flux per cell to vary from 1.0×10^{-18} to 2.4×10^{-15} $\text{g C cell}^{-1} \text{sec}^{-1}$, values consistent with the few direct measurements (Table 1). Assuming that the exudate is composed of small molecular weight compounds such as glycollate, an assumption that is consistent with HPLC analysis of phytoplankton exudate (Fogg 1983), we estimate that exudate fluxes range from 2.7×10^{-20} to 6.5×10^{-17} $\text{mol cell}^{-1} \text{sec}^{-1}$.

The variability in exudate fraction has received much attention (Sharp 1977, Fogg 1983, Wood et al. 1989) and discussion continues regarding the importance of exudation in the overall nutrition of marine bacterioplankton. While experimental biases have no doubt affected some *in situ* measurements, even recent measurements of exudation, conducted with full knowledge of possible experimental artifacts, show that a significant fraction of primary productivity is lost as dissolved organic carbon

(Wood et al. 1989). As pointed by Jumars et al. (1989), however, many of the *in situ* measurements of exudate release may be due in part to losses through grazing, either by lysis of damaged cells or through incomplete digestion and subsequent loss from sinking fecal pellets. The relative importance of each of these sources of dissolved organic carbon is at present undetermined, and considering procedural difficulties it seems reasonable to simulate a broad range of exudate flux per phytoplankton cell that combines variations in phytoplankton cell size, phytoplankton growth rate, and percent of productivity exuded.

Chemotactic Ability of Marine Bacteria - Detailed descriptions of marine bacterial swimming patterns are not available, but isolates from collections of heterotrophic marine bacteria have morphologies similar to species whose chemotactic behavior has been studied. Chemotactic swimming patterns have been described for the uni-flagellated marine photosynthetic bacteria *Rhodobacter* (Armitage and MacNab 1987) and the peritrichously flagellated enteric bacteria (e.g., MacNab and Koshland 1972, Berg and Brown 1972) and will be used in this study to simulate marine bacteria swimming patterns. Some descriptive information on the morphology of marine bacteria is available. All 788 strains in a culture collection of North Pacific bacteria are motile and most of the isolates are straight rods with with 1-3 polar flagella (Baumann and Baumann 1978). A smaller number of isolates possess peritrichous flagellation. Swimming speeds of chemotactic marine bacteria, both heterotrophic and photosynthetic, have also been measured, and they differ from that of the enteric bacteria. Peritrichously flagellated enteric bacteria swim at speeds ranging from 12 to 30 $\mu\text{m sec}^{-1}$ (MacNab and Koshland 1972, Berg and Brown 1972), while Azam and Ammerman (1984) observed heterotrophic marine bacteria swimming speeds of 20 to 40 $\mu\text{m sec}^{-1}$, and the medially flagellated photosynthetic marine bacteria *Rhodobacter* swims as fast as 80 $\mu\text{m sec}^{-1}$ (MacNab and Armitage 1987). A coastal pseudomonad has been

observed to move upstream against a uniform flow of approximately $100 \mu\text{m sec}^{-1}$ (Walsh and Mitchell 1978), but it is impossible to determine the exact bacterial swimming speed in this case because of possible wall effects and the uncertainty regarding the actual swimming pattern of the bacteria.

Capillary chemotaxis assays have shown that marine bacteria are attracted to a variety of small chain alcohols and sugars (Table 2). The minimum concentration in the capillary eliciting a chemotactic response ranges from 10^{-4} to 10^{-8} M, while the maximum response occurs at millimolar concentrations, as determined by counting the number of bacteria that swim into the capillary after a prescribed time period. Enteric bacteria respond to the same groups of organic compounds (Table 2) and threshold concentrations are also as low as 10^{-8} M. For enteric bacteria, the concentration in the capillary eliciting a maximum response has been shown to be an estimate of the chemoreceptor affinity K_d (Mesibov et al. 1972). Affinities measured this way range from 10^{-2} to 3×10^{-6} M (Table 2). Although the thresholds shown are useful for comparisons between organisms, it is the chemoreceptor affinity that must be quantified to describe chemotactic motion. Measurements from marine bacteria predict affinities in the millimolar range (Table 2), but considering the dilute nature of organic material in the ocean it seems likely that chemoreceptor affinities for marine bacteria are at least as low, and probably lower, than those for enteric bacteria.

Both the peritrichously flagellated bacteria such as *Escherichia coli* (e.g., Berg and Brown 1972) and *Salmonella typhimurium* (e.g., MacNab and Koshland 1972) and the medially flagellated *Rhodobacter* (Armitage and MacNab 1987) swim in a "run and tumble" pattern controlled by the direction of flagellar rotation. Constant velocity runs are interrupted by a tumbling reorientation of the bacteria and directed motion is accomplished by lengthening runs made in favorable directions.

Table 2. Chemoreceptor Affinity Measurements

Organism	Compound	Threshold Conc. (M)	Max.Resp. Conc. (M)	Reference
<i>Escherichia coli</i>	galactose	10^{-8}	3×10^{-6}	Mesibov et al. 1973
	glycero galctoside	4×10^{-7}	10^{-5}	
	fucose	7×10^{-5}	10^{-3}	
	methyl aspartate	3×10^{-7}	10^{-4}	
	methyl aspartate		1.6×10^{-4}	Berg and Tedesco 1975
	amino isobutyrate		3.1×10^{-3}	
	L-leucine		$.98 \times 10^{-2}$	Brown and Berg 1972
	glutamate	10^{-5}	2.3×10^{-3}	
<i>Salmonella typhimurium</i>	serine	10^{-6}	10^{-3}	Dahlquist et al. 1976
coastal pseudomonad	methionine	10^{-7}	10^{-3}	Chet and Mitchell 1976
	leucine	10^{-8}	10^{-2}	
	cysteine	10^{-8}	10^{-2}	
	proline	10^{-7}	10^{-2}	
	glutathione	10^{-6}	10^{-3}	
	glucose	10^{-7}	10^{-3}	
	fructose	10^{-4}	10^{-3}	
	galactose	10^{-6}	10^{-3}	
ribose	10^{-7}	10^{-3}		
<i>Aeromonas hydrophila</i>	amino acids	10^{-3}	10^{-1}	Hazen et al. 1984
	carbohydrates	10^{-4}	10^{-2}	
marine vibrio	L-arginine	10^{-6}	10^{-4}	Geesey and Morita 1979

Brown and Berg (1974) have proposed the following equation to describe the run duration T ,

$$T = T_0 \exp \left[\alpha \frac{K_d}{(K_d + C)^2} \frac{dC}{dt} \right] \quad (2)$$

where T_0 is the average run time when no concentration gradients are present, α is a sensitivity factor, C is the chemoattractant concentration and the overbar indicates an effective temporal averaging. Temporal gradients are sensed by the bacterium by making comparisons of time averaged receptor occupancy (Segall et al. 1986), so that concentration signals are averaged over an adaptation time scale (T_m). The response latency time (T_{min}) is the minimum time required to change direction of flagellar rotation after an abrupt change in attractant concentration. For *E. coli*, T_m has been observed to be approximately 4 seconds and T_{min} approximately 0.2 seconds (Block et al. 1982, Segall et al. 1982). Experiments with enteric bacteria have shown that they can maintain a constant heading for no more than a few seconds because of contact from water molecules, an effect which can be quantified with a Brownian rotation coefficient (Berg 1983).

A parameter relating the exudation flux to the bacteria's chemotactic sensitivity can be derived from the model of bacterial run time regulation (Eq. 2). In motionless fluid the exudate concentration above background, $C(r) - C_\infty$, is given as (Carslaw and Jaeger 1959)

$$C(r) - C_\infty = \frac{F}{4\pi D r} \quad (3)$$

where D is the molecular diffusion coefficient, and r is the distance to the center of the phytoplankton. Since the range of exudate fluxes specified earlier results in

concentrations well below the range of chemoreceptor affinities K_d , we can simplify Eq. 2 as

$$\frac{T}{T_0} = \exp \left[\frac{\alpha}{K_d} \frac{dC}{dr} \frac{dr}{dt} \right] = \exp \left[\frac{\alpha}{K_d} \frac{F}{4\pi D r^2} V \cos \phi \right] \quad (4)$$

where V is the bacterial swimming velocity and ϕ is the angle between the bacterial heading and the direction to the phytoplankton. The concentration gradient term in Eq. 2 is specified by spatially differentiating Eq. 3 and assuming that temporal averaging effects are negligible. By combining each of the parameters in Eq. 4 except for the swimming velocity, which influences run distance independently from the run time, we can define a normalized exudation flux F_* as

$$F_* = \frac{F}{4\pi D K_d} \alpha \quad (\mu\text{m sec}) \quad (5)$$

This single parameter incorporates both the signal strength and the sensitivity of the bacterial response and therefore is useful in quantifying the expected response of the chemotactic bacteria surrounding an exuding phytoplankter. With a chemotactic sensitivity factor $\alpha = 660 \text{ sec}$ (Brown and Berg 1974), the normalized exudation rate is expected to vary from $F_* = 1.4 \times 10^{-3}$ to $1.14 \times 10^3 \mu\text{m sec}$ for the range of exudation fluxes and chemoreceptor affinities specified earlier.

Since the range of normalized exudation rates is based on chemotactic abilities of enteric bacteria and the exudate fluxes from a limited range of phytoplankton cell sizes, it is useful to consider how this estimate might vary for different sized phytoplankton and motile bacteria. Assuming that selective pressures have optimized bacterial chemotactic sensitivities, then the sensitivity parameter α should scale with the diffusion limited chemoattractant uptake rate, which means that it varies linearly with the bacteria cell radius. Since marine bacteria are

typically smaller than enteric bacteria (Bratbak 1985), the value of α used is probably an upper limit and may be too high for marine bacteria. However, the range of chemoreceptor affinities used ($K_d = 10^{-4} - 3 \times 10^{-6}$ M), also taken from enteric bacteria measurements, may underestimate the affinities of marine bacteria. As an estimate of the maximum chemoreceptor affinity we examine the range of bacterial uptake affinities and thresholds for chemotaxis by open-ocean cyanobacteria.

Uptake affinities for cyclic AMP are as low as 10^{-12} M (Ammerman and Azam 1982) and Willey (1988) has measured threshold concentrations for a cyanobacterium's chemotaxis towards nitrogen compounds as low as 10^{-10} M. As pointed out by Jackson (1987), however, chemotactic behavior will begin to be limited when the background concentration of chemoattractant approaches the chemoreceptor affinity. With background concentrations of low molecular weight sugars and amino acids of one to one hundred nM (Mopper and Lindroth 1982, Billen et al. 1980) we expect the minimum chemoreceptor affinity to be in the range of 10^{-8} to 10^{-8} M. By combining these estimates we see that an upper bound for normalized exudation for the phytoplankton cell sizes considered (1-10 μm) is no more than ten times the maximum value given earlier. Higher normalized exudation rates might be found for larger phytoplankton cells (Eq. 1) if the growth rate and fraction of productivity exuded were comparable to those used to estimate exudate flux (Eq. 1). However, considering the uncertainty associated with each parameter value it seems reasonable to use the previously calculated maximum exudation $F_* = 1140 \mu\text{m sec}$ as our limiting value.

The Effects of Fluid Motion - The microscale fluid motions experienced by a phytoplankter distort exudate concentration distributions by augmenting diffusive transport of exudate in the directions where fluid moves away from the phytoplankton. Irrotational shearing motion moves fluid towards the

phytoplankton along one or two principal axes of shear and away from the fluid along the other axes (Fig. 2). A characteristic shear strength E_b can be defined as $E_b = 0.5 \Sigma |E_i|$ where E_i is the velocity gradient along the i th principal axis. In a turbulent fluid the characteristic shear strength is related to the rate at which the fluid's viscosity dissipates mixing energy according to $E_{b_{avg}} \simeq 0.5 (\epsilon/\nu)^{\frac{1}{2}} \text{ sec}^{-1}$, where $E_{b_{avg}}$ is the time averaged shear strength, ϵ is the viscous dissipation rate, and ν is the fluid's kinematic viscosity. Oceanographic measurements of viscous dissipation rate vary with depth and meteorological forcing, ranging from $\epsilon = 10^{-2} \text{ cm}^2\text{sec}^{-3}$ near the surface under strong forcing to $\epsilon = 10^{-6} \text{ cm}^2\text{sec}^{-3}$ at the thermocline, or where shallow, temporary thermoclines limit vertical transport of mixing energy (Denmann and Gargett 1988). Many of the measurements of dissipation in the mixed layer for wind or convective mixing are near $10^{-3} \text{ cm}^2 \text{ sec}^{-3}$ (Shay and Gregg 1986, Osborn and Lueck 1985a, 1985b), a value that we will use to indicate "typical" conditions in the mixed layer. This dissipation rate corresponds to an average shear strength of $E_{b_{avg}} = 0.15 \text{ sec}^{-1}$.

The relative motion around a phytoplankton may also include rotational and uniform flow components. Rotation changes the position of fluid elements relative to the shear axes but does not move elements to or from the phytoplankton. Uniform flow around the phytoplankton results when the cell sinks or swims through the fluid. Sinking speeds of unicellular marine phytoplankton generally increase with cell size, although diatoms are known to regulate their density (Gross 1948) and reduced sinking speeds have been observed at the thermocline (Bienfang 1985). A "typical" sinking speed for a diatom with a radius of $10 \mu\text{m}$ is approximately $5 - 20 \mu\text{m sec}^{-1}$ (Smayda 1970, Bienfang 1980). This value is also a reasonable estimate for swimming speeds of phytoplankton in the size range simulated ($1-10 \mu\text{m}$).

Exudate concentration distributions surrounding phytoplankton cells neither sinking nor swimming have two distinctive shapes depending on the pattern of the

shearing and the orientation and strength of rotation (Fig. 2) (Bowen and Stolzenbach 1989). In a central core of size $l_s = (D/E_b)^{1/2}$ concentration distributions follow the solution for motionless diffusion (Eq. 3). The size of the diffusive core varies from 30 μm for the strongest shear rates in the upper mixed layer ($E_b = 1.0 \text{ sec}^{-1}$) to 300 μm at the thermocline ($E_b = 0.01 \text{ sec}^{-1}$), thus the phytoplankton cell is contained within the purely diffusive region. The concentration distribution near the cell will be given by the motionless solution (Eq. 3). Beyond the diffusive core the concentration distributions are stretched along the axes where fluid moves away from the phytoplankton (Bowen and Stolzenbach 1989), resulting in distinctive tube and disk shaped concentration distributions (Fig. 2).

Rotation modifies the distributions by reducing asymmetry in the plane perpendicular to the rotation axes. Strongly rotational flows have axisymmetric concentration distributions around the rotation axis (Batchelor 1979). Weak rotation does not change the shape of concentration contours but reorients the concentration contours away from the principal axes of shear (Bowen and Stolzenbach 1989). Regardless of the relative magnitudes of shear and rotation, however, exudate distributions surrounding phytoplankton in the oceanic mixed layer have distinctive tube and disk like shapes.

Exudate concentration distributions for a sinking or swimming phytoplankton have a character qualitatively similar to those resulting from shear flow (see Fig. 1, Jackson 1989). Within a region of size $l_a = D/w_s$ where w_s is the phytoplankton velocity, contours are undistorted by the fluid motion and are spherical. For a phytoplankter moving at 10 $\mu\text{m sec}^{-1}$ the region undistorted by fluid motions is approximately 100 μm . Beyond this region fluid motions distort concentration contours so that the long axis of the contours is aligned with the direction where

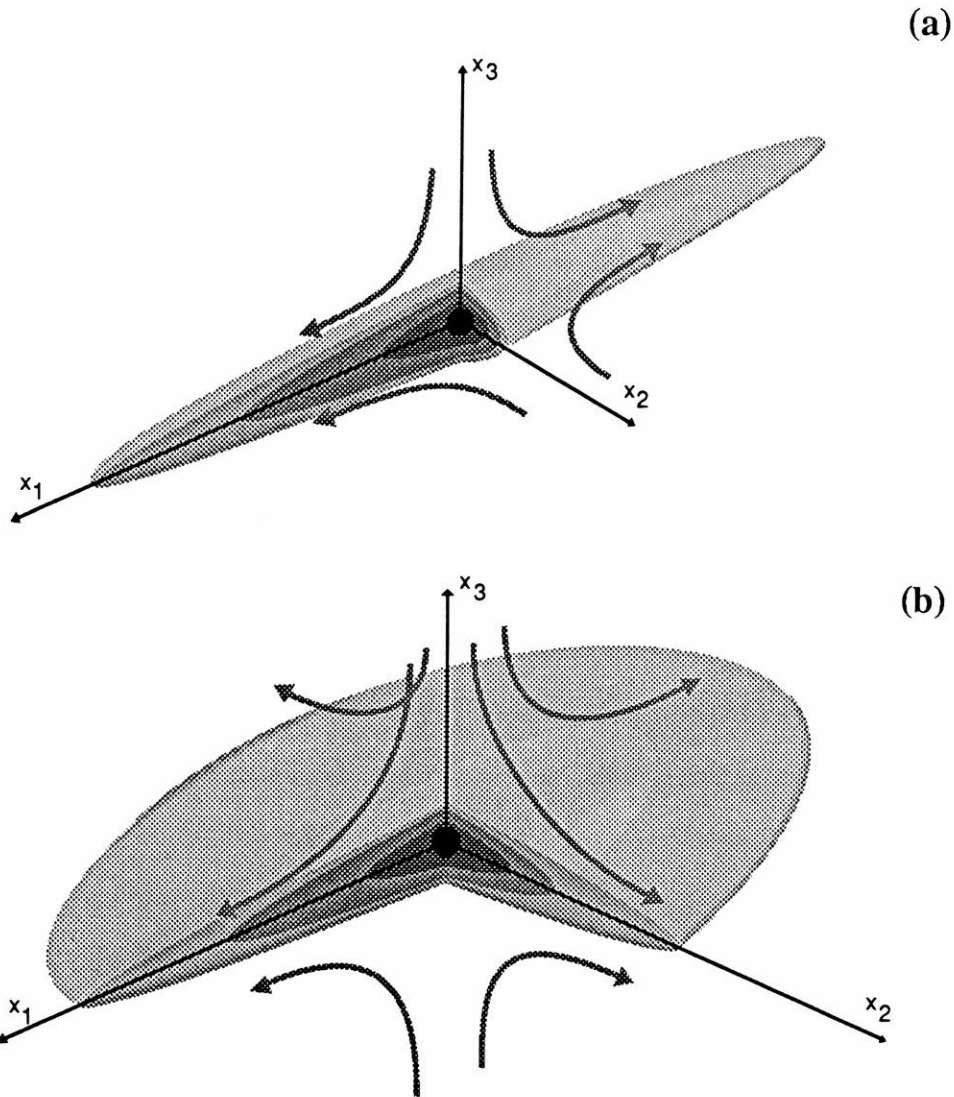


Figure 2. The fluid motion and concentration distributions surrounding a phytoplankton in a sheared fluid. The dark sphere at the origin has a radius of $(D/E_b)^{1/2}$ that indicates the size of the region unaffected by fluid motion. The lighter shading shows contours distorted by the shearing flow. The arrows indicate the direction of fluid motion relative to the cell.

(a) Tube: Fluid moves away from the cell along the x_1 axis and towards the cell along the x_2 and x_3 axes.

(b) Disk: Fluid moves away from the phytoplankton along the x_1 and x_2 axes and towards it along the x_3 axis.

fluid moves away from the source. Equations describing the distribution in this region were given by Brenner (1963) and Acrivos and Taylor (1962) and later used by Jackson (1989) to simulate the attraction of bacteria to falling phytoplankton.

An analysis of the effects of fluid motion must also account for the time varying nature of turbulent shearing. Multiple measurements of energy dissipation rates at a single location show a log-normal distribution with a high degree of unsteadiness (Baker and Gibson 1987), thus phytoplankton in the mixed layer experience long periods of relative calm punctuated by bursts of intense shearing motion. Because of the skewness of the distribution towards high values, the most frequently occurring dissipation rate may be an order of magnitude below the mean level (Baker and Gibson 1987). The size and orientation of the shear distorted concentration contours change with each new shear rate. The establishment time for concentration distributions is on the order of E_b^{-1} , so adjustment to a new shear pattern and intensity occurs within seconds for expected shear rates in the mixed layer. It has been hypothesized that each shear rate lasts for a time corresponding to the large scale motions (Lumley 1972, Corrsin 1963), which are significantly longer than E_b^{-1} for motion in the upper mixed layer, although this question is still a matter of debate (Monin and Yaglom 1975). Using this hypothesis regarding shear rate duration, we expect that concentration contours around an exuding phytoplankton in a turbulent ocean remain steady in size and orientation for a few minutes.

Simulation Model

Bacterial population densities surrounding the phytoplankton were calculated by simulating bacterial motion around a single phytoplankter and assuming that this represents the average conditions around other phytoplankton cells. The radius of the simulated region r_s was related to the phytoplankton density by $r_s = 3/(4\pi n_{tp})^{-1/3}$, where n_{tp} is the bulk average phytoplankton population density. The number of bacteria in the simulation was n_{tb}/n_{tp} , where n_{tb} is the bulk average bacterial population density. The values of n_{tb} and n_{tp} for our simulation (see Table 3) correspond to a simulation region of 620 μm radius that contains 1 phytoplankter and 1000 bacteria. These bulk average population densities of phytoplankton and bacteria represent "typical" values in the oceanic mixed layer (Beers et al. 1977, Fuhrman et al. 1980). Bacterial movement around a 10 μm radius phytoplankton was simulated, but since the phytoplankton could be considered to be a point source of exudate, the resulting concentration distribution depended only on the fluid motion and the exudate flux per phytoplankter, F . The relevance of phytoplankton cell size to the clustering of bacteria will be discussed in more detail in the results section.

The model was used to simulate the time history of a constant number of bacteria as they swim or are transported to the neighborhood of many phytoplankton cells. Bacterial cells transported out of the simulation region by fluid motion or swimming were randomly placed back on the region's boundary. A test procedure was used to check to see if fluid or swimming motion would bring the cell back into the region in the following time step. If not, then another random location on the boundary was selected and the test procedure repeated. In this way fluid and random swimming motions can move bacteria to and from the phytoplankton while the time history of a constant number of bacteria is being followed for long time periods. Each bacterium moved independently of the other bacteria and bacteria

Table 3. Model Parameters

Parameter	Symbol	Range of Values Used
exudation parameters		
exudate fraction	f	0.1 - 0.5
phytoplankton cell radius	a_p	1-10 μm
phytoplankton growth rate	μ	0.25 - 0.7 day^{-1}
cell carbon allometric constant	b	$1.52 \times 10^{-12} \text{ g C } \mu\text{m}^{-2.28}$
# carbon atoms in exudate molecule	n	3
molecular diffusion coefficient	D	$1000 \mu\text{m}^2 \text{ sec}^{-1}$
exudation rate	F	$1.0 \times 10^{-18} - 2.4 \times 10^{-15} \text{ g C cell}^{-1} \text{ sec}^{-1}$
Normalized Exudation Rate	F^*	$1.4 \times 10^{-3} - 1140 \mu\text{m sec}$
chemotaxis parameters		
bacterial swimming speed	V	$12.3 - 80 \mu\text{m sec}^{-1}$
chemoreceptor affinity	K_d	$3 \times 10^{-6} - 1.0 \times 10^{-4} \text{ mol liter}^{-1}$
average run time	T_o	1.0 sec
adaptation time scale	T_m	0.6 sec
response latency time	T_{min}	0.2 sec
rotational diffusion coefficient	D_r	$0.062 \text{ rad}^2 \text{ sec}^{-1}$
chemotaxis sensitivity factor	α	660 sec
fluid motion parameters		
viscous dissipation rate	ϵ	$10^{-2} - 10^{-6} \text{ cm}^2 \text{ sec}^{-3}$
characteristic shear rate	E_b	$0.0 - 0.30 \text{ sec}^{-1}$
sinking or swimming speed	w_s	$5 - 20 \mu\text{m sec}^{-1}$
other simulation parameters		
phytoplankton population density	n_{tp}	$1000 \text{ cells ml}^{-1}$
bacteria population density	n_{tb}	$10^6 \text{ cells ml}^{-1}$
radius of simulation region	r_s	$620 \mu\text{m}$

striking the phytoplankton cell in the simulations were reflected back into the fluid, thus adhesion to the phytoplankton surface was not modelled. The position, heading, and current and cumulative exudate concentration exposure of each bacterium was monitored with each time step of the model. For the steady shearing cases, bacterial population density distributions were calculated by averaging the instantaneous distributions over a time period long enough to filter out the randomness inherent in the stochastic description of bacterial behavior. The averaging of population densities began once the population average distance from the phytoplankton reached a steady value. Non-chemotactic control cases were simulated by setting the chemotactic sensitivity factor α to zero (see Eq. 2).

Exudate concentration distributions were simulated using approximate analytical solutions for the advection dominated region ($r > l_s$) (Bowen and Stolzenbach 1989) with a central diffusive core ($r < l_s$) (Eq. 3). A weighting function matched these two distributions in the region where transport was affected by both advection and diffusion. Concentration distributions for the sinking case used analytical solutions for uniform flow (Acrivos and Taylor 1962) in the same manner as Jackson (1989). The model assumed that bacterial uptake did not significantly affect the exudate concentration distribution, an assumption that will be examined in the results section. As a result of neglecting bacterial uptake, however, the bulk-average exudate concentration was found to decrease with increasing levels of fluid motion. To eliminate this bias when calculating time-averaged exudate exposures, the background concentration for each level of fluid motion was adjusted to give a bulk-average concentration equal to the motionless case. The magnitude of this adjustment was never more than 2.3 percent of the concentration at the phytoplankton cell surface and had no effect on the simulated bacterial population densities.

Bacterial swimming was simulated using the original Brown and Berg model (1974) modified to account for the response latency (Block et al. 1982) and temporal

averaging characteristics (Segall et al. 1986) quantified by more recent studies of bacterial chemotactic behavior. Unlike the original Brown and Berg (1974) model, where the temporal gradient of receptor occupancy is calculated and then temporally smoothed, the model simulates the sensing of temporal gradients by comparing instantaneous and time averaged receptor occupancy. The model uses a single averaging time, T_m , as in earlier simulations (Jackson 1987, 1989), foregoing the complexity of multiple time constants which have been used to describe bacterial processing of concentration signals (Segall et al. 1986). The averaging time used (Table 3) represents the minimum time necessary to average out random fluctuations in exudate concentrations in order to determine temporal gradients (Jackson 1987). The probability that a run ends during a given time step is linearly related to the calculated run time (Eq. 2), which is restricted to be no less than the response latency time T_{min} . Tumbles were considered to be instantaneous, and new headings were chosen randomly, since chemotactic behavior has been shown to be insensitive to turn angle distributions (Jackson 1987). The Brownian rotation rate was taken from the measured value for *E. coli* (Berg 1983), since no measurements are available for marine bacteria. Although the value for marine bacteria may be higher since their cell sizes are generally smaller than enteric bacteria (Bratbak 1985), it is not known how the presence of bacterial flagella affects Brownian rotation, so the use of the measured values for enteric bacteria seems reasonable.

The range of conditions in the mixed layer was simulated by varying three key parameters: the bacterial swimming speed V , the strength of fluid motions from phytoplankton movement, w_s , or fluid shearing, E_b , and the normalized exudation rate F_* (Eq. 5). Each of the parameters was varied according to the ranges established in the literature. A variety of shear patterns were simulated initially and the results were found to be insensitive to these changes (data not shown), so all subsequent simulations used a shear pattern giving axisymmetric tubes. Our

simulations dealt mainly with the effect of shear rather than uniform motion because the latter has been dealt with extensively by Jackson (1989).

To facilitate comparisons of time-averaged exudate exposures, the normalized exudation, F_* , was varied by fixing the phytoplankton exudation rate and adjusting the chemoreceptor affinity K_d . The exudate concentration at the phytoplankton surface ($r = 10 \mu\text{m}$) was fixed at $5.2 \times 10^{-7} \text{ M}$ and the chemoreceptor affinity varied from a minimum of $3 \times 10^{-6} \text{ M}$, giving the maximum normalized exudation rate, $F_* = 1140 \mu\text{m sec}$. From this maximum the normalized flux was reduced by increasing the chemoreceptor affinity until the fraction clustered approached zero and the cumulative exudate exposure approached the non-chemotactic control. The minimum F_* simulated ($100 \mu\text{m sec}$) was therefore larger than the minimum possible considering the full range of exudation rates and chemoreceptor affinities.

In addition to the simulations of steady fluid motion, a number of simulations were run with a shear rate that varied in time. The time averaged shear rate ($E_{b_{\text{avg}}} = .15 \text{ sec}^{-1}$) and the variance around the average ($\sigma^2 = 1.5$) were taken from measurements of the turbulent motions due to convective or wind induced shearing in the oceanic mixed layer (Osborn and Lueck 1985a, Shay and Gregg 1986). Individual shear intensities were randomly selected from a log-normal distribution, in keeping with measurements of energy dissipation in the oceanic mixed layer (e.g., Baker and Gibson 1987). Orientation of the principal axes of shear changed randomly with each new shear rate, which remained steady for a time equivalent to $5 E_b^{-1}$, a duration consistent with theory (Lumley 1972). For each bacterial swimming speed, initial bacterial density distributions were taken from the steady shearing cases and simulations were run long enough to give many bursts of mixing with intervening periods of relative calm fluid motion.

Results and Discussion

General Characteristics of Bacterial Clusters - The simulation of bacterial chemotactic motion in steady shearing revealed a characteristic bacteria population density distribution surrounding the phytoplankton. Population densities were highest near the phytoplankton, but decreased rapidly with increasing distance (Fig. 3). The density decrease varied with swimming speed over the range of shear strengths and exudation rates, so that for weak fluid motion ($E_b = 0.05 \text{ sec}^{-1}$) and high normalized exudation rates ($F_* = 1140 \mu\text{m sec}$) (Fig. 3a), the maximum population density was highest for the slowest bacteria swimming speed ($V = 12 \mu\text{m sec}^{-1}$). At the maximum cell density ($\approx 10^{10} \text{ cells ml}^{-1}$) bacteria were separated by approximately $5 \mu\text{m}$, a large distance relative to bacteria cell radii of 0.2 to $0.6 \mu\text{m}$ (Bratbak 1985). The distance at which bacterial densities approached background levels increased with weaker fluid motions (Fig. 3a, 3b) or stronger exudation rates (Fig. 3c), but in all cases was less than $300 \mu\text{m}$, so bacterial clusters never occupied more than 10 per cent of the simulation region ($r_s = 620 \mu\text{m}$). Motile bacteria achieved high population densities with frequent, brief visits to a cluster since for all swimming speeds and exudation rates a bacteria's average duration in a cluster was less than one minute when shearing fluid motions were present.

Simulated distributions of bacterial population densities have a characteristic form described by the following equation (Fig. 4)

$$n(r) = n_b + n_p \exp\left(-\frac{r-a_p}{l}\right) \quad (6)$$

where n_b is the background population density, n_p is the maximum density which occurs at the phytoplankton cell surface ($r = a_p$), and l is an inner length scale describing the variation in density near the phytoplankter. Bowen et al. (1989) have shown that a bacterial density distribution as described by Eq. 6 results when

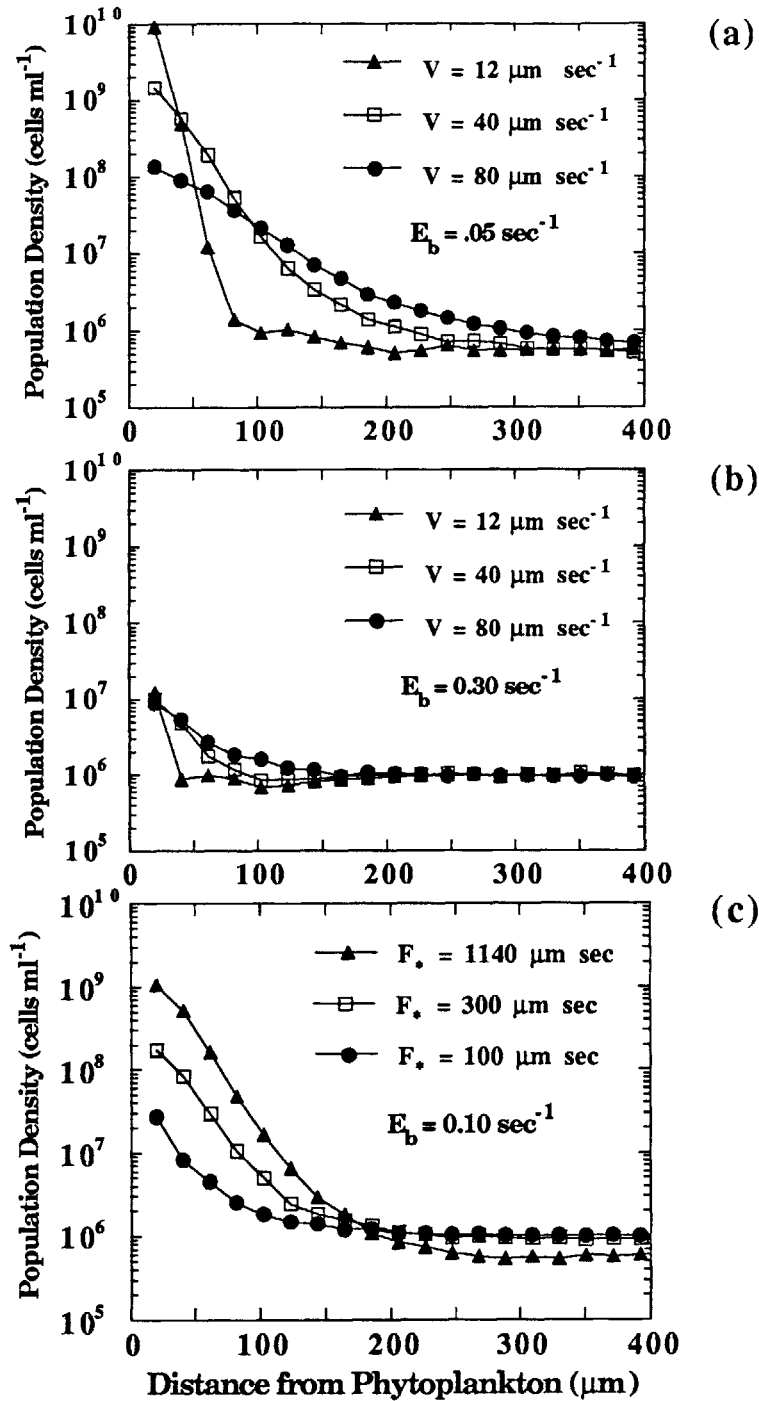


Figure 3. Simulated bacterial population densities versus the distance from the center of the phytoplankton cell.

- (a) Weak shearing motion ($E_b = 0.05 \text{ sec}^{-1}$), at the maximum normalized exudation rate ($F_* = 1140 \text{ } \mu\text{m sec}$), for a range of swimming speeds.
- (b) Strong shearing motion ($E_b = 0.30 \text{ sec}^{-1}$), at the minimum normalized exudation rate ($F_* = 100 \text{ } \mu\text{m sec}$), for a range of swimming speeds.
- (c) Intermediate shear strength ($E_b = 0.10 \text{ sec}^{-1}$), for a single swimming speed ($V = 40 \text{ } \mu\text{m sec}^{-1}$), over a range of normalized exudation rates.

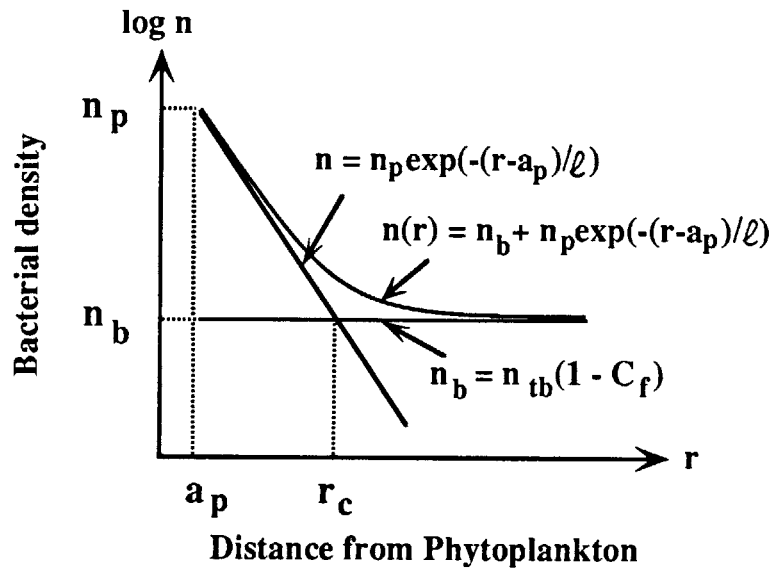


Figure 4. Parameterized bacterial population density distribution surrounding a phytoplankton cell (log of population density vs. distance from cell center). Near the phytoplankton the population density decreases exponentially with a peak density n_p at the phytoplankton surface. Far from the phytoplankton the population density approaches a uniform background level n_b . The sum of these two limiting distributions defines the population density $n(r)$.

the bacterial motion near the phytoplankton is the sum of a saturated chemotactic response and a random component of bacterial motion. For each simulation the inner length scale l and peak density n_p was determined from a linear regression of the logarithm of bacterial density versus distance for the distribution near the phytoplankton. The background density n_b was calculated by counting the cells beyond a distance of $350 \mu\text{m}$ from the phytoplankton and dividing by the volume of this region. For all simulations it was found that population densities were constant in this region except for random fluctuations. The fraction of the bacteria population in a cluster, C_f , was calculated from the bacterial densities according to $C_f = 1 - n_b/n_{tb}$.

Fraction of Population in a Bacterial Cluster for Steady Shearing - Addressing the effects of bacterial clustering on carbon flow through the microbial food web raises the following question: What percentage of the chemotactic population could realistically be clustered around the phytoplankton at any given time and what are the critical parameters that determine this percentage? If this percentage is large the phytoplankton grazers may also be important grazers of bacteria. For motionless fluid at the highest exudation rate ($F_* = 1140 \mu\text{m sec}$) 70–90 per cent of the bacterial cells are clustered, with the highest fraction at the slower swimming speeds (Table 4). Reducing the normalized exudation flux by a factor of ten, ($F_* = 100 \mu\text{m sec}$), reduces the fraction clustered to approximately 5 per cent for the entire range of swimming speeds simulated (Table 4).

Once fluid motions begin to reduce the fraction clustered, faster swimming speeds result in higher clustered fractions (Table 4). At the slowest bacterial swimming speed ($V = 12 \mu\text{m sec}^{-1}$) the fraction clustered is less than 5 per cent for shear strengths expected in the mixed layer ($E_b > 0.1 \text{ sec}^{-1}$) whereas the fastest swimming speed ($V = 80 \mu\text{m sec}^{-1}$) has at least 5 percent clustered up to the highest level of shear simulated ($E_b = 0.3 \text{ sec}^{-1}$) (Table 4). The fraction clustered is above

Table 4. Fraction of Bacterial Population Clustered

Bacterial Swimming Speed, V ($\mu\text{m sec}^{-1}$)	Normalized Exudation Rate, F^* ($\mu\text{m sec}$)	Shear Strength E_B (sec^{-1})						Phytoplankton Velocity, w_s ($\mu\text{m sec}^{-1}$)		
		0.00	0.05	0.10	0.15	0.20	0.30	5.0	10.0	20.0
12.3	1140	0.95	0.82	0.23	0.05	0.01	0.00	0.72	0.02	0.01
	570	0.61	0.40	0.12	0.02	0.01	0.00			
	300	0.10	0.08	0.03	0.01	0.00	0.00			
	200	0.05	0.02	0.01	0.01	0.00	0.00			
	100	0.04	0.01	0.01	0.01	0.00	0.00			
40.0	1140	0.95	0.84	0.42	0.16	0.07	0.02	0.86	0.37	0.05
	570	0.61	0.49	0.20	0.13	0.05	0.01			
	300	0.19	0.14	0.09	0.03	0.02	0.01			
	200	0.05	0.05	0.02	0.02	0.01	0.00			
	100	0.03	0.02	0.02	0.01	0.00	0.00			
80.0	1140	0.83	0.46	0.35	0.20	0.12	0.05	0.68	0.41	0.10
	570	0.34	0.34	0.18	0.10	0.06	0.02			
	300	0.10	0.10	0.06	0.05	0.03	0.01			
	200	0.05	0.06	0.04	0.03	0.02	0.00			
	100	0.03	0.04	0.02	0.01	0.00	0.00			

20 percent only for relatively weak shear strengths ($E_b \leq 0.10 \text{ sec}^{-1}$), which occur only under relatively calm conditions or near the thermocline. For shear strengths more typical of the oceanic surface layers ($E_b > 0.15 \text{ sec}^{-1}$) only a small percentage of the chemotactic bacteria are in a cluster at any given time, even though population densities are orders of magnitude above background levels. Even if all clustered bacteria are grazed with the phytoplankton, the fraction clustered is under most circumstances too low to represent a significant source of reduced carbon to grazers.

Enhancement of Exudate Exposure in Steady Shearing - How much of an advantage in time-averaged exudate exposure does a population of chemotactic bacteria receive by clustering, as compared to a non-chemotactic bacteria population? The exudate exposure enhancement factor is defined as the time-averaged exudate exposure of a chemotactic bacteria population divided by the corresponding value for a non-chemotactic population. The modelling results showed significant enhancement factors for nearly the entire range of simulated shear strengths (Table 5). Enhancement factors were highest for conditions maximizing the peak bacterial density n_p , i.e., weak shearing motions, high exudation rates, and slow swimming speeds (Table 5). Chemotactic behavior may increase average exudate exposure of the bacteria population by more than a factor of 25 for these conditions.

At higher levels of fluid motion, where faster swimming is needed to overcome fluid motion, the intermediate swimming speed ($V = 40 \mu\text{m sec}^{-1}$) gave the highest enhancement of exudate exposure. Chemotactic motion continued to enhance exposure by a factor of 30 percent up to the highest shear strength simulated ($E_b = 0.3 \text{ sec}^{-1}$) for the intermediate swimming speed (Table 5). For bacteria swimming in a run and tumble pattern, swimming provided both effective chemotactic motion and random diffusive-like motion. Both these motion

Table 5. Exudate Exposure Enhancement Factors

Bacterial Swimming Speed, V ($\mu\text{m sec}^{-1}$)	Normalized Exudation Rate, F* ($\mu\text{m sec}$)	Shear Strength E_b (sec^{-1})						Phytoplankton Velocity, w_s ($\mu\text{m sec}^{-1}$)		
		0.00	0.05	0.10	0.15	0.20	0.30	5.0	10.0	20.0
12.3	1140	25	22	6.6	1.9	1.3	1.1	17	1.3	1.0
	570	15	11	3.6	1.4	1.1	1.0			
	300	2.5	2.3	1.6	1.2	1.1	1.0			
	200	1.8	1.3	1.2	1.1	1.0	1.0			
	100	1.4	1.2	1.1	1.0	1.0	1.0			
40.0	1140	11	10	5.0	2.5	1.7	1.3	8.6	3.6	1.2
	570	6.2	5.6	2.8	2.1	1.5	1.1			
	300	2.1	2.0	1.7	1.3	1.2	1.1			
	200	1.3	1.3	1.2	1.1	1.1	1.1			
	100	1.1	1.1	1.1	1.1	1.1	1.0			
80.0	1140	4.8	3.2	2.5	1.9	1.6	1.2	3.7	2.5	1.4
	570	2.3	2.4	1.8	1.4	1.3	1.1			
	300	1.3	1.4	1.3	1.2	1.2	1.1			
	200	1.2	1.2	1.2	1.1	1.1	1.1			
	100	1.1	1.1	1.1	1.1	1.0	1.0			

components increase with faster swimming speeds. The intermediate swimming of $40 \mu\text{m sec}^{-1}$ seemed to provide sufficient directed chemotactic motion to overcome shearing motions while minimizing random motions that limited the ability of the bacteria to stay near the phytoplankton cell. At the intermediate swimming speed, exudate exposures of chemotactic bacteria were doubled (Table 5) at conditions where the fraction clustered was only 13 percent (Table 4).

Simulations of Clusters in Unsteady Shearing - The implications of unsteady shearing were investigated by simulating the time series of shear intensities expected in a turbulent surface layer. The simulated shear pattern for the upper mixed layer had several intervals of a few minutes each with $E_b < 0.05 \text{ sec}^{-1}$, a larger number of intervals with $E_b \approx 0.10 \text{ sec}^{-1}$, and occasional short-lived bursts of strong shear ($E_b > 0.3 \text{ sec}^{-1}$) (Fig. 5). As a surrogate for a time-averaged fraction clustered, which assumes steady density distributions, the fraction of the population within $133 \mu\text{m}$ of the phytoplankton was determined for each time. This region represents 1 percent of the fluid volume and is used as a rough estimate of the size of bacterial clusters.

According to our simulations intense bursts of mixing dispersed clusters for swimming speeds of $V = 12 \mu\text{m sec}^{-1}$ and $V = 40 \mu\text{m sec}^{-1}$ but the response to the subsequent calm periods differed between the two swimming speeds. The high shear rates sweep nearly all clustered bacteria away from the phytoplankton during a burst, decreasing the fraction clustered to less than 5 percent (Fig. 5). In subsequent calm periods the clustered fraction increased more rapidly for the faster swimming speed. During the long simulated calm period with $E_b \approx 0.05 \text{ sec}^{-1}$, the fraction clustered for $V = 40 \mu\text{m sec}^{-1}$ approached the 49 percent clustered expected for steady shearing (Table 4), but for $V = 12 \mu\text{m sec}^{-1}$ the fraction clustered increased to only 10 percent (Fig. 5), far from the steady shear value of 40 percent (Table 4). The fraction clustered during these calm periods, however, is several

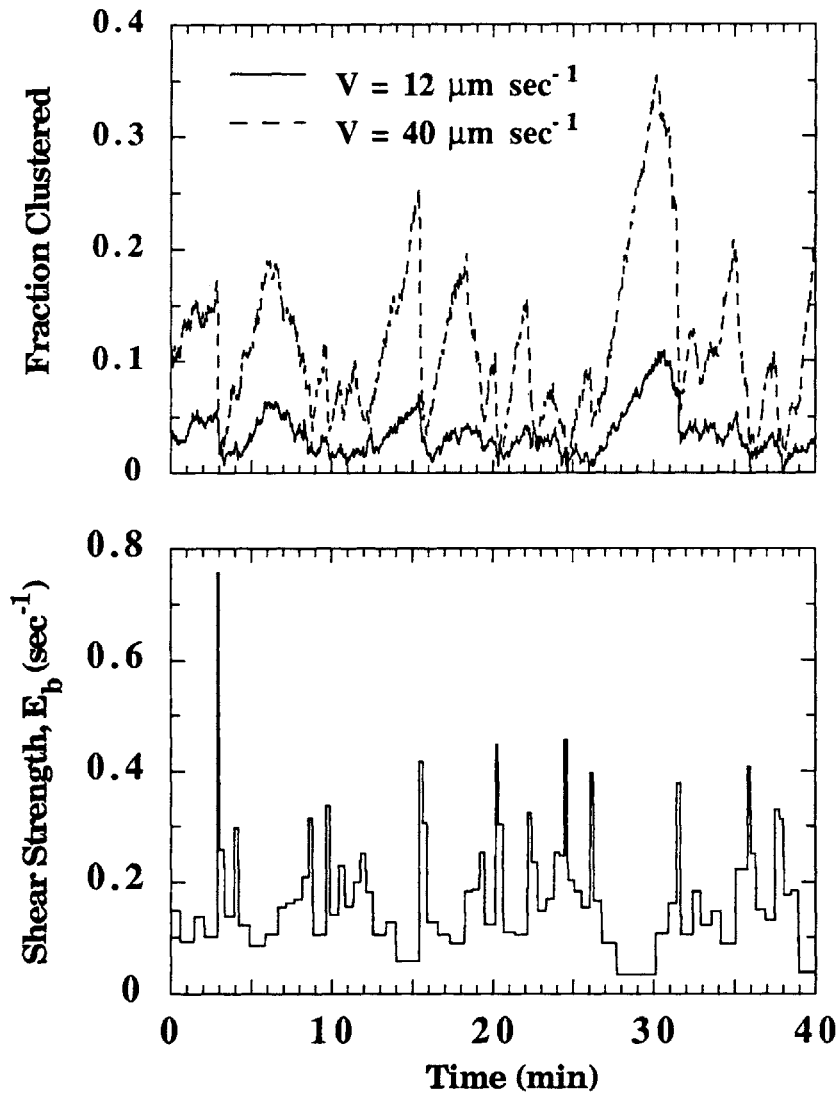


Figure 5. Simulation of time varying shear and the resulting clustering of the motile bacteria population. The shear rate E_b has a log-normal distribution with an average value $E_{b_{avg}} = 0.15 \text{ sec}^{-1}$. Each shear value lasts a time equal to $5 E_b^{-1}$. The ordinate shows the fraction of the bacteria population within $133 \mu\text{m}$ of the exuding phytoplankton, a region occupying 1% of the total fluid volume. Normalized flux $F^* = 570 \mu\text{m sec}$.

times that expected for a steady shear of $E_b = 0.15 \text{ sec}^{-1}$. Clustered fractions of 2 and 13 percent are expected for swimming speeds of $V = 12$ and $V = 40 \mu\text{m sec}^{-1}$ respectively (Table 4). For the slowest swimming speed, time varying shear limits the fraction clustered by dispersing clusters before they reach steady-state levels. Nonetheless, unsteadiness results in periods of weak mixing, during which the degree of clustering exceeds the levels corresponding to time-average shear rates.

The changing shear intensities also affected the bacteria's cumulative exudate exposure. For the steady state case ($E_b = 0.15 \text{ sec}^{-1}$) the exudate exposure enhancement factor was 1.4 for the slow swimming speed ($V = 12 \mu\text{m sec}^{-1}$) and 2.1 for the faster swimming speed ($V = 40 \mu\text{m sec}^{-1}$) (Table 5, $F_* = 570 \mu\text{m sec}$). The unsteady shearing also showed higher enhancement factors for faster swimming speeds (1.6 for $V = 12 \mu\text{m sec}^{-1}$, and 2.2 for $V = 40 \mu\text{m sec}^{-1}$). These factors were calculated using the steady shearing, non-chemotactic case to normalize exudate exposure, indicating that unsteady shearing results in higher exudate exposures than steady conditions. Unsteadiness increased cumulative exudate exposures by 15 and 6 percent for the swimming speeds of 12 and $40 \mu\text{m sec}^{-1}$, thus unsteadiness seemed to favor slower swimming speeds but the absolute cumulative exposure was highest for a swimming speed of $40 \mu\text{m sec}^{-1}$. Chemotaxis provides a significant advantage in exudate exposure, even though clusters are periodically dispersed by bursts of strong mixing.

Clustering Around Moving Phytoplankton Cells - For a phytoplankton moving at $10 \mu\text{m sec}^{-1}$, a reasonable velocity for sinking or swimming of phytoplankton of 1-10 μm radius (Smayda 1970), bacterial population density distributions showed a form very similar to that for shearing flows (Fig. 6). Near the phytoplankton cell surface, bacterial densities were orders of magnitude above background levels, approaching $10^9 \text{ cells ml}^{-1}$ for $V = 40 \mu\text{m sec}^{-1}$ and $F_* = 1140 \mu\text{m sec}$.

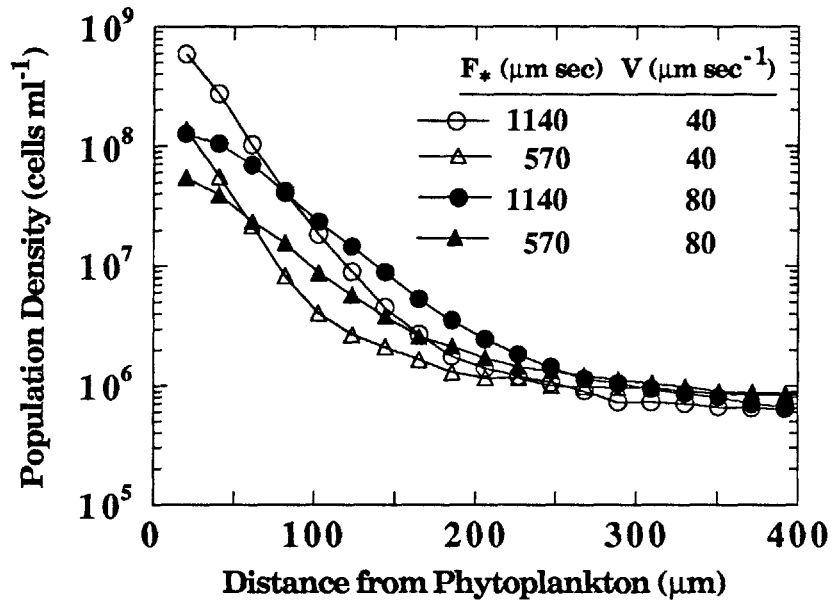


Figure 6. Simulated bacterial population densities surrounding a phytoplankton cell with the phytoplankton sinking at $10 \mu\text{m sec}^{-1}$ for varying normalized exudation rates F_* and bacteria swimming speeds V .

Population densities decreased rapidly with increasing distance from the phytoplankton, at rates similar to those for shearing flows (Fig 3). The size of the cluster increased with increasing bacterial swimming speed or increasing normalized exudation rate, just as in the shearing case. The fraction of the population in a cluster seemed more sensitive to changing exudation rates, decreasing from 41 to 11 percent for $V = 40 \mu\text{m sec}^{-1}$ and from 39 to 17 percent for $V = 80 \mu\text{m sec}^{-1}$ as the normalized exudation rate decreased from $F_* = 1140 \mu\text{m sec}$ to $F_* = 570 \mu\text{m sec}$.

Simulations over a range of bacterial swimming speeds and phytoplankton velocities showed results analogous to the shearing case, as the bacterial swimming speed giving the highest exudate exposure enhancement increased with increasing phytoplankton velocity (Tables 4 and 5). For the highest phytoplankton velocity simulated ($w_s = 20 \mu\text{m sec}^{-1}$), exudate exposures and fractions clustered were maximized for the fastest swimming speed ($V = 80 \mu\text{m sec}^{-1}$). This differs from the shearing case where exudate exposures were maximized for the intermediate swimming speed, but in both cases chemotactic motions may increase exudate exposures by an order of magnitude (Table 5).

Effects of Clustering on Exudate Distribution - The cumulative uptake of dissolved organic carbon by clustered bacteria can affect the exudate concentration surrounding the phytoplankton. In doing so, motile chemotactic bacteria gain an additional competitive advantage over non-chemotactic strains by removing the exuded carbon from the medium before it is available to the randomly distributed non-chemotactic bacteria. An estimate of this effect was made by including a term for bacterial uptake in the exudate transport equation. To simplify the analysis we examined only the motionless case, which was a reasonable simplification since the clustered region had diffusion dominated transport even in shearing flows.

Assuming that bacterial uptake is diffusion limited results in the following exudate

concentration equation

$$\frac{d^2C}{dr^2} + \frac{2}{r} \frac{dC}{dr} - 4\pi a_b [n_b + n_p \exp(-(r-a_p)/l)] C = 0 \quad (7)$$

where a_b is the bacterial cell radius. The first two terms give the radial change in diffusive transport which must balance bacterial uptake, given by third term with Eq. 6 used to represent the bacteria's population density distribution. If the bacteria population is unclustered ($n_p = 0$, $n_b = n_{bt}$), then the exudate distribution is the same as for diffusive transport with first order reaction (Carslaw and Jaeger 1959).

$$C = C_0(r) \exp[-r(4\pi a_b n_{bt})^{\frac{1}{2}}] \quad (8)$$

where $C_0(r)$ is the concentration expected from motionless diffusion without uptake (Eq. 3). The term $(4\pi a_b n_{bt})^{\frac{1}{2}}$ represents the inverse of a length scale where uptake begins to affect the concentration distribution. For bacteria with a cell radius of $0.5 \mu\text{m}$ and a density of $1000 \text{ cells } \mu\text{l}^{-1}$, this length scale is $400 \mu\text{m}$, thus over most of the simulation region unclustered bacteria do not significantly change the exudate distribution.

No analytical solutions were available for the clustered case, but Eq. 7 can be solved numerically to predict the clustered bacteria's effect on exudate concentrations. The parameters describing the bacterial population density in Eq. 7 were taken from the model simulation for the motionless case, with a swimming speed of $40 \mu\text{m sec}^{-1}$, and exudation rates, $F_* = 300$ and $200 \mu\text{m sec}$, giving 18 and 5 percent clustered respectively (Table 4). When 18 percent of chemotactic bacteria were clustered, uptake in the cluster lowered the exudate concentration by a factor of approximately three (Fig. 7a). The exudate concentration was depressed by

approximately 30 percent when 5 percent of the chemotactic population was clustered (Fig. 7a). Bacteria in the cluster took up a significant part of the exudate: approximately 30 and 70 percent for 5 and 18 percent clustered respectively (Fig. 7b). Beyond the cluster ($r > 115 \mu\text{m}$), the concentration distributions for clustered and unclustered cases decreased at similar rates but the cumulative uptake of the bacteria population was nearly twice as high for the 18 percent clustered case (83 percent of exudate) as compared with the unclustered case (44 percent of exudate).

Bacterial uptake of DOC distribution could increase the chemotactic exudate enhancement factor by lowering the background concentration of exudate. Using the modified concentration distribution that accounted for bacterial uptake while retaining the original bacterial distribution increased the calculated exudate exposure enhancement factor from 2.1 to 5.7 for 18 percent clustered and from 1.3 to 2.0 for 5 percent clustered. A more complete analysis would also account for these uptake effects in determining the chemotactic response and thus the distribution of bacteria. It seems unlikely, however, that bacterial uptake effects would have significantly altered the simulated bacterial population densities or time-averaged exudate exposures. Far from the phytoplankton, there was a significant decrease in concentration due to the cumulative uptake of the bacteria (Fig. 7a), but in this region the bacteria moved randomly through swimming and fluid motion. Near the phytoplankton, where chemotactic motions were important, the uptake effect was smaller and in fact, the concentrations nearest the cell had steeper spatial gradients in the case where uptake was considered. Likewise, since the majority of the bacteria's exudate exposure occurred near the phytoplankton, where the depression of exudate concentration through bacterial uptake was relatively small, we expect that the simulated time-averaged exudate exposures accurately reflected the effects of bacterial clustering. Even though the clustered population represented a minor

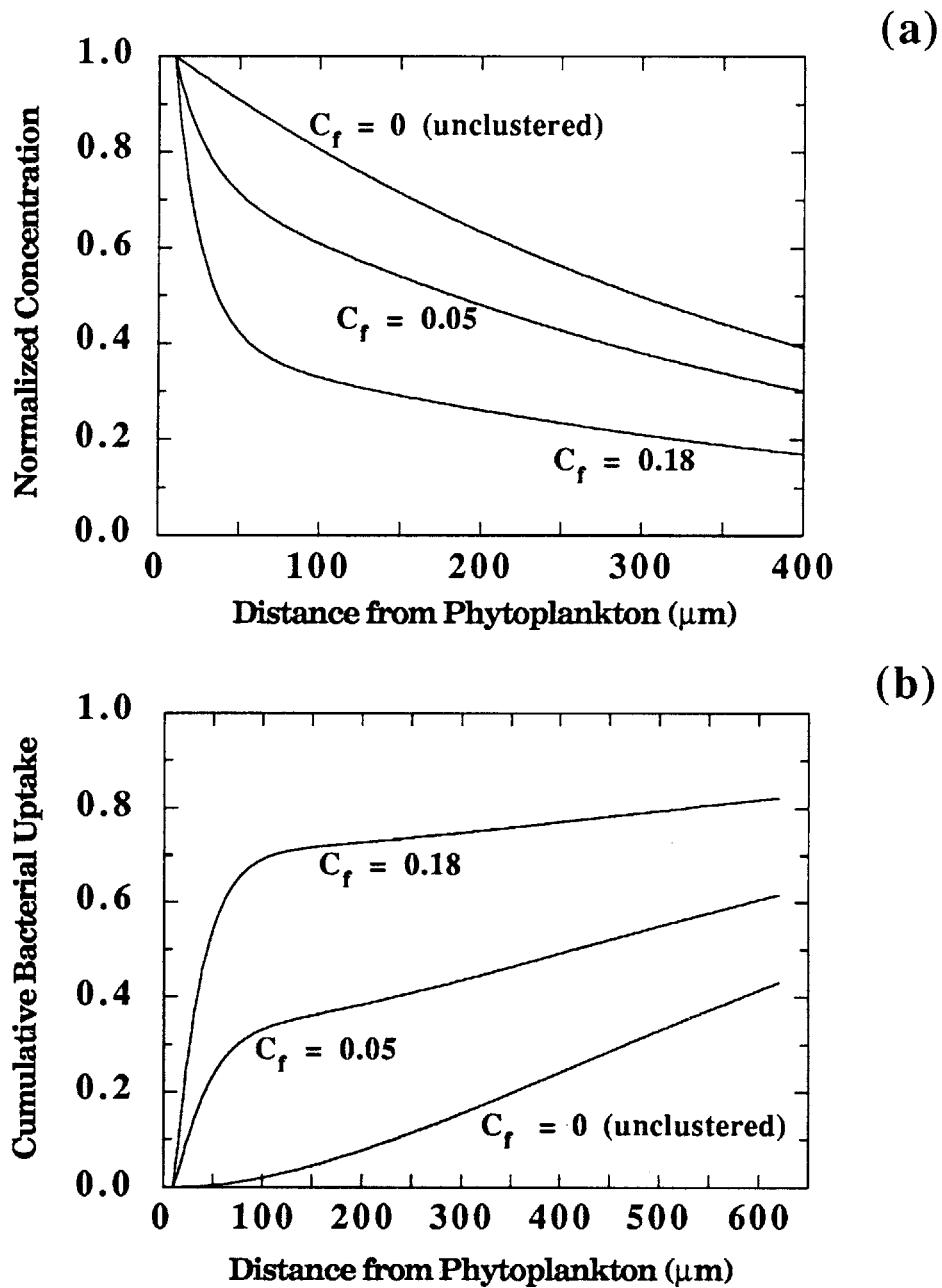


Figure 7. The effects of bacterial uptake on exudate distributions in motionless fluid. The average bacterial population density is 10^6 ml^{-1} . For the clustered cases, the population density distributions are taken from the results of the simulation model ($E_b = 0.0 \text{ sec}^{-1}$, $F^* = 200$ and $300 \mu\text{m sec}$).

- exudate concentration normalized by the corresponding value for motionless diffusion without bacterial uptake.
- cumulative uptake by the bacteria within the given distance to the phytoplankton.

portion of the total number of bacteria, their location in the region of highest exudate concentration means that they could take up a majority of the material exuded by the phytoplankton cell.

Effects of Clustering on Inorganic Nitrogen Distribution - As the bacteria in a cluster take up exudate they may also take up inorganic nitrogen and therefore lower the concentration of nitrogen near the phytoplankton. Estimating this effect of clustering required calculation of the relative nitrogen fluxes into the phytoplankton cell and the surrounding bacteria population. Bacterial biomass has been measured to be approximately 5-20 per cent of phytoplankton biomass (Williams 1981) and the C:N ratio for bacteria and phytoplankton are approximately 3.5 and 7.0 respectively (Lancelot and Billen 1985). Since growth rates of marine bacteria are no more than twice phytoplankton growth rates (Williams 1981), we expect that the total flux of nitrogen into the bacterial population will be comparable to the phytoplankton flux.

The inorganic nitrogen concentration distribution was predicted using an analysis like that used for exudate distributions which accounted for both transport and uptake effects on concentration distributions. Far from the phytoplankton the nitrogen concentration was assumed to approach a uniform background. Uptake by the phytoplankton was at the diffusion limited rate so as to maximize the potential effect of bacterial competition for nutrients. The bacterial uptake was assumed to saturate at a level giving a cumulative flux twice the phytoplankton flux. Even for this unrealistically high estimate of bacterial uptake, the effects of clustering on the flux of nitrogen to the phytoplankton were negligible. When 18 percent of the chemotactic bacteria population was clustered, the flux of nutrients to the phytoplankton was reduced by only 3 percent from the flux expected when the bacteria were uniformly distributed around the phytoplankton cell. Bacteria take up large amounts of exudate because they have high population densities in the

regions of high concentration. However, because of phytoplankton uptake of nutrients, the region where bacteria congregate has a concentration of nitrogen below background levels. This tends to decrease the effects of clustering on the distribution of inorganic nutrients. Clustered bacteria do not significantly alter the uptake of inorganic nitrogen by the exuding phytoplankton.

Comparison of Results with Previous Studies - The simulation results for clustering in moving fluids showed trends predicted by earlier investigations of marine bacteria chemotaxis. We agree with Mitchell et al. (1985) that fluid motions, from both turbulent shearing and phytoplankton sinking, limit bacterial clustering in the oceanic mixed layer. However, we find that clustering can occur for the shear intensities and phytoplankton sinking speeds expected in the oceanic mixed layer because even transient association of bacteria with phytoplankton can result in significant enhancement of bacterial exposure to exudate. Thus the assumption made by Mitchell et al. that clustering is precluded whenever bacteria cannot remain with a phytoplankton is unnecessarily restrictive. Our results also showed the strong dependence on exudation rates as seen by Jackson (1987) for the transient behavior of marine bacteria surrounding exuding phytoplankton in motionless fluid. When fluid motion effects are present, our results showed higher time-average exudate exposures for higher exudation rates and faster swimming speeds (Table 5), as seen by Jackson (1989) for his short-term analysis of sinking phytoplankton cells. Our simulations showed slightly higher rates of bacterial chemotaxis than Jackson because of differences in the assumed values of K_d (Jackson used 10^{-4} M while we used a range from 10^{-3} to 3×10^{-6} M), which results in higher normalized exudation rates F_* (Eq. 5). The standard conditions used by Jackson for computations of chemotaxis towards a sinking phytoplankton in low Peclet number flow (Jackson 1989) are equivalent to a normalized exudation rate F_* of $350 \mu\text{m sec}$ (see Eq. 5), while our simulations span a range of values from 100 to

1140 $\mu\text{m sec}$. In addition, our simulation results did not predict variations in clustering due solely to the size of the phytoplankton cell as seen by Jackson (1987). Bacterial density distributions calculated for a motionless fluid with constant normalized exudation rate ($F_* = 200 \mu\text{m sec}$) but varying phytoplankton cell sizes showed no differences for phytoplankton cell sizes of 2, 10 or 20 μm (Fig. 8). This result was not a reflection of differences in the respective models of chemotactic motion, as equivalent results were obtained using the unmodified Brown and Berg (1974) chemotaxis model implemented by Jackson (1987). We believe that given a sufficient chemotactic signal, as quantified by the normalized exudation F_* , Jackson's model would show bacteria approaching a 2 μm phytoplankter. The inability of bacteria to approach picoplankton as observed by Jackson (1987) should only be attributed to the lower assumed exudation rates of these cells. We agree that algal cell size strongly influences clustering by affecting exudation rate, but we find no limit based solely on the physical size of the phytoplankton cell.

Summary

In summary we believe that a small but not inconsequential fraction of the chemotactic bacteria population may be clustered around exuding phytoplankton cells in the ocean's upper mixed layer. Although the fraction clustered may be relatively small for shear levels in the mixed layer, increases in exudate exposure through chemotactic behavior can be significant, giving chemotactic bacteria a competitive advantage over non-chemotactic bacteria. The advantage in exudate exposure occurs both from the extra time spent by chemotactic bacteria in areas of high exudate concentration and from the resulting reduction in average exudate concentration experienced by non-chemotactic bacteria due to uptake in the cluster. The cumulative exudate exposure of chemotactic populations may be an order of magnitude higher than that predicted by bulk average conditions, therefore

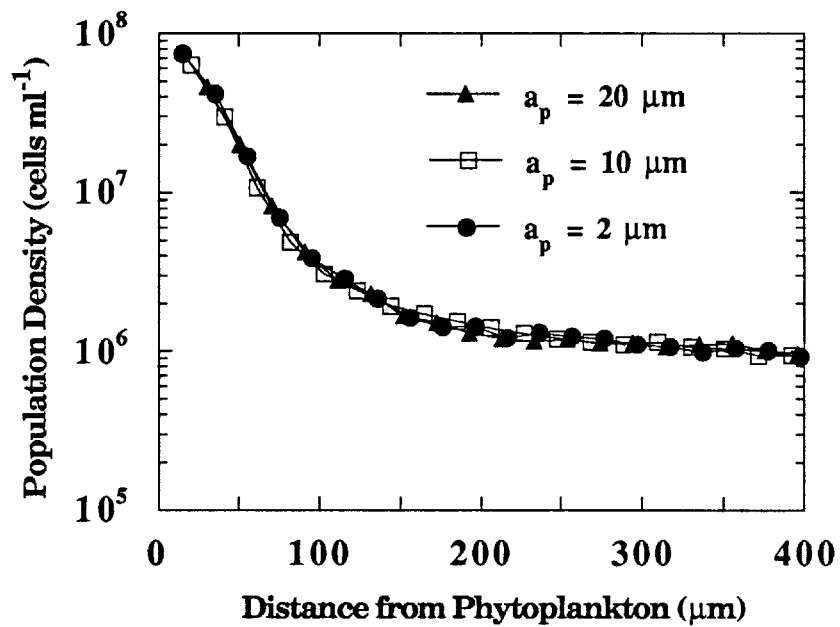


Figure 8. Bacterial population densities surrounding phytoplankton with cell radii a_p varying from 2.0 to 20.0 μm , for a normalized exudation rate $F^* = 200 \mu\text{m sec}$ and bacterial swimming speed $V = 40 \mu\text{m sec}^{-1}$.

additions of labelled DOC added in bulk may seriously underestimate bacterial activity by ignoring the effects of clustering. In fact, there is evidence showing turnover of labelled DOC increasing by an order of magnitude when the label is introduced through phytoplankton exudation rather than added in bulk to the sample (Azam and Ammerman 1984).

While clustering may have important consequences to the uptake and distribution of exudate, its effect on the spatial distribution of bacteria is less dramatic. Unsteady shearing and uniform fluid motions limit clusters to less than 15 percent of the motile population for a majority of conditions expected in the mixed layer. Therefore, it seems unlikely that clustering significantly affects the fate of bacterial secondary production in the microbial food web. According to our simulations, bursts of intense shearing motion almost completely disperse clusters of bacteria, but they do not prevent cluster formation and the accompanying enhancement of exudate exposure. Unsteady shearing actually results in occasional periods when the degree of clustering is well above that expected for the corresponding mean shear rate.

The picture that emerges from our simulations of bacterial motion is one in which chemotactic bacteria are transported to the phytoplankton cell primarily by fluid motion and random swimming rather than by directed chemotactic motion. Shearing motions typical of the upper mixed layer ($E_b = 0.15 \text{ sec}^{-1}$) exceed any directed bacterial swimming motions, for bacteria swimming at $40 \mu\text{m sec}^{-1}$, in at least 90 percent of the volume occupied by a phytoplankter ($1 \mu\text{l}$ for typical phytoplankton densities). Once the bacterium is brought near the cell, chemotactic motions are effective in keeping the bacterium near the phytoplankton thereby increasing its time-averaged exudate exposure. Near the phytoplankton, fluid motions are weakest and concentration gradients steepest, conditions which can

increase a bacterium's residence time near the phytoplankter by several orders of magnitude. In the region where significant chemotactic response occurs, exudate concentration distributions are not distorted by fluid motion. As a result, the degree of bacterial clustering and the level of exudate exposure enhancement is relatively insensitive to the concentration distribution in the region where fluid motion distorts the concentration distributions, i.e. whether a disk or tube shaped exudate concentration distribution is formed. Random swimming and fluid motions end the association between the bacterium and the phytoplankton cell within a minute for the conditions expected in the mixed layer, transporting the bacterium to other phytoplankton where the chemotactic process is repeated.

References

- Acrivos, A., and T.D. Taylor. 1962. Heat and mass transfer from single spheres in Stokes flow. *Phys. Fluids* 5: 387-394.
- Ammerman, J.W., and F. Azam. 1982. Uptake of cyclic AMP by natural populations of marine bacteria. *Applied and Environmental Microbiology*. 43: 689-.
- Armitage, J.P., and R.M. MacNab. 1987. Unidirectional, intermittent rotation of the flagellum of *Rhodobacter sphaeroides*. *Journal of Bacteriology*. 169: 514-518.
- Azam, F., and Hodson R.E. 1981. Multiphasic kinetics for D-glucose uptake by assemblages of natural marine bacteria. *Marine Ecology Progress Series*. 6: 213-
- Azam, F., and J.W. Ammerman. 1984. Cycling of organic matter by bacterioplankton in pelagic marine ecosystems: microenvironmental considerations, in: M.J.R. Fasham [ed.], "Flows of energy and materials in marine ecosystems," Plenum, pp. 345-360.
- Baker, M.A., and C.H. Gibson. 1987. Sampling turbulence in the stratified ocean: Statistical consequences of strong intermittency. *Journal of Physical Oceanography*. 17: 1817-1836.
- Banse, K. 1984. Review of "Marine Pelagic Protozoa and Microzooplankton Ecology." *Limnology and Oceanography*. 29: 445-446.
- Batchelor, G.K. 1979. Mass transfer from a particle suspended in fluid with a steady linear ambient velocity distribution. *Journal of Fluid Mechanics*. 95: 369-400.
- Baumann, P., and L. Baumann. 1978. The marine gram-negative eubacteria: Genera *Photobacterium*, *Beneckea*, *Alteromonas*, *Pseudomonas*, and *Alicagenes*. in: N.R. Krieg and J.G. Holt, eds. *Bergeys Manual of Systematic Bacteriology*. Williams and Wilkins. pp. 1301-1331.
- Beers, J.R., F.M.H. Reid, and G.L. Stewart. 1980. Microplankton population structure in southern California nearshore waters in late Spring. *Marine Biology*. 60: 209-226.
- Bell, W.H., and R. Mitchell. 1972. Chemotactic and growth responses of marine bacterial to algal extracellular products, *Biological Bulletin*, 143: 265-277.
- Berg, H.C. 1983. "Random Walks in Biology." Princeton University Press. Princeton, New Jersey. 142 pp.
- Berg, H.C., and D.A. Brown. 1972. Chemotaxis in *Escherichia coli* analysed by three-dimensional tracking. *Nature*. 239: 500-504.
- Bienfang, P.K. 1980. Phytoplankton sinking rates in oligotrophic waters off Hawaii, USA. *Marine Biology*. 61: 69-77.

- Bienfang, P.K. 1985. Size structure and sinking rates of various microparticulate constituents in oligotrophic Hawaiian waters. *Marine Ecology Progress Series*. 23: 143-151.
- Blaauboer, M.C.I., R. Van Keulen, and Th. E. Cappenberg. 1982. Extracellular release of photosynthetic products by freshwater phytoplankton populations, with special reference to the algal species involved, *Freshwater Biology*. 12: 559-572.
- Block, S.M., J.E. Segall, and H.C. Berg. 1982. Impulse responses in bacterial chemotaxis. *Cell*. 31: 215-226.
- Bowen, J.D., and K.D. Stolzenbach. 1989. Concentration distributions around continuous point sources in a fluid with a steady linear velocity distribution, submitted to the *Journal of Fluid Mechanics*.
- Bowen, J.D., S.W. Chisholm, and K.D. Stolzenbach. 1989. Microbial chemotaxis around a continuous point source of attractant. in prep.
- Bratbak, G. 1985. Bacterial biovolume and biomass estimations. *Applied and Environmental Microbiology*. 49: 1488-1493.
- Bratbak, G., and T.F. Thingstad. 1985. Phytoplankton-bacteria interactions: an apparent paradox? Analysis of a model system with both competition and commensalism. *Marine Ecology Progress Series*. 25: 23-30.
- Brenner, H. 1963. Forced convection heat and mass transfer at small Peclet numbers from a particle of arbitrary shape. *Chemical Engineering Science*. 18: 109-122.
- Brown, D.A., and H.C. Berg, 1974, Temporal stimulation of chemotaxis in *Escherichia coli*, *Proceedings of the National Academy of Sciences of the U.S.A.* 71: 1388-1392.
- Carslaw, H.S., and J.C. Jaeger. 1959. *Conduction of Heat in Solids*. Oxford University Press.
- Chet, I., and R. Mitchell, 1976, The relationship between chemical structure of attractants and chemotaxis by a marine bacterium, *Canadian Journal of Microbiology*, 22: 1206-1208.
- Corrsin, S. 1963. Estimates of the relation between Eulerian and Lagrangian scale in large Reynolds number turbulence, *J. Atmos. Sci.* 20, 115- .
- Denman, K.L., and A.E. Gargett, 1988, Multiple thermoclines are barriers to vertical exchange in the subarctic Pacific during SUPER, May 1984, *Journal of Marine Research*, 46: 77-103
- Ducklow, H.W., D.A. Purdue, P.J. LeB. Williams, and J.M. Davies. 1986. Bacterioplankton: A sink for carbon in a coastal marine plankton community, *Science*. 232: 865-867.
- Fenchel, T. 1988. Marine plankton food chains. *Annual Review of Ecology and Systematics*. 19: 19-38.

- Fogg, G.E. 1983. The ecological significance of extracellular products of phytoplankton photosynthesis. *Botanica Marina*. 26: 3-14.
- Fuhrman, J.A., J. Ammerman, and F. Azam. 1980. Bacterioplankton in the coastal euphotic zone: Distribution, activity, and possible relationships with phytoplankton. *Marine Biology*. 66: 109-120.
- Gallucci, K.K., and H.W. Paerl, 1984. *Pseudomonas aeruginosa* chemotaxis associated with blooms of N₂-fixing blue-green algae (Cyanobacteria). *Applied and Environmental Microbiology*. 45: 557-562.
- Geesey, G.G., and R.Y. Morita. 1979. Capture of arginine at low concentrations by a marine psychrophilic bacterium. *Applied and Environmental Microbiology*. 38: 1092-1097.
- Gross, F., and E. Zeuthen. 1948. The buoyancy of plankton diatoms: A problem of cell physiology. *Proc. Roy. Soc. Ser. B*. 135: 382-389.
- Hazen, T.C., R.F. Dimock Jr, G.W. Esch, A. Mansfield, and M.L. Raker. 1984. Chemotactic behavior of *Aeromonas hydrophila*, *Current Microbiology*. 10: 13-18.
- Jackson, G.A. 1987. Simulating chemotaxis by marine microorganisms, *Limnology and Oceanography*. 32: 1253-1266.
- Jackson, G.A. 1989. Simulation of bacterial attraction and adhesion to falling particles in an aquatic environment. *Limnology and Oceanography*. 34: 514-530.
- Jones, A.K., and Cannon, R.C. 1986. The release of micro-algal photosynthate and associated bacterial uptake and heterotrophic growth. *British Phycological Journal*. 21: 341-358.
- Jumars, P.A., D.L Penry, J.A. Baross, M.J. Perry, and B.W. Frost. 1989. Closing the microbial loop: dissolved carbon pathway to heterotrophic bacteria from incomplete ingestion, digestion and absorption in animals, *Deep-Sea Research*. 36: 483-495.
- Lancelot, C., and G. Billen. 1985. Carbon-nitrogen relationships in nutrient metabolism of coastal marine ecosystems. *Advances in Aquatic Microbiology*, 3: 263-321.
- Lumley, J.L. 1972. On the solution of equations describing small scale deformation. In *Symposia Matematica: Convegno sulla Teoria della Turbolenza al Istituto Nazionale di Alta Matematica*. pp. 315-334. Academic Press.
- Macnab, R.M., and D.E. Koshland Jr. 1972. The gradient-sensing mechanism in bacterial chemotaxis. *Proceedings of the National Academy of Sciences of the U.S.A.* 69: 2509-2512.
- Mague, T.H., E. Friberg, D.J. Hughes, and I. Morris. 1980. Extracellular release of carbon by marine phytoplankton: a physiological approach. *Limnology and Oceanography*. 25, 262-279.

- Mesibov, R., G.W. Ordal, and J. Adler. 1973. The range of attractant concentrations for bacterial chemotaxis and the threshold and size of response over this range. *Journal of General Physiology*. 62: 203-223.
- Mitchell, J.G., A. Okubo, and J.A. Fuhrman. 1985. Microzones surrounding phytoplankton form the basis for a stratified microbial ecosystem. *Nature*. 316: 58-59.
- Mopper, K., and P. Lindroth. 1982. Diel and depth variations in dissolved free amino acids and ammonium in the Baltic Sea determined by shipboard HPLC analysis. *Limnology and Oceanography*. 27: 336-347.
- Monin, A.S. and A.M. Yaglom. 1975. *Statistical Fluid Mechanics*. Vol. 2. MIT Press.
- Mullin, M.M., P.R. Sloan, and R.W. Eppley. 1966. Relationship between carbon content, cell volume, and area in phytoplankton. *Limnology and Oceanography*. 11: 307-311.
- Nalewajko, C., T.G. Dunstall, and H. Shear. 1976. Kinetics of extracellular release in axenic algae and in mixed algal-bacterial cultures: Significance in estimation of total (gross) phytoplankton excretion rates. *Journal of Phycology*. 12: 1-5.
- Osborn, T.R., and R.G. Lueck. 1985a. Turbulence measurements from a towed body, *Journal of Atmospheric and Oceanic Technology*. 2: 517-527.
- Osborn, T.R., and R.G. Lueck, 1985b, Turbulence measurements with a submarine. *Journal of Physical Oceanography*, 15: 1502-1520.
- Segall, J.E., M.D. Manson, and H.C. Berg. 1982. Signal processing times in bacterial chemotaxis. *Nature*. 296: 855-857.
- Segall, J.E., S.M. Block, and H.C. Berg. 1986. Temporal comparisons in bacterial chemotaxis. *Proc. Natl. Acad. Sci. USA*. 83: 8987-8991.
- Sharp, J.H. 1977. Excretion of organic matter by marine phytoplankton: Do healthy cells do it? *Limnology and Oceanography*. 22: 381-399
- Sharp, J.H. 1984. Inputs into microbial food chains. in: Hobbie, J.E., and Williams, P.J. LeB. [eds.], "Heterotrophic Activity in the Sea." Plenum Press. New York.
- Shay, T.J., and M.C. Gregg. 1986. Convectively driven turbulent mixing in the upper ocean. *Journal of Physical Oceanography*. 16: 1777-1798.
- Smayda, T.J. 1970. Normal and accelerated sinking of phytoplankton in the sea. *Marine Geology*. 11: 105-122.
- Sondergaard, M., B. Riemann, and N.O.G. Jorgensen. 1985. Extracellular organic carbon (EOC) released by phytoplankton and bacterial production. *Oikos*. 45, 323-332.

- Sugimura, Y., and Y. Suzuki. 1988. A high-temperature catalytic oxidation method for the determination of non-volatile dissolved organic carbon in seawater by direct injection of a liquid sample. *Marine Chemistry*. 24: 105-131.
- Tennekes, H., and J.L. Lumley. 1972. *A First Course in Turbulence*. MIT Press.
- Walsh, F., and R. Mitchell. 1978. Bacterial chemotactic responses in flowing water. *Microbial Ecology*. 4: 165-168.
- Wheeler, P.A., and David L. Kirchman. 1986. Utilization of inorganic and organic nitrogen by bacteria in marine systems. *Limnology and Oceanography*. 31: 998-1009.
- Wiley J.M. 1988. Characterization of swimming motility in a marine unicellular cyanobacterium. *PH.D. Thesis. MIT/WHOI*. WHOI-88-18. pp. 80-146.
- Williams, P.J.LeB. 1981. Incorporation of microheterotrophic processes into the classical paradigm of the planktonic food web, *Kieler Meeresforsch.* 5: 1-28.
- Williams, P.J.LeB. 1984. Bacterial production in the marine food chain: The emperor's new suit of clothes? in: M.J.R. Fasham [ed.], "Flows of energy and materials in marine ecosystems." Plenum. pp. 345-360.
- Wolter, K. 1982. Bacterial incorporation of inorganic substances released by natural phytoplankton populations. *Marine Ecology Progress Series*. 7: 287-295.
- Wood, A.M., and Van Valen, L.M. 1989. Paradox Lost? On the excretion of energy-rich compounds by phytoplankton. *Marine Microbial Food Webs*. In Press.
- Wood, M.A., H. Rai, J. Garnier, T. Kairesalo, S. Gressens, E. Orive, and B. Ravail. 1989. Practical Approaches to algal excretion: A report from GAP88. submitted to *Marine Microbial Food Webs*.
- Zlotnik, I., and Z. Dubinsky. 1989. The effect of light and temperature on DOC excretion by phytoplankton. *Limnology and Oceanography*. 34: 831-839.

Appendix A. Model Validation and Sensitivity Analysis

The following appendix is provided as validation for the model of chemotactic bacterial motion used in Chapter 5. The exudate concentration distribution surrounding the source was modelled by matching two asymptotic solutions. Near the source the concentration followed that for a continuous input into a motionless fluid. Far from the source the distribution was assumed to approach the approximate analytical solutions developed in Chapter 2. The asymptotic solutions were matched in the region where the transport is affected by both diffusion and advection. The calculated exudate concentration was compared to an exact solution calculated by numerically convolving the instantaneous point source solution (Figures A.1, A.2, and A.3).

Initially, the model of bacterial motion was validated by simulating the motion of bacteria in motionless and shearing fluid around a phytoplankton that is not exuding. In the first numerical simulation, a population of bacteria were placed near the phytoplankton cell. The bacteria cells moved randomly away from the phytoplankton, with the average distance of the bacteria population increasing as $(V^2T_0t)^{\frac{1}{2}}$, where V is the bacterial swimming speed, T_0 is the average run time, and t is the time since bacterial addition (Figure A.4). Eventually the bacteria population reached a uniform density, although the calculated population density in the slowest swimming speed case ($V=12 \mu\text{m sec}^{-1}$) showed a significant level of random fluctuation (Figure A.5). A second validation step consisted of comparing the results of the simulation model for the motionless case against a previous simulation presented by Jackson (1987) (see Chp. 5 for reference). The simulated transient behavior of the chemotactic population agreed well with the corresponding simulation presented by Jackson (1987) (Figure A.6).

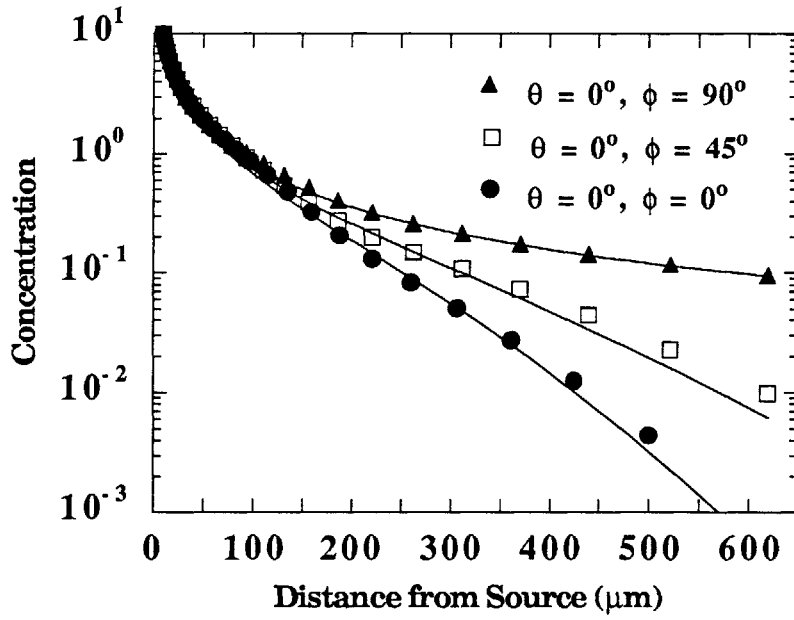
The calculated bacterial population densities had a characteristic form that showed an exponential decrease in density near the source (see Chapter 4). The

population densities decreased as $\exp(-r/l)$, where r is the distance from the source and l is a characteristic length scale. This exponential behavior was seen in motionless fluid, in fluid with shearing motion, and in fluid with a uniform flow due to sinking or swimming of the phytoplankton. The characteristic length scale l was found to be linearly related to the bacterial swimming speed, V , and the minimum run time of the bacteria, T_{\min} (Figure A.7).

The sensitivity of the model results to the form of the concentration distribution was analyzed by simulating the motion of bacteria in a moving fluid with an exudate concentration distribution described by the motionless result (see Chapter 5). Bacterial movement was also simulated for a variety of shear patterns giving disk and tube shaped exudate concentration distributions. It was found that the simulated bacterial population densities were insensitive to the pattern of shearing motion for all bacterial swimming speeds simulated (Figure A.8). At the intermediate swimming speed ($V = 40 \mu\text{m sec}^{-1}$), it was found that the calculated densities were not sensitive to the degree of distortion in the exudate distributions in the advection dominated region. Population densities for bacterial movement in the presence of shearing fluid motions, but with exudate distributions described by the motionless result, were identical to the case where the shearing motion distorted the exudate distribution into a tube (Figure A.9). There was a significant difference, however, for the fastest simulated bacterial swimming speed ($V = 80 \mu\text{m sec}^{-1}$) (Figure A.10).

Figure A.1. Validation of the approximate analytical solutions for concentration distributions surrounding a continuous point source in a shear flow. The solid line is obtained by numerical convolution of the exact solution for an instantaneous point source (Batchelor 1979). The symbols represent concentrations calculated using approximate analytical solutions for the sheared region (Bowen and Stolzenbach 1989) and the motionless diffusion solution (Carslaw and Jaeger 1959) for the central diffusive core. In the region where transport is due to both diffusion and advection, the two solutions are matched with an empirically determined weighting function. Concentrations are calculated along lines emanating from the source with orientations given in polar coordinates such that $\theta = 0^\circ$, $\phi = 90^\circ$ lies along the x_1 axis, $\theta = 90^\circ$, $\phi = 90^\circ$ lies along the x_2 axis, and $\theta = 0^\circ$, $\phi = 0^\circ$ lies along the x_3 axis. The shear strength E_b is 0.05 sec^{-1} in (a) and 0.5 sec^{-1} in (b). The shear tensor symmetry factor s is fixed at -1 , thus the principal strain rates are: $E_1 = E_b$, $E_2 = -1/2 E_b$, $E_3 = -1/2 E_b$.

(a)



(b)

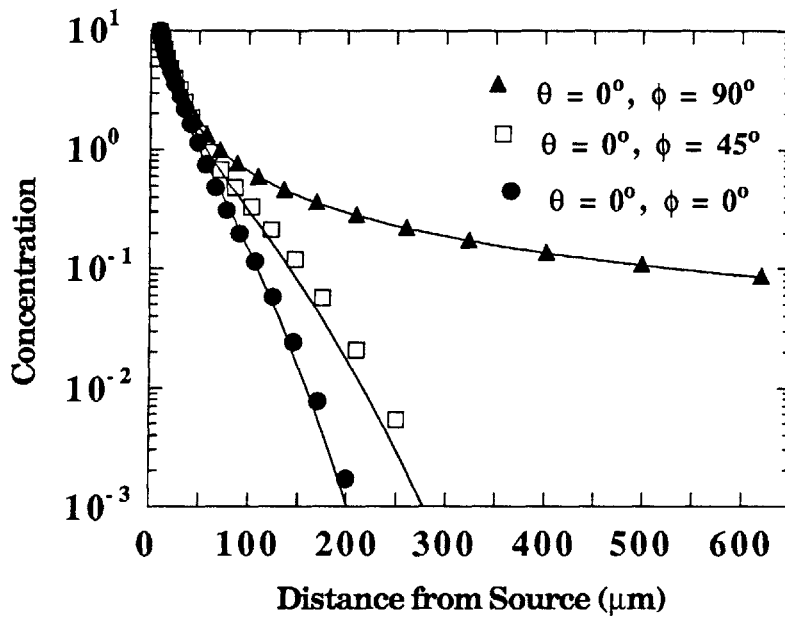
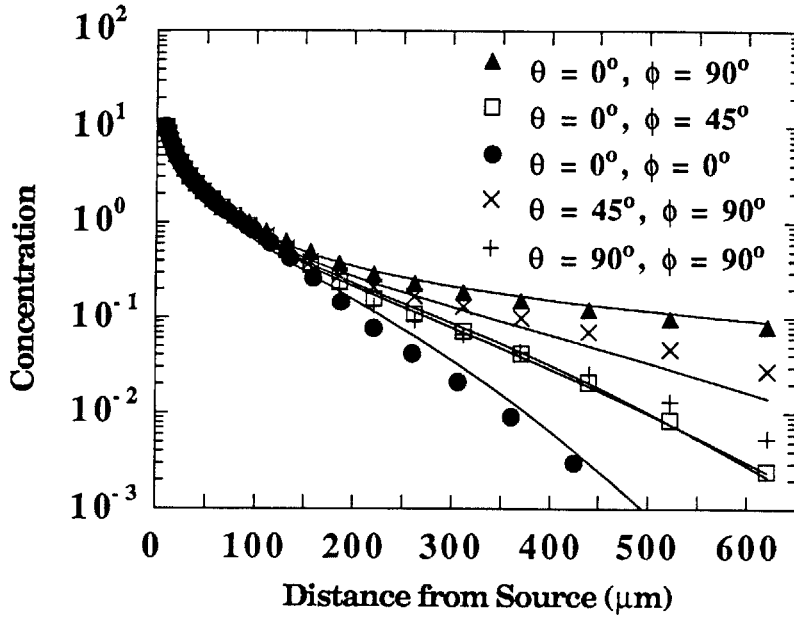


Figure A.2. Validation of the approximate analytical solutions for a non-axisymmetric tube-shaped concentration distribution. Concentrations are calculated using the matched approximate analytical solution described in A.1 (symbols) and the convolution of the exact instantaneous solution (lines). Orientation of each line is as described in A.1. The shear strength E_b is 0.05 sec^{-1} in (a) and 0.5 sec^{-1} in (b). The shear tensor symmetry factor s is given as $s = -0.5$ so that $E_1 = E_b$, $E_2 = -1/4 E_b$, $E_3 = -3/4 E_b$.

(a)



(b)

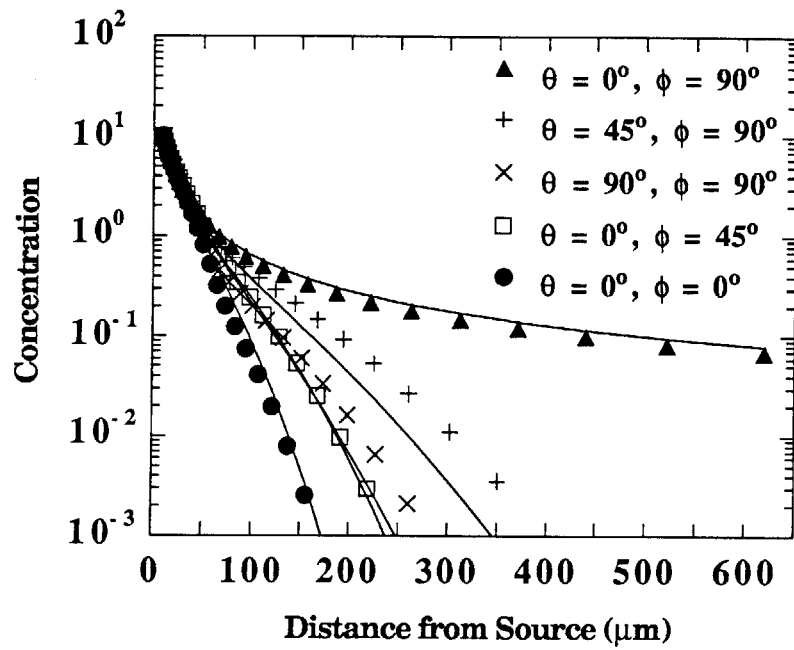
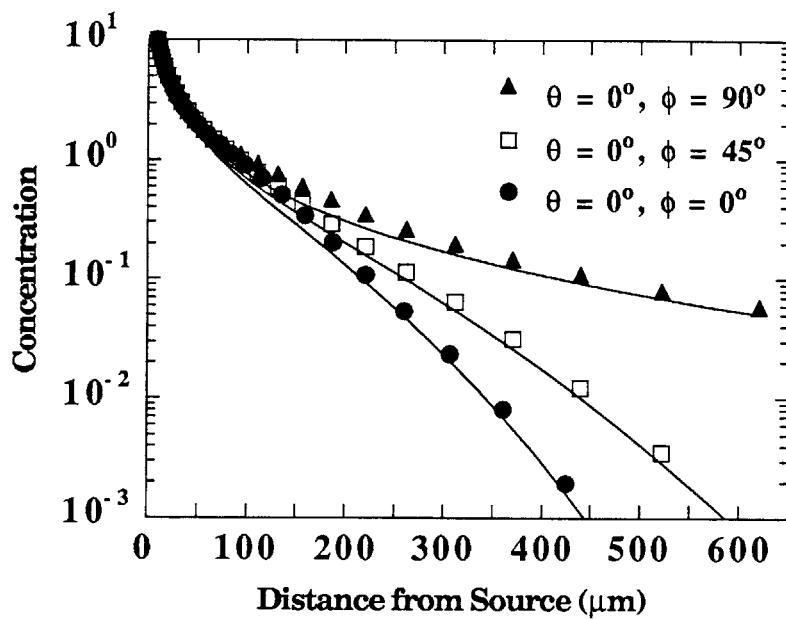


Figure A.3. Validation of the approximate analytical solutions for an axisymmetric disk-shaped concentration distribution. Concentrations are calculated using the matched approximate analytical solution described in A.1 (symbols) and the convolution of the exact instantaneous solution (lines). Orientation of each line is as described in A.1. The shear strength E_b is 0.05 sec^{-1} in (a) and 0.5 sec^{-1} in (b). The shear tensor symmetry factor s is given as $s = 1.0$ so that $E_1 = 1/2 E_b$, $E_2 = 1/2 E_b$, $E_3 = -E_b$.

(a)



(b)

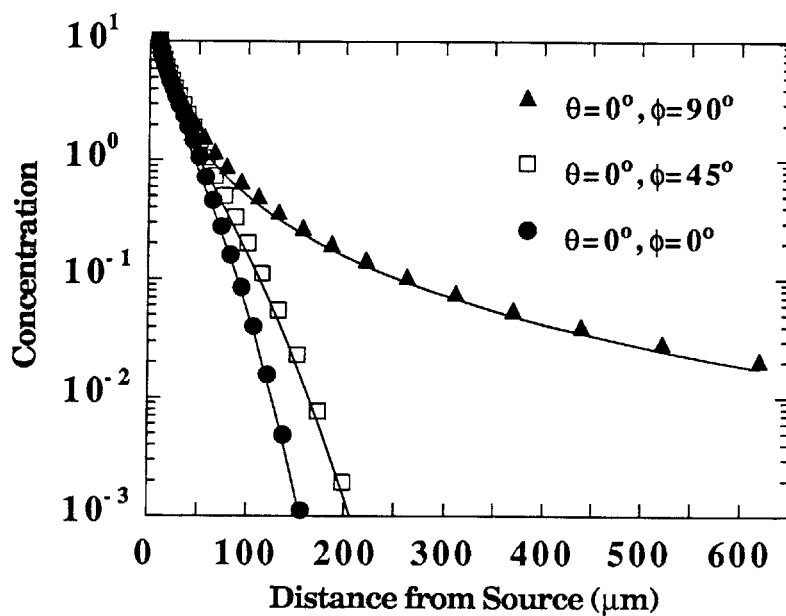


Figure A.4. Validation of the model of bacterial motion when the fluid is motionless and without exudate concentration gradients. 2000 cells were placed at $r = 11 \mu\text{m}$ initially, where r is the distance from the center of the phytoplankton which has a radius of $10 \mu\text{m}$. The solid lines are fitted by linear regression. The linear relationship indicates a constant random diffusion coefficient. The slopes for the three swimming speeds are 16.0 for $V = 12.3 \mu\text{m sec}^{-1}$, 51.0 for $V = 40.0 \mu\text{m sec}^{-1}$, and 100.4 for $V = 80 \mu\text{m sec}^{-1}$. If the random motion diffusion coefficient D_S is assumed to be determined by $D_S = 1/3 V T_0$ (Dahlquist and Lovely 1975), where T_0 is the average run time, then the predicted slopes are 17.0 for $V = 12.3 \mu\text{m sec}^{-1}$, 56.6 for $V = 40.0 \mu\text{m sec}^{-1}$, and 113.1 for $V = 80 \mu\text{m sec}^{-1}$.

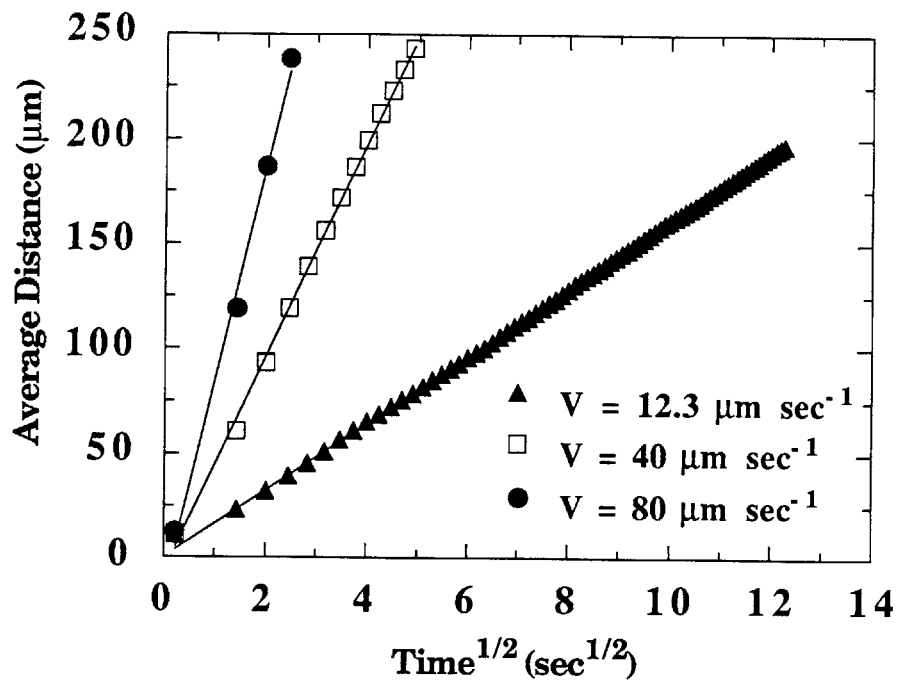


Figure A.5. Validation of the model of bacterial motion when the fluid is motionless and without exudate concentration gradients. The model simulates the random motion of 2000 cells placed randomly in the simulation region. The exudate flux from the phytoplankton is set equal to zero, so no directed chemotactic motion is possible. Time averaged bacteria population density distributions are calculated for the three swimming speeds. Although random fluctuations in density are apparent for each swimming speed, the population density is essentially uniform throughout the simulation region.

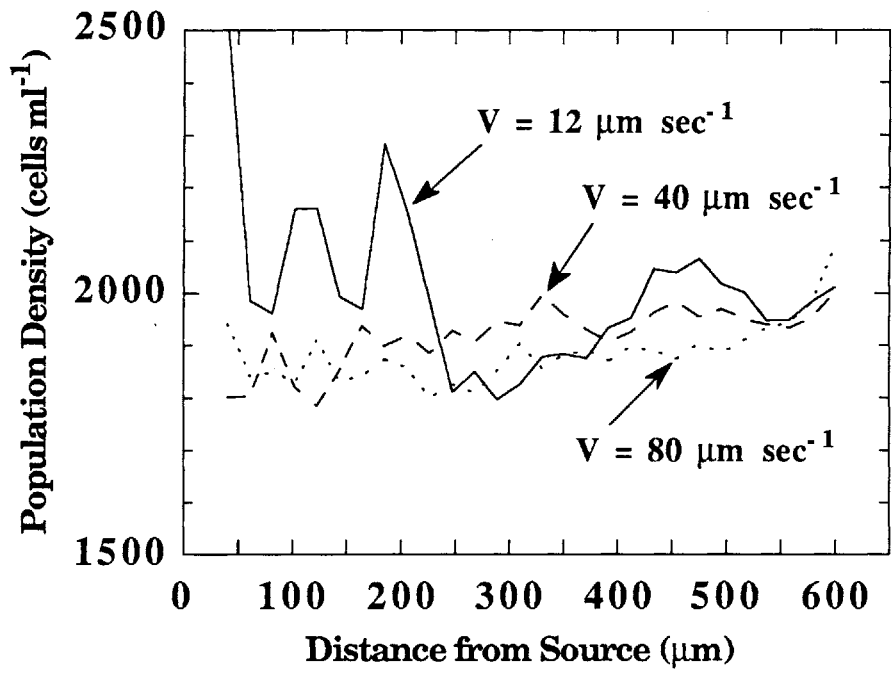


Figure A.6. Transient behavior of a population of 3500 bacterial cell distributed randomly in a spherical simulation region with a radius of 100 μm . The phytoplankton cell radius is 10 μm . The average distance for each time step is calculated by finding the linear average of the distance to the center of the phytoplankton for the population of 3500 bacteria cells. The normalized flux values F^* are calculated using parameter values taken from Jackson (1987). The solid line shows the transient response of the population due to chemotactic behavior as computed by the model described by Bowen et al. (1989), while the dashed line shows the corresponding results from Jackson's model (see Figure 3, Jackson 1987). The fluid is motionless.

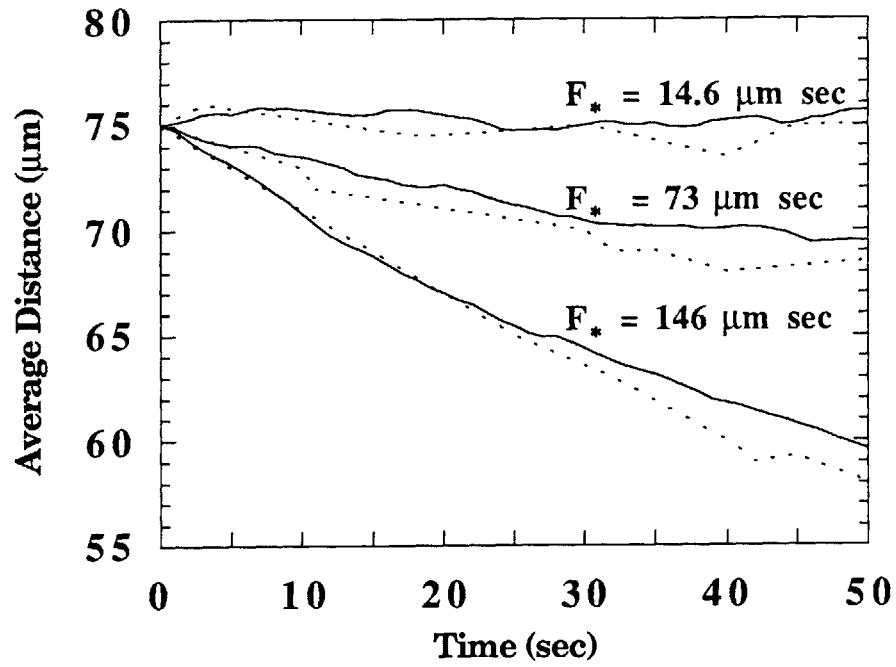


Figure A.7. Inner length scales for model runs with sinking motion and shearing motion. V is the bacterial swimming speed and T_{\min} is the response latency. Runs differ in shear strength, sinking speed, and normalized exudation rate. The open symbols indicate results for shearing motions, while the closed symbols indicate results from sinking fluid motions.

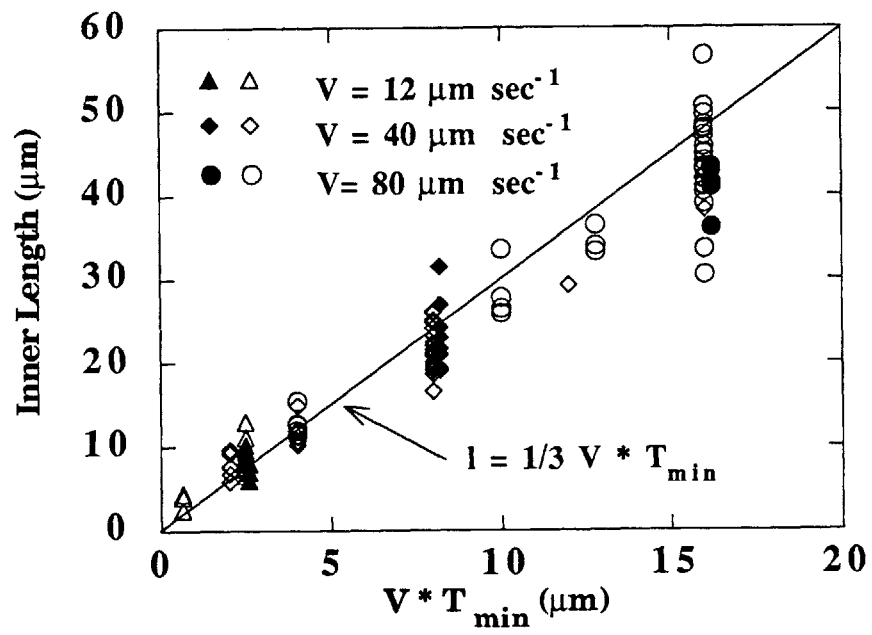
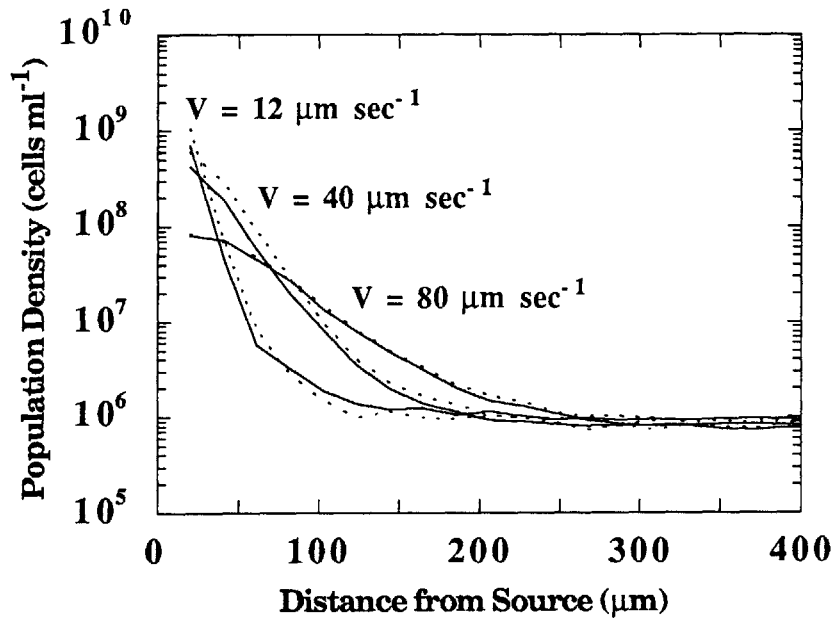


Figure A.8. Sensitivity of calculated bacterial population density distributions to the pattern of the shearing motions. The bacterial swimming speed V varies from $V = 12 \mu\text{m sec}^{-1}$ to $V = 80 \mu\text{m sec}^{-1}$. The normalized exudation rate F^* is constant at $F^* = 1140 \mu\text{m sec}$. The solid lines show the calculated population density distributions when the shearing pattern is characterized by an axisymmetric compressive flow in the x_2 - x_3 plane. This shearing pattern gives axisymmetric tube-shaped concentration distributions. The dashed lines show the calculated population density distributions when the shearing pattern is characterized by an axisymmetric expansive flow in the x_2 - x_3 plane. This shearing pattern gives axisymmetric disk-shaped concentration distributions. (a) Shear strength $E_b = .15 \text{ sec}^{-1}$. (b) Shear strength $E_b = 0.3 \text{ sec}^{-1}$.

(a)



(b)

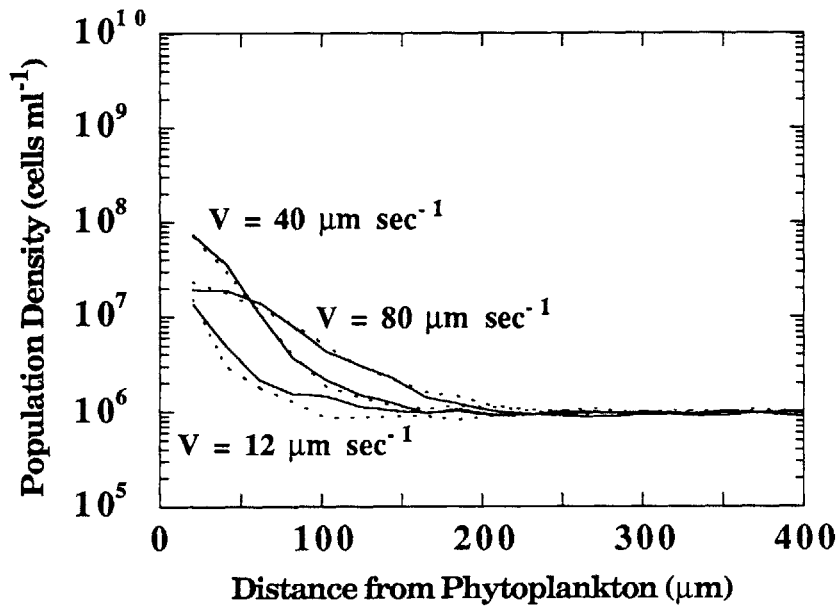
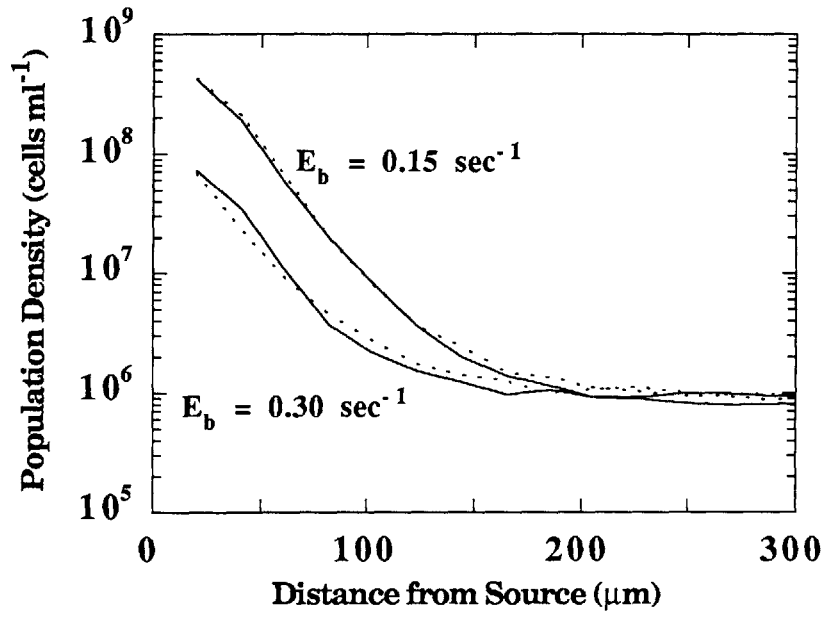


Figure A.9. Sensitivity of the calculated bacterial population density distributions to the variations in the exudate concentration distributions at the intermediate swimming speed $V = 40 \mu\text{m sec}^{-1}$. Bacterial motion is dependent on chemotactic swimming and shearing fluid motion. The solid lines show the bacterial population densities when the concentration distribution is a tube distorted by the shearing flow. The dashed lines show the density distribution when the exudate concentration distribution is described by the motionless diffusion solution. The shear strength E_b varies from $E_b = .15 \text{ sec}^{-1}$ to $E_b = .30 \text{ sec}^{-1}$.
(a) Normalized exudation rate F^* at the maximum value $F^* = 1140 \mu\text{m sec}$.
(b) Normalized exudation F^* reduced by a factor of two from the maximum value ($F^* = 570 \mu\text{m sec}$).

(a)



(b)

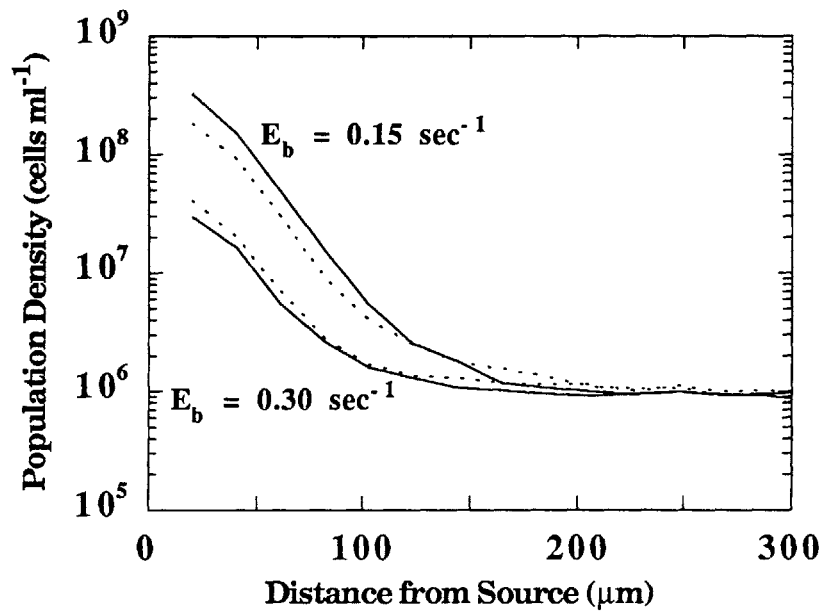
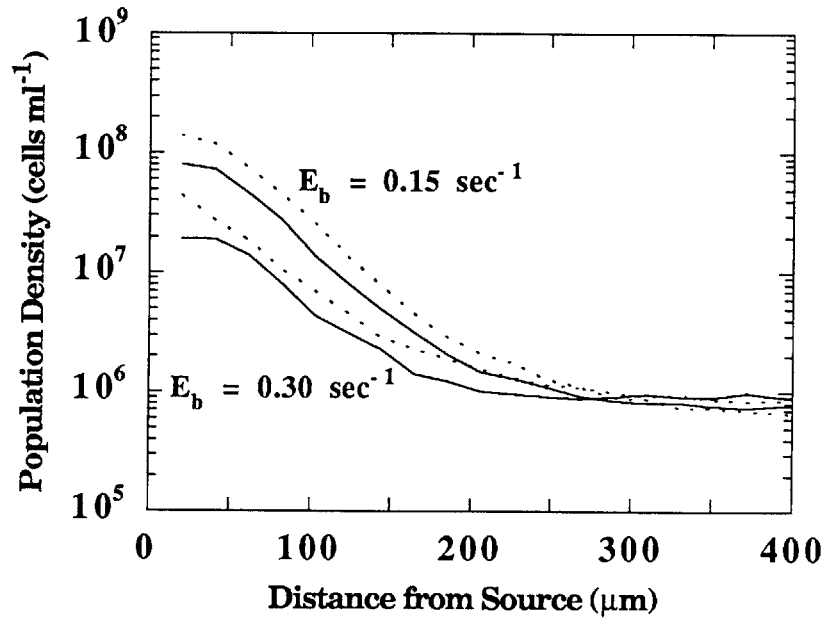
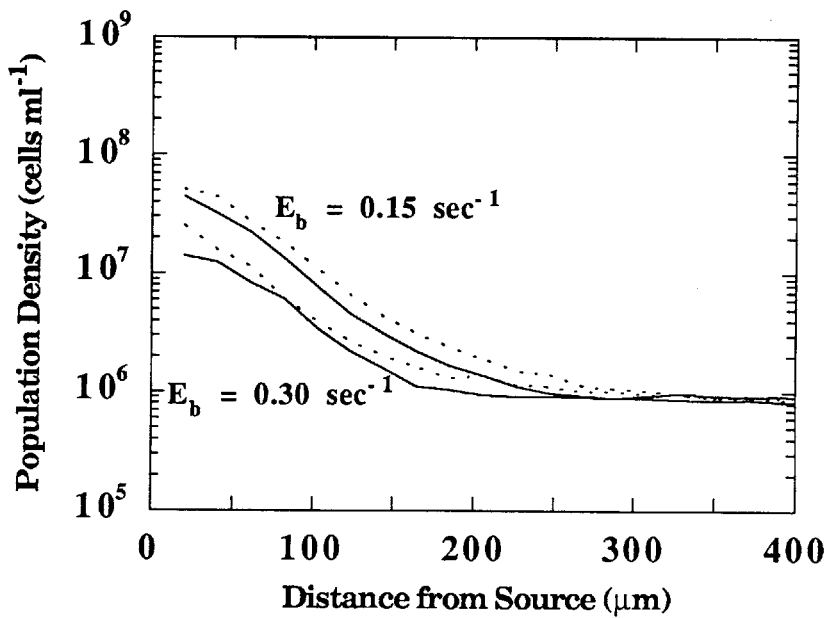


Figure A.10. Sensitivity of the calculated bacterial population density distributions to the variations in the exudate concentration distributions at the maximum swimming speed $V = 80 \mu\text{m sec}^{-1}$. Bacterial motion is dependent on chemotactic swimming and shearing fluid motion. The solid lines show the bacterial population densities when the concentration distribution is a tube distorted by the shearing flow. The dashed lines show the density distribution when the exudate concentration distribution is described by the motionless diffusion solution. The shear strength E_b varies from $E_b = .15 \text{ sec}^{-1}$ to $E_b = .30 \text{ sec}^{-1}$. (a) Normalized exudation rate F^* at the maximum value $F^* = 1140 \mu\text{m sec}$. (b) Normalized exudation F^* reduced by a factor of two from the maximum value ($F^* = 570 \mu\text{m sec}$).

(a)



(b)



Appendix B. Computer Codes

Computer codes are given for the bacterial clustering model and the program used to calculate the exact solution for a continuous point source into a fluid with a linear velocity distribution. The main program for the bacterial clustering model is called BCMD3. The main program calls the following subroutines:

- CHTAX - chemotaxis subroutine
- SHEAR - simulates shearing fluid motion
- CONC1 - calculates exudate distributions
- RMAL - generates a random number $N(0,1)$ from a normal distribution
- RANDOM - generates a random number from a uniform distribution
- PTOC - converts from polar to cartesian coordinates
- CTOP - converts from cartesian to polar coordinates
- GEN2 - randomly places bacteria in a spherical region
- SUMMRY - prints summary statistics
- TIMAV - calculates a time-averaged population density distribution
- HISTO - assembles histograms
- PRNPOS - prints the positions of a bacterial population
- READPO - reads the positions of a bacterial population

Additional documentation is available in the computer code. The main program for the calculation of concentration distributions surrounding a steady source in a fluid with a linear velocity distribution is called EXC1.FOR. See Chapter 2 for a description of this calculation. The main program has the following subroutines:

- EIGSRT - sorts the eigenvalues
- JACOBI - uses the Jacobi method to find eigenvalues
- ROT - transforms the shear tensor after a change in coordinates
- LUDCMP - solves a system of equations through matrix decomposition
- LUBKSB - back substitutes to solve a linear system of equations
- LUINV - finds the inverse of a matrix
- LUDET - finds the determinant of a matrix
- SETPL1 - determines the timing of each instantaneous pulse

The following subroutines were taken from the book "Numerical Recipes, The Art of Scientific Computing", by Press, W.H., B.P. Flannery, S.A. Teukolsky, and W.T. Vetterling, Cambridge University Press, 1986: EIGSRT, JACOBI, LUDCMP, LUBKSB, LUINV, and LUDET.

```

C
C      program BCMD3
C
C              SIMULATES THE MOVEMENT OF BACTERIA
C      INTRODUCES BACTERIA IN IN THE BACKGROUND
C      CONCENTRATION MODEL IS PULSE MODEL
C
C      NBAC      # BACTERIA IN PHYCO R<RB (# ADDED)
C      C          NEW CONCENTRATION
C      CON        OLD CONCENTRATION
C      NCELLS     # OF BACTERIA IN PHYCOSPHERE BACKGROUND
C      RB         PHYCOSPHERE RADIUS
C      A          PHYCO BAC DIRECTION
C      XP         AVERAGED CONCENTRATION
C      X          PHYCO BAC POSITION
C      EE         SHEAR TENSOR
C      V          SWIMMING SPEED
C      TNOT       AVERAGE RUN TIME
C      TTNOT      AVERAGE TWIDDLE TIME
C      TM         CONCENTRATION AVERAGING TIME
C      ALP        CHEMOTAXIS SENSITIVITY
C      XKD        CHEMORECEPTOR AFFINITY
C      XKMN       MINIMUM VALUE FOR KRUN
C      XKMX       MAXIMUM VALUE FOR KRUN
C
C      DM         DIFFUSION COEFF
C      DRC        IDENTITY MATRIX
C      RAV        AVERAGE POSITION OF PHYCO BAC EACH TIME
C      RMIN       MIN RAD FOR PLACEMENT OF NBAC BACTERIA
C      RMAX       MAX RAD FOR PLACEMENT OF NBAC BACTERIA
C      NCHFL      GIVES CHEMOTAXIS TYPE
C      CZ         BACKGROUND CONCENTRATION
C      MAXIN      MAX # OF BACTERIA IN PHYCO
C
C      CSUM       CUMULATIVE CONCENTRATION EXPOSURE
C      NTT1       HOW LONG EACH BAC HAS BEEN IN THIS TIME
C      NT1        HOW MANY TIMES BAC HAS BEEN THROWN OUT OF
VOLUME
C
C      NT2        HOW MANY TIMES BAC HAS ENTERED PHYCO (C
CRITERIA)
C      NTT2       TOTAL TIME SPENT IN PHYCO (C CRITERIA)
C      CSUM2      CUMULATIVE CONCEN
C
C      NT3        HOW MANY TIMES BAC BAC ENTERED PHYCO (R1
CRITERIA)
C      NTT3       TOTAL TIME SPENT IN PHYCO (R1 CRITERIA)
C      CSUM3      CUMULATIVE CONCEN
C
C      NT4        HOW MANY TIMES BAC ENTERED PHYCO (R2
CRITERIA)

```

```

C          NTT4          TOTAL TIME SPENT IN PHYCO          (R2
CRITERIA)
C          CSUM4          CUMULATIVE CONCEN
C
C          F1 F2 F3          C AND 2 R CRITERIA
C SUBROUTINES
C          SETPL1          FINDS TIME STEPS FOR EACH INSTANTANEOUS PULSE
C          GEN2           PLACES BACTERIA RANDOMLY IN SPHERICAL REGION
C          CONC1          CALCULATES CONCENTRATIONS USING SUPERPOSITION
C          PTOC           CONVERTS POLAR TO CARTESIAN
C          CTOP           CARTESIAN TO POLAR
C          CHTAX          CHEMOTAXIS SUBROUTINE
C          SHEAR          MOVEMENT IN SHEAR FIELD
C

```

```

PROGRAM BCMD
DIMENSION X(3500,3),A(3500,2)
DIMENSION C(3500),CON(3500),XP(3500)
DIMENSION NUMOUT(3500),ROLD(3500)
DIMENSION EE(3,3)
DIMENSION TAVC(50),TAVD(50)
DIMENSION CSUM(3500),CSUM2(3500),CSUM3(3500),CSUM4(3500)
INTEGER*2 NTT1(3500),NT1(3500),NT2(3500),NTT2(3500),NT3(3500)
INTEGER*2 NTT3(3500),NT4(3500),NTT4(3500)
COMMON /CONN/ DRC(3,3),DM,N1,N2
INTEGER*4 L
INTEGER SUMII,SUMIO,SUMOI,SUMOO,IT
CHARACTER*1 EXIN(3500),TEST,TCON,T
CHARACTER*8
BACHA(24),BACHB(24),BACHC(24),BACPOS(24),BACOUT(24)
CHARACTER*1 RORT(3500)
CHARACTER*8 XL
CHARACTER*8 BACTIM(24)
CHARACTER*12 FNAME(24),BOUT,SUMFIL
DATA T/' '/
DATA BACHA/'CA01.DAT','CA02.DAT','CA03.DAT','CA04.DAT',
*'CA05.DAT','CA06.DAT','CA07.DAT','CA08.DAT','CA09.DAT',
*'CA10.DAT','CA11.DAT','CA12.DAT','CA13.DAT','CA14.DAT',
*'CA15.DAT','CA16.DAT','CA17.DAT','CA18.DAT','CA19.DAT',
*'CA20.DAT','CA21.DAT','CA22.DAT','CA23.DAT','CA24.DAT'/
DATA BACHB/'CB01.DAT','CB02.DAT','CB03.DAT','CB04.DAT',
*'CB05.DAT','CB06.DAT','CB07.DAT','CB08.DAT','CB09.DAT',
*'CB10.DAT','CB11.DAT','CB12.DAT','CB13.DAT','CB14.DAT',
*'CB15.DAT','CB16.DAT','CB17.DAT','CB18.DAT','CB19.DAT',
*'CB20.DAT','CB21.DAT','CB22.DAT','CB23.DAT','CB24.DAT'/
DATA BACHC/'CC01.DAT','CC02.DAT','CC03.DAT','CC04.DAT',
*'CC05.DAT','CC06.DAT','CC07.DAT','CC08.DAT','CC09.DAT',
*'CC10.DAT','CC11.DAT','CC12.DAT','CC13.DAT','CC14.DAT',
*'CC15.DAT','CC16.DAT','CC17.DAT','CC18.DAT','CC19.DAT',
*'CC20.DAT','CC21.DAT','CC22.DAT','CC23.DAT','CC24.DAT'/
DATA BACPOS/'CP01.DAT','CP02.DAT','CP03.DAT','CP04.DAT',

```

```

*'CP05.DAT','CP06.DAT','CP07.DAT','CP08.DAT','CP09.DAT',
*'CP10.DAT','CP11.DAT','CP12.DAT','CP13.DAT','CP14.DAT',
*'CP15.DAT','CP16.DAT','CP17.DAT','CP18.DAT','CP19.DAT',
*'CP20.DAT','CP21.DAT','CP22.DAT','CP23.DAT','CP24.DAT'/
  DATA BACOUT/'CS01.DAT','CS02.DAT','CS03.DAT','CS04.DAT',
*'CS05.DAT','CS06.DAT','CS07.DAT','CS08.DAT','CS09.DAT',
*'CS10.DAT','CS11.DAT','CS12.DAT','CS13.DAT','CS14.DAT',
*'CS15.DAT','CS16.DAT','CS17.DAT','CS18.DAT','CS19.DAT',
*'CS20.DAT','CS21.DAT','CS22.DAT','CS23.DAT','CS24.DAT'/
  DATA BACTIM/'CT01.DAT','CT02.DAT','CT03.DAT','CT04.DAT',
*'CT05.DAT','CT06.DAT','CT07.DAT','CT08.DAT','CT09.DAT',
*'CT10.DAT','CT11.DAT','CT12.DAT','CT13.DAT','CT14.DAT',
*'CT15.DAT','CT16.DAT','CT17.DAT','CT18.DAT','CT19.DAT',
*'CT20.DAT','CT21.DAT','CT22.DAT','CT23.DAT','CT24.DAT'/
  DATA XPI /3.1415926/
  DATA MAXIN/3500/
  DO 10 I=1,3
  DO 10 J=1,3
  DRC(I,J)=0.0
10   IF(I.EQ.J)DRC(I,J)=1.0
  DM=1000.
  N1=3
  N2=3
  WRITE(*,*)' GIVE INPUT FILENAME'
  READ(*,'(A12)')SUMFIL
  OPEN(9,FILE=SUMFIL)
  WRITE(*,*)' GIVE SUMMARY FILENAME'
  READ(*,'(A12)')SUMFIL
  OPEN(10,FILE=SUMFIL)
  WRITE(*,*)' GIVE LABEL IDENTIFIER (a8) '
  READ(*,'(A8)')XL
  READ(9,*)NRS,NRUN
  NPOS=NRS-1
  DO 15 NR=1,NRUN
15  READ(9,1998)FNAM1(NR)
  CLOSE(9)
  DO 8000 NR=NRS,NRUN

C
C   INITIALIZE RUN
C
  NDIV=0
  NDIV1=0
  SUM=0.0
  JOUT=0
  TOUT=0.0
  MTOUT=0
  COUT=0.0
  NTAV=0
  DO 18 J=1,50
  TAVC(J)=0.0

```

```

18   TAVD(J)=0.0
      OPEN(2,FILE=BACOUT(NR))
      OPEN(3,FILE=BACHA(NR))
      OPEN(4,FILE=BACHB(NR))
C    UNIT 5 IS FOR BACTERIA POSITION
      OPEN(6,FILE=BACHC(NR))
      OPEN(12,FILE=BACTIM(NR))
      OPEN(9,FILE=FNAM1(NR))
      READ(9,*)VOLPHY,F1,F2,F3
      RB=(0.75*VOLPHY/XPI)**(1./3.)*1000.
      WRITE(*,*)'RADIUS PHYCOSPHERE=',RB
      READ(9,*)NBAC,NBAC1
      READ(9,*)V,TNOT,TM,ALP,TTNOT,XKD,DR,NCHFL
      READ(9,*)XKMN,XKMX
      READ(9,*)DTT,AR,CZ

C
C          CALCULATE CHEMOTAXIS PARAMETERS
C
      FR=EXP(-DTT/TM)
      IF(NCHFL.LE.5)THEN
        ALZ=ALOG(TNOT)
      ELSE
        ALZ=TNOT
      ENDIF

C
C          RUN LENGTH, ROTATIONAL FACTOR
C
      RAD=DTT*V
      FAC=SQRT(12.*DR*DTT)

C
      READ(9,*)NT,NTCZ
      READ(9,*)L,JOUTF
      RMIN=RANDOM(L)
      READ(9,*)RMIN,RMAX,RMIN1,RMAX1
      READ(9,'(I5,A12)')NINF1,BOUT
      IF(NINF1.NE.0)
        *OPEN(11,FILE=BOUT,ACCESS='SEQUENTIAL',FORM='BINARY')
        DO 1222 I=1,3
          READ(9,*)EE(I,1),EE(I,2),EE(I,3)
1222  CONTINUE
      READ(9,*)VS,FLUX
      FLUX1=FLUX
      FLUX=(FLUX1-CZ)*4.*XPI*AR*DM
      READ(9,*)NSF,NSI
      READ(9,*)NPF,NPI
      READ(9,*)NTF,NTI,ICD,CONF,CONL,IDD,DISF,DISL

C
C    ENTER 1 FOR MOTIONLESS DIFFN C W/SHEAR MOTION
C
      READ(9,*)IMDC

```

```

C
C           CALCULATE SHEAR FACTORS
C
      IF (VS.LE.0.0) THEN
      EB=0.5*(ABS (EE (1, 1)) +ABS (EE (2, 2)) +ABS (EE (3, 3)))
      IF (EB.GT.0.0) THEN
      SYM=2.*EE (2, 2) /EB
      XN=SQRT (DM/EB)
      ELSE
      SYM=-1.
      XN=1.E9
      ENDIF
      CN=FLUX/16./ATAN (1.0) /DM/XN
      ELSE
      EB=VS
      SYM=999.
      XN=DM/VS
      CN=FLUX/16./ATAN (1.0) /DM/XN
      EE (1, 1)=VS
      EE (2, 2)=999.
      ENDIF
      EB1=EB
      IF (IMDC.EQ.1) THEN
      EB1=0.0
      SYM=-1.
      XN=1.E9
      CN=FLUX/16./ATAN (1.0) /DM/XN
      ENDIF
      WRITE (*, *) ' EB, SYM, XN, CN', EB, SYM, XN, CN
      IF (NINF1.NE.0) THEN
      NBAC=NBAC+NBAC1
      WRITE (*, *) 'CALLING READPO'
      CALL READPO (NBAC, X (1, 1), X (1, 2), X (1, 3), A (1, 1),
* A (1, 2), C, XP, NTT1, CSUM)
      WRITE (*, *) NBAC, ' CELLS INITIALLY IN PHYCOSPHERE'
C
C           FINDING INITIAL CONCENTRATIONS AND INITIALIZING
C
      RUNFAC=TNOT/ (TNOT+TTNOT)
      IF (NINF1.NE.2) THEN
      DO 2028 I=1, NBAC
      NTT1 (I)=0
      CSUM (I)=0.0
2028 CONTINUE
      ENDIF
      DO 2029 I=1, NBAC
      NT1 (I)=0
      NT2 (I)=0
      NTT2 (I)=0
      NT3 (I)=0

```

```

    NTT3 (I)=0
    NT4 (I)=0
    NTT4 (I)=0
    IF (RANDOM (L) .LE .RUNFAC) THEN
    RORT (I)='R'
    ELSE
    RORT (I)='T'
    ENDIF
2029  CONTINUE
    DO 2039 I=1,NBAC
    CSUM2 (I)=0.0
    CSUM3 (I)=0.0
    CSUM4 (I)=0.0
    ROLD (I)=SQRT (X (I, 1) *X (I, 1)+X (I, 2) *X (I, 2)+X (I, 3) *X (I, 3) )
    EXIN (I)='Y'
    IF (ROLD (I) .LE .F2)NT3 (I)=1
    IF (ROLD (I) .LE .F3)NT4 (I)=1
    IF (ROLD (I) .LE .F1)NT2 (I)=1
2039  CONTINUE
C
    ELSE
C
C           FIND THE INITIAL POSITIONS AND DIRECTIONS
C           AND INITIALIZE CONCENTRATIONS
C
    NSTART=1
    CALL GEN2 (X,NSTART,NBAC,RMIN,RMAX,L,MAXIN)
    IF (NBAC1.GT.0)
*CALL GEN2 (X,NBAC+1,NBAC+NBAC1,RMIN1,RMAX1,L,MAXIN)
    NBAC=NBAC+NBAC1
    WRITE (*,*)NBAC,' CELLS INITIALLY IN PHYCOSPHERE'
C
C           FINDING INITIAL CONCENTRATIONS AND INITIALIZING
C
    RUNFAC=TNOT/(TNOT+TTNOT)
    DO 202 I=1,NBAC
    NTT1 (I)=0
    NT1 (I)=0
    NT2 (I)=0
    NTT2 (I)=0
    NT3 (I)=0
    NTT3 (I)=0
    NT4 (I)=0
    NTT4 (I)=0
    IF (RANDOM (L) .LE .RUNFAC) THEN
    RORT (I)='R'
    ELSE
    RORT (I)='T'
    ENDIF
    A (I, 1)=XPI*2.*RANDOM (L)

```

```

A(I,2)=ACOS(2.*RANDOM(L)-1.)
202 CONTINUE
CALL CONC1(NBAC,X,FLUX,C,CON,CZ,EB1,SYM,XN,CN,AR,MAXIN)
C
C      STEPPING BACTERIA
C
NCH=0
CALL CHTAX(NCH,NBAC,X,A,C,CON,XP,DTT,ALZ,ALP,XKD,RAD,
*AR,L,FR,TTNOT,RORT,XKMN,XKMX,MAXIN,MAXIN)
IF(EB.NE.0.0)CALL SHEAR(NBAC,X,EE,DTT,AR,MAXIN)
C
C      MOVED BACTERIA FIND CONCENTRATION
C
CALL CONC1(NBAC,X,FLUX,C,CON,CZ,EB1,SYM,XN,CN,AR,MAXIN)
C
C      INITIALIZE BACTERIA
C
IF(NCHFL.EQ.2 .OR. NCHFL.EQ.4 .OR. NCHFL.EQ.5)THEN
DO 204 I=1,NBAC
204 XP(I)=CON(I)/(CON(I)+XKD)
ELSE
DO 205 I=1,NBAC
205 XP(I)=XKD/(XKD+C(I))/(XKD+C(I))*(C(I)-CON(I))/DTT
ENDIF
DO 203 I=1,NBAC
C(I)=CON(I)
CSUM(I)=0.0
CSUM2(I)=0.0
CSUM3(I)=0.0
CSUM4(I)=0.0
ROLD(I)=SQRT(X(I,1)*X(I,1)+X(I,2)*X(I,2)+X(I,3)*X(I,3))
EXIN(I)='Y'
IF(ROLD(I).LE.F2)NT3(I)=1
IF(ROLD(I).LE.F3)NT4(I)=1
IF(ROLD(I).LE.F1)NT2(I)=1
203 CONTINUE
C
C      END INITIALIZATION
C
ENDIF
C
C      CALCULATE THE OUTER RADIUS
C
ROUT=RB*EXP(EB*DTT*1.1)+RAD*1.1
IF(SYM.EQ.999.)ROUT=RB+VS*DTT*1.1+RAD*1.1
WRITE(*,*)' OUTER RAD',ROUT
IF(NSF.LE.NT)
* WRITE(2,920)NR,XL,NR,NR,NR,NR,NR
C

```

```

C          START THE TIME LOOP
C
      WRITE(*,*) ' STARTING TIME LOOP '
      WRITE(*,*) '   RUN      STEP      SUMII SUMIO  SUMOI  SUMOO
AVDISI
      *N AVDISOU'
      DO 100 IT=1,NT
C
C          FIND CONCENTRATIONS
C
      WRITE(*,*) ' CALLING CONC '
      CALL CONC1(NBAC,X,FLUX,C,CON,CZ,EB1,SYM,XN,CN,AR,MAXIN)
C
C          PRINT THE POSITION OF EACH POINT
C
      IF((IT.GE.NPF).AND.(MOD(IT-NPF,NPI).EQ.0)) THEN
      NPOS=NPOS+1
      WRITE(*,*) ' PRINTING POSITIONS '
      OPEN(5,FILE=BACPOS(NPOS),ACCESS='SEQUENTIAL',FORM='BINARY')
      CALL
PRNPOS(NBAC,X(1,1),X(1,2),X(1,3),A(1,1),A(1,2),C,XP,NTT1,
      * CSUM)
      CLOSE(5)
      ENDIF
C
C          ADVANCE CONCENTRATION AND DURATION
C
      DO 135 IN=1,NBAC
      IF(IT.GE.NTCZ) CSUM(IN)=CSUM(IN)+C(IN)
      IF(EXIN(IN).EQ.'Y') THEN
      NTT1(IN)=NTT1(IN)+1
      ELSE
      NTT1(IN)=1
      ENDIF
135  CONTINUE
C
C          CHEMOTAX
C
      WRITE(*,*) ' CALLING CHTAX '
      NCH=NCHFL
      CALL CHTAX(NCH,NBAC,X,A,C,CON,XP,DTT,ALZ,ALP,XKD,RAD,AR
*,L,FR,TTNOT,RORT,XKMN,XKMX,MAXIN,MAXIN)
C
C          ADVECT IN SHEAR FLOW
C
      WRITE(*,*) ' CALLING SHEAR '
      IF(EB.NE.0.0) CALL SHEAR(NBAC,X,EE,DTT,AR,MAXIN)
C
C          START CRITTER LOOP
C

```

```

C      WRITE(*,*) ' START CRITTER LOOP '
SUMIO=0
SUMII=0
SUMOI=0
SUMIO=0
SUMOO=0
NOUT=0
RSUMIN=0.0
RSUMOU=0.0
DO 50 IN=1,NBAC
R=SQRT(X(IN,1)*X(IN,1)+X(IN,2)*X(IN,2)+X(IN,3)*X(IN,3))
C
C      CHECK FOR BACTERIA OUT OF BOUNDS
C
IF(R.GT.RB) THEN
  RSUMOU=RSUMOU+R
  IF (EXIN(IN) .EQ. 'Y') THEN
    NT1(IN)=NT1(IN)+1
    SUMIO=SUMIO+1
    IF (IT.GE.JOUTF) THEN
      JOUT=JOUT+1
      TOUT=TOUT+FLOAT(NTT1(IN))*DTT
      MTOUT=MAX0(MTOUT,NTT1(IN))
      COUT=COUT+CSUM(IN)/FLOAT(IT)
    ENDIF
    EXIN(IN)='N'
  ELSE
    SUMOO=SUMOO+1
  ENDIF
  A(IN,1)=XPI*2.*RANDOM(L)
  A(IN,2)=ACOS(2.*RANDOM(L)-1.)
  NOUT=NOUT+1
  NUMOUT(NOUT)=IN
ELSE
  RSUMIN=RSUMIN+R
  IF (EXIN(IN) .EQ. 'N') THEN
    SUMOI=SUMOI+1
    EXIN(IN)='Y'
  ELSE
    SUMII=SUMII+1
  ENDIF
ENDIF
ENDIF
C
C
C
C
C      ACCOUNT FOR ROTATIONAL DIFFUSION
C
A(IN,1)=A(IN,1)+(RANDOM(L)-0.5)*FAC
A(IN,2)=A(IN,2)+(RANDOM(L)-0.5)*FAC
C

```

```

C          CHECK FOR BACTERIA IN PHYCO (C AND R CRITERIA)
C
      IF (R.LE.F2) THEN
      NTT3 (IN)=NTT3 (IN) +1
      CSUM3 (IN)=CSUM3 (IN) +C (IN)
      IF (ROLD (IN) .GT.F2) NT3 (IN) =NT3 (IN) +1
      ENDIF
      IF (R.LE.F3) THEN
      NTT4 (IN)=NTT4 (IN) +1
      CSUM4 (IN)=CSUM4 (IN) +C (IN)
      IF (ROLD (IN) .GT.F3) NT4 (IN) =NT4 (IN) +1
      ENDIF
      IF (R.LE.F1) THEN
      NTT2 (IN)=NTT2 (IN) +1
      CSUM2 (IN)=CSUM2 (IN) +C (IN)
      IF (ROLD (IN) .GT.F1) NT2 (IN) =NT2 (IN) +1
      ENDIF
      ROLD (IN)=R
C
C          END CRITTER LOOP
C
50    CONTINUE
C
C          PLACE THE OUTER GUYS
C
      DO 4600 IN=1,NOUT
4500  X1NEW=(RANDOM(L)-0.5)*2.*ROUT
      X2NEW=(RANDOM(L)-0.5)*2.*ROUT
      X3NEW=(RANDOM(L)-0.5)*2.*ROUT
      R=SQRT (X1NEW*X1NEW+X2NEW*X2NEW+X3NEW*X3NEW)
      IF (R.LT.RB) GOTO 4500
      IF (R.GT.ROUT) GOTO 4500
      CALL PTOC (RAD,A (IN,1),A (IN,2),AA,BB,CC)
      X1NEW=X1NEW+AA
      X2NEW=X2NEW+BB
      X3NEW=X3NEW+CC
      IF (SYM.EQ.999) THEN
      X3NEW=X3NEW+VS*DTT
      ELSE
      X1NEW=X1NEW+DTT*(EE (1,1)*X1NEW+EE (1,2)*X2NEW+EE (1,3)*X3NEW)
      X2NEW=X2NEW+DTT*(EE (2,1)*X1NEW+EE (2,2)*X2NEW+EE (2,3)*X3NEW)
      X3NEW=X3NEW+DTT*(EE (3,1)*X1NEW+EE (3,2)*X2NEW+EE (3,3)*X3NEW)
      ENDIF
      R=SQRT (X1NEW*X1NEW+X2NEW*X2NEW+X3NEW*X3NEW)
      IF (R.GT.RB) GOTO 4500
      X (NUMOUT (IN),1)=X1NEW
      X (NUMOUT (IN),2)=X2NEW
      X (NUMOUT (IN),3)=X3NEW
4600  CONTINUE
C

```

```

C          DO STATISTICS
C
IF ( (MOD (IT-NSF, NSI) .EQ. 0) .AND. (IT.GE.NSF) ) THEN
  WRITE (*, *) ' DOING STATISTICS '
  SUMR=0.0
  SUMF1=0.0
  SUMF2=0.0
  SUMF3=0.0
  CYSUM=0.0
  CZSUM=0.0
  DO 5000 IN=1, NBAC
  CYSUM=CYSUM+C (IN)
  IF (IT.GE.NTCZ) CZSUM=CZSUM+C (IN)
  RA=SQRT (X (IN, 1) *X (IN, 1) +X (IN, 2) *X (IN, 2) +X (IN, 3) *X (IN, 3) )
  SUMR=SUMR+RA
  IF (RA.LE.F2) SUMF2=SUMF2+1.
  IF (RA.LE.F3) SUMF3=SUMF3+1.
  IF (RA.LE.F1) SUMF1=SUMF1+1.
5000 CONTINUE
  CYSUM=CYSUM/FLOAT (NBAC)
  IF (IT.GE.NTCZ) CZSUM=CZSUM/FLOAT (IT-NTCZ+1) /FLOAT (NBAC)
  RAV=SUMR/FLOAT (NBAC)
  SUMF1=SUMF1/FLOAT (NBAC)
  SUMF2=SUMF2/FLOAT (NBAC)
  SUMF3=SUMF3/FLOAT (NBAC)
  TIM=FLOAT (IT) *DTT
  IF (IT.GE.NTCZ) THEN
  WRITE (2, 998) TIM, RAV, SUMF1, SUMF2, SUMF3, CYSUM, CZSUM
  ELSE
  WRITE (2, 998) TIM, RAV, SUMF1, SUMF2, SUMF3, CYSUM
  ENDIF
  ENDIF
C
C          FIND THE TIME AVERAGES
C
IF ( (MOD (IT-NTF, NTF) .EQ. 0) .AND. (IT.GE.NTF) ) THEN
  WRITE (*, *) ' FINDING TIME AVERAGES '
  NTAV=NTAV+1
  DISINC=(DISL-DISF) /FLOAT (IDD-1)
  CONINC=(CONL/CONF) ** (1./FLOAT (ICD) )
  DO 350 IN=1, NBAC
  R=SQRT (X (IN, 1) *X (IN, 1) +X (IN, 2) *X (IN, 2) +X (IN, 3) *X (IN, 3) )
  DO 300 I=1, IDD
  IF (R.LE.DISINC*FLOAT (I-1) +DISF) THEN
  TAVD (I) =TAVD (I) +1.
  GOTO 310
  ENDIF
300 CONTINUE
310 DO 330 I=1, ICD-1
  IF (C (IN) .GE.CONF*CONINC** (I) ) THEN

```

```

TAVC(I)=TAVC(I)+1.
ENDIF
330 CONTINUE
IF(C(IN).GE.CONL)TAVC(ICD)=TAVC(ICD)+1
350 CONTINUE
ENDIF
C
C           END TIME LOOP
C
NOUT=MAX0(1,SUMIO+SUMOO)

IF(MOD(IT,10).EQ.1)WRITE(*,970)NR,NRUN,IT,NT,SUMII,SUMIO,SUMOI,
*SUMOO,RSUMIN/FLOAT(SUMII+SUMOI),RSUMOU/FLOAT(NOUT)
100 CONTINUE
WRITE(*,*)' END TIME LOOP'
C
C           PRINT SUMMARY STATISTICS
C
WRITE(*,*)' CALLING SUMMRY'
CALL SUMMRY(NR,NBAC,VOLPHY,F1,F2,F3,V,TNOT,TM,ALP,TTNOT,XKD,
*NCHFL,XKMN,XKMX,EB,SYM,FLUX1,AR,CZ,CSUM,CSUM2,CSUM3,NTT1,X,XP,
*NTT2,NT3,NTT3,COUT,JOUT,TOUT,MTOUT,DTT,C,NT,NT2,NT4,NTT4,CSUM4,
*NT1,RB,NTCZ)
C
C           FIND HISTOGRAMS
C
WRITE(*,*)' CALLING HISTO'
WRITE(3,900)NR,NR,NR,F1,NR,F2,NR,F3
900 FORMAT(1X,I2,'CON ',I2,'TOTL ',3(I2,'C',E9.4,1X))
WRITE(4,890)NR,NR,NR,NR,NR,NR,NR,NR,NR
890 FORMAT(1X,I2,'PHY ',I2,'#PHY ',I2,'F1 ',I2,'#IN1 ',I2,'F2
',I2,
*'#IN2 ',I2,'F3 ',I2,'#IN3 ')
WRITE(6,880)NR,NR,NR,NR,NR,NR,NR,NR,NR
880 FORMAT(1X,I2,'TMPHY ',I2,'#PHY ',I2,'TF1 ',I2,'#TM1 ',I2,'TF2
',
*I2,'#TM2 ',I2,'TF3 ',I2,'#TM3 ')
CALL HISTO(CSUM,CSUM2,CSUM3,CSUM4,NT1,NT2,NT3,NT4,NTT1,NTT2,
*NTT3,NTT4,NBAC,DTT,NT)
C
C           PRINT TIME AVERAGES
C
WRITE(*,*)' CALLING TIMAV'
IF(NT.GE.NTF)CALL TIMAV(NR,TAVD,TAVC,ICD,IDD,CONF,CONL,DISF,
*DISL,AR,NTAV,NBAC,XL)
C
C           CLOSE OUTPUT FILES
C
CLOSE(2)

```

```
CLOSE (3)
CLOSE (4)
CLOSE (6)
CLOSE (9)
CLOSE (12)
C
8000 CONTINUE
110  FORMAT(4F7.2,5E11.4)
320  FORMAT(F7.2,14F8.1)
920  FORMAT(' TIME ',I2,'AV',A8,' ',I2,'F1 ',I2,'F2 ',I2,'F3 ',I2;
*'INCN ',I2,'AVCN ')
940  FORMAT(' TIME ',I2,'TOT')
950  FORMAT(1X,F10.4,1X,E12.5,1X,E12.5)
970  FORMAT(I2,' OF',I2,1X,I6,' OF',I6,4I6,2F10.2)
980  FORMAT(F8.3,1X,4I5)
998  FORMAT(2F10.3,3F7.4,2E12.5,F10.2)
1998 FORMAT(A12)
125  FORMAT(E11.4,1X,10F8.2)
      STOP
      END
```

```

SUBROUTINE CHTAX (NCHFL, NBAC, X, A, C, CON, XP, DTT, ALZ, ALP, XKD, RAD,
* AR, L, FR, TTNOT, RORT, XKMN, XKMX, MAX1, MAX2)
DIMENSION X (MAX1, 3), A (MAX1, 2)
DIMENSION C (MAX1), CON (MAX1), XP (MAX1)
CHARACTER*1 RORT (MAX1)
ITM=ITM+1
TIME=FLOAT (ITM) *DTT
XPI=4.*ATAN (1.)
STP=RAD*ALZ/DTT
TM=-DTT/ALOG (FR)
XKNOT=EXP (-ALZ)
IF (TTNOT.LE.DTT) THEN
XPTT=1.0
ELSE
XPTT=DTT/TTNOT
ENDIF
DO 50 IN=1, NBAC
C
C      TWIDDLERS
C
IF (RORT (IN) .EQ. 'T') THEN
IF (NCHFL.EQ.4 .OR. NCHFL.EQ.2 .OR. NCHFL.EQ.5) THEN
XPONE=C (IN) / (C (IN) +XKD)
XP (IN) = (1.-FR) *XPONE+FR*XP (IN)
ENDIF
IF (RANDOM (L) .LE. XPTT) THEN
C
C      RUN
C
RORT (IN) = 'R'
CALL PTOC (RAD, A (IN, 1), A (IN, 2), AA, BB, CC)
C      WRITE (*, *) ' R, RAD, A', AA, BB, CC
X (IN, 1) =X (IN, 1) +AA
X (IN, 2) =X (IN, 2) +BB
X (IN, 3) =X (IN, 3) +CC
ELSE
C
C      TUMBLE
C      CHOOSE NEW ANGLES
C
A (IN, 2) =ACOS (2.*RANDOM (L) -1.)
A (IN, 1) =2.*RANDOM (L) *XPI
ENDIF
C
C      RUNNERS
C
ELSE
C
C      CALCULATE RUN LENGTH

```

```

C
IF (NCHFL.EQ.0) THEN
C
C   UNBIASED RANDOM WALK
C
  XX=ALZ
  IF (XX.GT.20.) XX=20.
  IF (XX.LT.-20.) XX=-20.
  XPT=DTT/EXP (XX)

C
C   BROWN & BERG (EXACT DPDT THEN TIME AVERAGED)
C   and now with a maximum (10/15)
C
ELSEIF (NCHFL.EQ.1) THEN
  DPDT=XKD / (XKD+C (IN)) / (XKD+C (IN)) * (C (IN) -CON (IN)) /DTT
  XP (IN) = (1.-FR) *DPDT+FR*XP (IN)
  XX=ALZ+ALP*XP (IN)
  IF (EXP (-XX) .GT.XKMX) XX= -ALOG (XKMX)
  IF (XX.LT.-20.) XX=-20.
  XPT=DTT/EXP (XX)

C
C   B&B W/ DIFFERENT DPDT CALCULATION
C   AND NOW A MAXIMUM AS WELL (6/29)
C
ELSEIF (NCHFL.EQ.2) THEN
  XPONE=C (IN) / (C (IN) +XKD)
  XP (IN) = (1.-FR) *XPONE+FR*XP (IN)
  DPDT= (XPONE-XP (IN)) /TM
  XX=ALZ+ALP*DPDT
  IF (EXP (-XX) .GT.XKMX) XX= -ALOG (XKMX)
  IF (XX.LT.-20.) XX=-20.
  XPT=DTT/EXP (XX)

C
C   BLOCK WITH OLD DPDT (EXACT DPDT THEN TIME AVERAGED)
C
ELSEIF (NCHFL.EQ.3) THEN
  DPDT=XKD / (XKD+C (IN)) / (XKD+C (IN)) * (C (IN) -CON (IN)) /DTT
  XP (IN) = (1.-FR) *DPDT+FR*XP (IN)
  XKR=XKNOT* (1.-ALP*XP (IN))
  IF (XKR.LT.0.0) XKR=0.0
  XPT=DTT*XKR

C
C   NEW CHEMOTAXIS FROM BLOCK WITH UPPER AND LOWER LIMITS
C
ELSEIF (NCHFL.EQ.5) THEN
  XPONE=C (IN) / (C (IN) +XKD)
  XP (IN) = (1.-FR) *XPONE+FR*XP (IN)
  DPDT= (XPONE-XP (IN)) /TM
  IF (DPDT.GE.0) XKR=XKNOT+ (XKMN-XKNOT) * (1.-EXP (ALP*DPDT*XKNOT/

```

```

* (XKMN-XKNOT) ) )
  IF (DPDT.LT.0) XKR=XKNOT+(XKMX-XKNOT) * (1.-EXP (ALP*DPDT*XKNOT/
* (XKMX-XKNOT) ) )
  XPT=DTT*XKR
C
C      NEW CHEMOTAXIS FROM BLOCK ET AL. '83
C
ELSEIF (NCHF.L.EQ.4) THEN
  XPONE=C (IN) / (C (IN) +XKD)
  XP (IN) = (1.-FR) *XPONE+FR*XP (IN)
  DPDT= (XPONE-XP (IN) ) /TM
  XKR=XKNOT*(1.-ALP*DPDT)
  IF (XKR.LT.0.0) XKR=0.0
  XPT=DTT*XKR
C
C      SIMPLE CHEMOTAXIS
C
ELSEIF (NCHF.L.EQ.6) THEN
  IF (ALP.EQ.0.0) THEN
    RAD1= (-RAD) *C (IN) / (1.+C (IN) )
  ELSE
    DPDT=XKD/ (XKD+C (IN) ) / (XKD+C (IN) ) * (C (IN) -CON (IN) ) /DTT
    XP (IN) = (1.-FR) *DPDT+FR*XP (IN)
    RAD1= (-RAD) *XP (IN) / (XP (IN) +ALP)
  ENDIF
ELSE
  RAD1=-RAD
ENDIF
C
C      DECIDE WHETHER RUN ENDS
C
IF (NCHF.L.LE.5) THEN
  IF (RANDOM (L) .LT.XPT) THEN
C
C      TUMBLE
C      CHOOSE NEW ANGLES
C
    A (IN, 2) =ACOS (2. *RANDOM (L) -1.)
    A (IN, 1) =2. *RANDOM (L) *XPI
    RORT (IN) = 'T'
    IF (RANDOM (L) .LE.XPTT) THEN
      RORT (IN) = 'R'
      CALL PTOC (RAD, A (IN, 1) , A (IN, 2) , AA, BB, CC)
      X (IN, 1) =X (IN, 1) +AA
      X (IN, 2) =X (IN, 2) +BB
      X (IN, 3) =X (IN, 3) +CC
    ENDIF
  ELSE
C
C      RUN

```

```

C
      CALL PTOC (RAD, A (IN, 1), A (IN, 2), AA, BB, CC)
C
      WRITE (*, *) ' R, RAD, A', AA, BB, CC
      X (IN, 1) = X (IN, 1) + AA
      X (IN, 2) = X (IN, 2) + BB
      X (IN, 3) = X (IN, 3) + CC
      ENDIF

C
      SIMPLE CHEMOTAXIS
C
      ELSE
      CALL CTOP (X (IN, 1), X (IN, 2), X (IN, 3), RR, TH, XPH)
      CALL PTOC (RAD1, TH, XPH, AA, BB, CC)
      X (IN, 1) = X (IN, 1) + AA
      X (IN, 2) = X (IN, 2) + BB
      X (IN, 3) = X (IN, 3) + CC
      TH = ACOS (2. * RANDOM (L) - 1.)
      XPH = 2. * RANDOM (L) * XPI
      CALL PTOC (STP, TH, XPH, AA, BB, CC)
      X (IN, 1) = X (IN, 1) + AA
      X (IN, 2) = X (IN, 2) + BB
      X (IN, 3) = X (IN, 3) + CC
      ENDIF
      ENDIF

C
      REFLECT IF NECESSARY
C
      R = SQRT (X (IN, 1) * X (IN, 1) + X (IN, 2) * X (IN, 2) + X (IN, 3) * X (IN, 3))
C
      TUMBLE WITH REFLECTION
C
      IF (R.LT.AR) THEN
      CALL CTOP (X (IN, 1), X (IN, 2), X (IN, 3), DIST, A1, A2)
      R = 2. * AR - DIST
      CALL PTOC (R, A1, A2, X (IN, 1), X (IN, 2), X (IN, 3))
      A (IN, 2) = ACOS (2. * RANDOM (L) - 1.)
      A (IN, 1) = 2. * RANDOM (L) * XPI
      ENDIF
50  CONTINUE
      RETURN
      END

```

```

C
C      SUBROUTINE SHEAR
C      MOVES BACTERIA IN SHEAR FLOW
C
C      SUBROUTINE SHEAR(NBAC,X,EE,DTT,AR,MAX)
C      DIMENSION X(MAX,3),EE(3,3),U(3),UE(3)
C
C      FIND MAXIMUM SHEAR RATE
C
C      MOVE FOR SINKING EE(1,1)=VS
C
C      IF(EE(2,2).EQ.999.) THEN
C      VS=EE(1,1)
C      NMAX=0
C      NMAX1=0
C      DO 5 N=1,NBAC
C      R=SQRT(X(N,1)*X(N,1)+X(N,2)*X(N,2)+X(N,3)*X(N,3))
C      AR1=AR/R
C
C      LIMIT STEP TO .01(R-AR)
C
C      NS=IFIX(100.*DTT*VS/(R-AR))
C      NS=MAX0(NS,1)
C      NS=MIN0(NS,10)
C      IF(NS.EQ.10)NMAX=NMAX+1
C      WRITE(*,*)'NS=',NS
C      DO 5 IT=1,NS
C      R=SQRT(X(N,1)*X(N,1)+X(N,2)*X(N,2)+X(N,3)*X(N,3))
C      IF(R.LE.AR) THEN
C      NMAX1=NMAX1+1
C      CALL CTOP(X(N,1),X(N,2),X(N,3),R,XTH,XPH)
C      R=2.*AR-R
C      CALL PTOC(R,XTH,XPH,X(N,1),X(N,2),X(N,3))
C      ENDIF
C      AR1=AR/R
C      X(N,1)=X(N,1)-VS*DTT/FLOAT(NS)*.75*(AR1-AR1**3)/R/R*
C      *X(N,1)*X(N,3)
C      X(N,2)=X(N,2)-VS*DTT/FLOAT(NS)*.75*(AR1-AR1**3)/R/R*
C      *X(N,2)*X(N,3)
C      X(N,3)=X(N,3)+DTT/FLOAT(NS)*VS*(1-.75*AR1-.25*AR1**3-.75*
C      *(AR1-AR1**3)/R/R*X(N,3)*X(N,3))
C      CONTINUE
C      IF(NMAX1.GT.0)WRITE(*,*)'#NS10 #COLL',NMAX,NMAX1
C      RETURN
C      ENDIF
C
C      MOVE FOR SHEAR
C
C      EMAX=EE(1,1)

```

```

DO 10 I=1,3
DO 10 J=1,3
10 EMAX=AMAX1(EMAX,EE(I,J))
C
C          LIMIT TIME STEP TO .5% CHAR TIME
C
NS=IFIX(200.0*DTT*EMAX)
IF(NS.LT.1)NS=1
C   WRITE(*,*)' SHEAR STEPS=',NS
C   WRITE(*,*)' NBAC,DT',NBAC,DT
DT=DTT/FLOAT(NS)
C
C          START TIME LOOP
C
DO 200 I=1,NS
DO 100 N=1,NBAC
C
C          FIND NORMALIZED DISTANCE
C
ARR=AR/SQRT(X(N,1)*X(N,1)+X(N,2)*X(N,2)+X(N,3)*X(N,3))
IF(ARR.GT.0.5)THEN
C
C   DO DISTURBANCE VELOCITY FOR SHEAR
C
SUM=0.0
DO 20 J=1,3
DO 20 K=1,3
20   SUM=SUM+EE(J,K)*X(N,K)*X(N,J)
DO 25 J=1,3
25   UE(J)=X(N,J)*2.5*(ARR**7-ARR**5)*SUM/AR/AR
FAC=ARR**5
ELSE
FAC=0.0
DO 28 J=1,3
28   UE(J)=0.0
ENDIF
C   WRITE(*,*)' I=',I
C
C          FIND VELOCITY
C
DO 35 J=1,3
35   U(J)=0.0
DO 40 J=1,3
DO 40 K=1,3
40   U(J)=U(J)+EE(J,K)*X(N,K)
C
C          MOVE BACTERIA
C
DO 50 J=1,3
50   X(N,J)=X(N,J)+(U(J)*(1-FAC)+UE(J))*DT

```

```
100 CONTINUE  
200 CONTINUE  
RETURN  
END
```

```

SUBROUTINE CONC1(NBAC,X,FLUX,C,CON,CZ,EB,SY,XN,CN,AR,MAXIN)
DIMENSION X(MAXIN,3),C(MAXIN)
DIMENSION CON(MAXIN)
COMMON /CONN/ DRC(3,3),DM,N1,N2
C
C      ZERO CONCENTRATIONS AND MOVE C TO CON
C
DO 65 IP=1,NBAC
CON(IP)=C(IP)
65  C(IP)=CZ
C
C      DO SINKING CONCENTRATIONS EB=SINKING VELOCITY VS
C
IF(SY.EQ.999.)THEN
DO 67 IP=1,NBAC
R=SQRT(X(IP,1)*X(IP,1)+X(IP,2)*X(IP,2)+X(IP,3)*X(IP,3))
67  C(IP)=C(IP)+CN*XN/R*EXP((X(IP,3)*EB-R*EB)/2./DM)
RETURN
ENDIF
C
C      FIND CONCENTRATIONS FOR MOTIONLESS DIFFUSION
C
IF(EB.EQ.0.0)THEN
DO 70 IP=1,NBAC
R=SQRT(X(IP,1)*X(IP,1)+X(IP,2)*X(IP,2)+X(IP,3)*X(IP,3))
70  C(IP)=C(IP)+CN*XN/R
RETURN
ENDIF
C
C      APPROXIMATE ANALYTICAL SOLUTION
C
C      TUBE
C
IF(SY.LT.0.0)THEN
C      WRITE(*,*)' XN=',XN
DO 75 IP=1,NBAC
X1=ABS(X(IP,1))
R1=SQRT(X(IP,2)*X(IP,2)+X(IP,3)*X(IP,3))
R1=AMAX1(R1,AR)
R=SQRT(X(IP,1)*X(IP,1)+X(IP,2)*X(IP,2)+X(IP,3)*X(IP,3))
IF(X1.LT.AR) THEN
FAC=(-SY)*(SY+2.)*.5
AA=CN*XN/AR*FAC
ELSE
AA=CN*XN/X1*(XN/(X1+XN) - X1/(X1+XN)*.5*SY*(SY+2.))
ENDIF
BB=EB/2./DM*(.5*SY*X(IP,2)*X(IP,2)-(1+.5*SY)*X(IP,3)*X(IP,3))
C(IP)=C(IP) + CN*XN/R * EXP((-R/XN)**3) + (1.-EXP((-R/XN)**3))
**AA*EXP(BB)*(1+XN/(X1+XN)*(AR/R1-1))

```

```

75  CONTINUE
    RETURN
    ENDIF

C
C          DISK
C

    IF (SY.EQ.1.0) THEN
    DO 77 IP=1,NBAC
    R1=SQRT (X (IP, 1) *X (IP, 1) +X (IP, 2) *X (IP, 2))
    R11=AMAX1 (R1, AR)
    X3=AMAX1 (ABS (X (IP, 3)), AR)
    R=SQRT (X (IP, 1) *X (IP, 1) +X (IP, 2) *X (IP, 2) +X (IP, 3) *X (IP, 3))
    AA=(CN*XN/R11*XN/(R1+XN) + R1/(R1+XN)*CN*SQRT (2./ATAN (1.)) *XN*
*XN/R11/R11) *0.75
    BB=EB/2./DM*X3*X3
    C (IP)=C (IP) + CN*XN/R * EXP ((-R/XN)**3) + (1.-EXP ((-R/XN)**3))
**AA*EXP (-BB) * (1+XN/(R1+XN)) * (AR/X3-1))
77  CONTINUE
    RETURN
    ENDIF

C
C          CAN'T DO NON-AXISYMMETRIC DISKS
C

    WRITE (*, *) ' CANT DO NON-AXISYMMETRIC DISKS, SYM=', SY
    STOP
    END

```

```

C
C           FUNCTION RMAL
C
C           GENERATES A NUMBER FROM A NORMAL DISTRIBUTION
WITH
C           MEAN =0 AND VARIANCE=1.0
C
FUNCTION RMAL(L)
INTEGER*4 L
X=0.0
DO 10 I=1,12
10 X=X+RANDOM(L)
RMAL=X-6.0
RETURN
END

C
C           FUNCTION RANDOM
C
C           GENERATES A RANDOM NUMBER BETWEEN 0 AND 1
C
C           NEEDS A SEED WHICH GETS UPDATED
C
FUNCTION RANDOM(L)
INTEGER*4 L
DOUBLE PRECISION DL
DL=DMOD(16807.0D0*DBLE(L),2147483647.0D0)
L=IDINT(DL)
RANDOM=SNGL(DL*4.6566128752458D-10)
RETURN
END

C
C           SUBROUTINE PTOC
C
C           CONVERTS FROM POLAR(R, THETA, PHI) TO
C           CARTESIAN
C
SUBROUTINE PTOC(R, THETA, PHI, A, B, C)
REAL PHI
A=R*COS(THETA)*SIN(PHI)
B=R*SIN(THETA)*SIN(PHI)
C=R*COS(PHI)
RETURN
END

C
C           CONVERTS FROM CARTESIAN TO POLAR
C           (RADIUS, ANGLE W/XAXIS, ANGLE W/ZAXIS)
C
SUBROUTINE CTOP(X1, X2, X3, R, THETA, PHI)
REAL PHI
R=SQRT(X1*X1+X2*X2+X3*X3)

```

```
PHI=ACOS (X3/R)
THETA=ACOS (X1/R/SIN (PHI))
IF (X2.LT.0.0) THETA=-THETA
RETURN
END
```

```
SUBROUTINE GEN2 (X, NSTART, NBAC, RMIN, RMAX, L, MAX)
DIMENSION X (MAX, 3)
INTEGER*4 L
10 I=NSTART
20 IF (I.GT.NBAC-NSTART+1) RETURN
X(I,1)=2.*RMAX*(RANDOM(L)-0.5)
X(I,2)=2.*RMAX*(RANDOM(L)-0.5)
X(I,3)=2.*RMAX*(RANDOM(L)-0.5)
R=SQRT(X(I,1)*X(I,1)+X(I,2)*X(I,2)+X(I,3)*X(I,3))
IF (R.LT.RMIN) GOTO 20
IF (R.GT.RMAX) GOTO 20
I=I+1
GOTO 20
END
```

```

SUBROUTINE
SUMMRY (NR, NBAC, VOLPHY, F1, F2, F3, V, TNOT, TM, ALP, TTNOT, XKD,
      *NCHFL, XKMN, XKMX, EB, SYM, FLUX1, AR, CZ, CSUM, CSUM2, CSUM3, NTT1, X, XP,
*NTT2, NT3, NTT3, COUT, JOUT, TOUT, MTOUT, DTT, C, NT, NT2, NT4, NTT4, CSUM4,
*NT1, RB, NTCZ)
  DIMENSION X(3500,3), C(3500)
  DIMENSION XP(3500)
  DIMENSION CSUM(3500), CSUM2(3500), CSUM3(3500), CSUM4(3500)
  INTEGER*2 NTT1(3500), NT2(3500), NTT2(3500), NT3(3500)
  INTEGER*2 NTT3(3500), NT4(3500), NTT4(3500), NT1(3500)
C
C      WRITE SUMMARY
C
  WRITE(10,*) ' RUN ', NR, ' FINAL # BACTERIA', NBAC
  WRITE(10, '( ' ' RB F1 F2 F3 ' ', 4F9.1, ) ' ) RB, F1, F2, F3
  WRITE(10, '( ' ' V, TNOT, TM, ALP ' ', 4F10.3 ' ) ' ) V, TNOT, TM, ALP
  WRITE(10,*) ' TTNOT, XKD, NCHFL', TTNOT, XKD, NCHFL
  WRITE(10,*) ' XKMN, XKMX', XKMN, XKMX
  WRITE(10,*) ' EB=', EB, ' S=', SYM
  WRITE(10,*) ' FLUX, CELL SIZE, BCKGND', FLUX1, AR, CZ
  SUMC=0.0
  SUMC2=0.
  SUMC3=0.
  SUMC4=0.
  NSUM=0
  AVEN2=0.
  NBC2=0
  NBC3=0
  NBC4=0
  AVEN3=0.
  AVEN4=0.
  MAXNTT1=0
  SUMRA=0.0
  SUMXP=0.0
  SUMP1=0
  SUMP11=0
  SUMP2=0
  SUMP22=0
  SUMP3=0
  SUMP33=0
  SUMST=0.0
  SUMAR=0.0
  ARST=AR+1.0
  DO 650 I=1, NBAC
  NT11=NT1(I)+1
  SUMC=SUMC+CSUM(I)/FLOAT(NT-NTCZ+1)
  SUMC2=SUMC2+CSUM2(I)
  SUMC3=SUMC3+CSUM3(I)

```

```

SUMC4=SUMC4+CSUM4 (I)
NSUM=NSUM+NTT1 (I)
MAXNTT1=MAX0 (MAXNTT1, NTT1 (I))
RA=SQRT (X (I, 1) *X (I, 1) +X (I, 2) *X (I, 2) +X (I, 3) *X (I, 3))
IF (RA.LE.ARST) SUMST=SUMST+1.0
IF (RA.LE.2.*AR) SUMAR=SUMAR+1.0
SUMXP=SUMXP+ABS (XP (I))
SUMRA=SUMRA+RA
SUMPH1=SUMPH1+FLOAT (NTT2 (I))
SUMPH11=SUMPH11+FLOAT (NT2 (I))
SUMPH2=SUMPH2+FLOAT (NTT3 (I))
SUMPH22=SUMPH22+FLOAT (NT3 (I))
SUMPH3=SUMPH3+FLOAT (NTT4 (I))
SUMPH33=SUMPH33+FLOAT (NT4 (I))
AVEN2=AVEN2+FLOAT (NT2 (I)) /NT11
IF (NT2 (I) .GT.0) NBC2=NBC2+1
AVEN3=AVEN3+FLOAT (NT3 (I)) /NT11
IF (NT3 (I) .GT.0) NBC3=NBC3+1
AVEN4=AVEN4+FLOAT (NT4 (I)) /NT11
IF (NT4 (I) .GT.0) NBC4=NBC4+1
650 CONTINUE
IF (NCHFL.EQ.2 .OR. NCHFL.EQ.4 .OR. NCHFL.EQ.5) THEN
SUMXP=0.0
DO 670 I=1, NBAC
DPDT= (C (I) / (C (I) +XKD) -XP (I)) /TM
SUMXP=SUMXP+ABS (DPDT)
670 CONTINUE
ENDIF
WRITE (10, *) ' PHYCOSPHERE STATISTICS '
WRITE (10, *) ' AVERAGE RADIUS ', SUMRA/FLOAT (NBAC)
WRITE (10, *) ' AVERAGE DURATION (sec) ', FLOAT (NSUM/NBAC) *DTT
WRITE (10, *) ' MAXIMUM DURATION (sec) ', FLOAT (MAXNTT1) *DTT
WRITE (10, *) ' AVERAGE CONCENTRATION ', SUMC/FLOAT (NBAC)
WRITE (10, *) ' AVG DPDT*ALP ', SUMXP*ALP/FLOAT (NBAC)
WRITE (10, *) ' R1 TIME TO, TIME IN ', FLOAT (NBAC*NT) /SUMPH11*
*DTT, SUMPH1/SUMPH11*DTT
WRITE (10, *) ' VIS/PHY % EXPSR ', AVEN2/FLOAT (NBC2), SUMC2
*/FLOAT (NT) /SUMC*100.
CFCT2=SUMPH2/FLOAT (NBAC*NT) * (RB/F2) **3
WRITE (10, *) ' R2 TIME TO, TIME IN ', FLOAT (NBAC*NT) /SUMPH22*
*DTT, SUMPH2/SUMPH22*DTT
WRITE (10, *) ' CON FACT (R1) ', CFCT2
WRITE (10, *) ' VIS/PHY % EXPSR ', AVEN3/FLOAT (NBC3), SUMC3
*/FLOAT (NT) /SUMC*100.
WRITE (10, *) ' R3 TIME TO, TIME IN ', FLOAT (NBAC*NT) /SUMPH33*
*DTT, SUMPH3/SUMPH33*DTT
CFCT3=SUMPH3/FLOAT (NBAC*NT) * (RB/F3) **3
WRITE (10, *) ' CON FACT (R2) ', CFCT3
WRITE (10, *) ' VIS/PHY % EXPSR ', AVEN4/FLOAT (NBC4), SUMC4
*/FLOAT (NT) /SUMC*100.

```

```
      WRITE(10,*)' % STUCK, % W/I  
2*AR',SUMST*100./FLOAT(NBAC),SUMAR*  
*100./FLOAT(NBAC)  
      WRITE(10,*)' '  
      WRITE(10,*)'      EXITING BACTERIA STATISTICS '  
      IF(JOUT.GT.0)THEN  
      CV=COUT/FLOAT(JOUT)  
      TV=TOUT/FLOAT(JOUT)  
      WRITE(10,*)' AVERAGE DURATION (sec)',TV  
      WRITE(10,*)' AVERAGE CONCENTRATION ',CV  
      ENDIF  
      WRITE(10,*)' MAXIMUM DURATION (sec)',MTOUT*DTT  
      WRITE(10,*)' '  
      RETURN  
      END
```

```

SUBROUTINE TIMAV(NR, TAVD, TAVC, ICD, IDD, CONF, CONL, DISF,
*DISL, AR, NTAV, NBAC, XL)
  DIMENSION TAVC(50), TAVD(50)
  CHARACTER*8 XL
  XPI=4.*ATAN(1.)
  TAVNSM=0.0
  DO 8880 I=1, IDD
8880  TAVNSM=TAVNSM+TAVD(I)
  TAVN=0.0
  IF(ICD.LT.IDD) THEN
  WRITE(12, 900)NR, XL, NR, XL, NR
900  FORMAT(' DIS ', I2, 'TVN', A8, ' ', I2, 'TVC', A8, ' CON', I2, 'TVC')
  DO 1500 I=1, ICD
  CTAV=CONF*(CONL/CONF)**(FLOAT(I)/FLOAT(ICD))
  CTAV=-ALOG10(CTAV)
  DTAV=DISF+FLOAT(I-1)/FLOAT(IDD-1)*(DISL-DISF)
  IF(I.EQ.1) THEN
  DTAV1=AR
  ELSE
  DTAV1=DISF+FLOAT(I-2)/FLOAT(IDD-1)*(DISL-DISF)
  ENDIF
  DDVOL=4./3.*XPI*(DTAV**3-DTAV1**3)/1.E9*FLOAT(NTAV)
  TAVN=TAVN+TAVD(I)
1500  WRITE(12, 890)DTAV, TAVN/TAVNSM, TAVD(I)/DDVOL, CTAV
  *, TAVC(I)/FLOAT(NTAV)/FLOAT(NBAC)
  DO 1510 I=ICD+1, IDD
890  FORMAT(5E12.5)
  DTAV=DISF+FLOAT(I-1)/FLOAT(IDD-1)*(DISL-DISF)
  IF(I.EQ.1) THEN
  DTAV1=AR
  ELSE
  DTAV1=DISF+FLOAT(I-2)/FLOAT(IDD-1)*(DISL-DISF)
  ENDIF
  DDVOL=4./3.*XPI*(DTAV**3-DTAV1**3)/1.E9*FLOAT(NTAV)
  TAVN=TAVN+TAVD(I)
1510  WRITE(12, 890)DTAV, TAVN/TAVNSM, TAVD(I)/DDVOL
  ELSE
  WRITE(12, 880)NR, NR, NR
880  FORMAT(' CON ', I2, 'TAVC DIS ', I2, 'TVN ', I2, 'TVC')
  DO 1600 I=1, IDD
  DTAV=DISF+FLOAT(I-1)/FLOAT(IDD-1)*(DISL-DISF)
  IF(I.EQ.1) THEN
  DTAV1=AR
  ELSE
  DTAV1=DISF+FLOAT(I-2)/FLOAT(IDD-1)*(DISL-DISF)
  ENDIF
  DDVOL=4./3.*XPI*(DTAV**3-DTAV1**3)/1.E9*FLOAT(NTAV)
  CTAV=CONF*(CONL/CONF)**(FLOAT(I)/FLOAT(ICD))
  CTAV=-ALOG10(CTAV)

```

```
      TAVN=TAVN+TAVD (I)
1600  WRITE (12, 890) CTAV, TAVC (I) /FLOAT (NTAV) /FLOAT (NBAC) ,DTAV,
      *TAVN/TAVNSM, TAVD (I) /DDVOL
      DO 1610 I=IDD+1, ICD
      CTAV=CONF* (CONL/CONF) ** (FLOAT (I) /FLOAT (ICD))
      CTAV=-ALOG10 (CTAV)
1610  WRITE (12, 890) CTAV, TAVC (I) /FLOAT (NTAV) /FLOAT (NBAC)
      ENDIF
      RETURN
      END
```

```

SUBROUTINE HISTO(CSUM,CSUM2,CSUM3,CSUM4,NT1,NT2,NT3,NT4,NTT1,
*NTT2,NTT3,NTT4,NBAC,DTT,NT)
  DIMENSION CSUM(3500),CSUM2(3500),CSUM3(3500),CSUM4(3500)
  DIMENSION XMXC(4),XMNC(4),XMXT(4),XMNT(4),XH(4)
  DIMENSION XINCC(4),XINCN(4),XINCT(4)
  INTEGER*2 NT1(3500),NT2(3500),NT3(3500),NT4(3500),NDIV(4)
  INTEGER*2 NTT1(3500),NTT2(3500),NTT3(3500),NTT4(3500)
  INTEGER*2 NHC(4,50),NHN(4,50),NHT(4,50),MNN(4),MXN(4)

C
C      INITIALIZING
C
  DO 20 I=1,4
    XMXC(I)=0.0
    XMNC(I)=1.E9
    MXN(I)=0
    MNN(I)=9999
    XMXT(I)=0.0
    XMNT(I)=1.E9
  DO 20 J=1,50
    NHC(I,J)=0
    NHN(I,J)=0
    NHT(I,J)=0
20  CONTINUE
C
C      CONCENTRATION HISTOGRAMS
C
  DO 50 I=1,NBAC
    XMXC(1)=AMAX1(XMXC(1),CSUM(I))
    XMXC(2)=AMAX1(XMXC(2),CSUM2(I))
    XMXC(3)=AMAX1(XMXC(3),CSUM3(I))
    XMXC(4)=AMAX1(XMXC(4),CSUM4(I))
    XMNC(1)=AMIN1(XMNC(1),CSUM(I))
    XMNC(2)=AMIN1(XMNC(2),CSUM2(I))
    XMNC(3)=AMIN1(XMNC(3),CSUM3(I))
    XMNC(4)=AMIN1(XMNC(4),CSUM4(I))
50  CONTINUE
    YMNC=XMNC(1)
    YMXC=XMXC(1)
  DO 58 J=2,4
    YMNC=AMIN1(YMNC,XMNC(J))
    YMXC=AMAX1(YMXC,XMXC(J))
58  CONTINUE
  DO 60 J=1,4
    XMNC(J)=YMNC
    XMXC(J)=YMXC
    XINCC(J)=(YMNC-XMNC)/50.
60  CONTINUE
  DO 100 I=1,NBAC
    NN=IFIX((CSUM(I)-XMNC(1))/XINCC(1))+1

```

```

NN=MIN0 (NN, 50)
NHC (1, NN) = NHC (1, NN) +1
NN=IFIX ( (CSUM2 (I) -XMNC (2)) /XINCC (2)) +1
NN=MIN0 (NN, 50)
NHC (2, NN) = NHC (2, NN) +1
NN=IFIX ( (CSUM3 (I) -XMNC (3)) /XINCC (3)) +1
NN=MIN0 (NN, 50)
NHC (3, NN) = NHC (3, NN) +1
NN=IFIX ( (CSUM4 (I) -XMNC (4)) /XINCC (4)) +1
NN=MIN0 (NN, 50)
NHC (4, NN) = NHC (4, NN) +1
100 CONTINUE
C
C      PRINT CONCENTRATION HISTOS
C
DO 120 I=1, 50
XXH=XMNC (1) /FLOAT (NT) +FLOAT (2*I-1) * .5*XINCC (1) /FLOAT (NT)
WRITE (3, 890) XXH, (NHC (J, I), J=1, 4)
120 CONTINUE
890 FORMAT (1X, E9.4, 4I5)
900 FORMAT (4 (1X, E9.4, I5))
C
C      TIME HISTOGRAMS
C
DO 150 I=1, NBAC
XMXT (1) =AMAX1 (XMXT (1), FLOAT (NTT1 (I)))
XMXT (2) =AMAX1 (XMXT (2), FLOAT (NTT2 (I)))
XMXT (3) =AMAX1 (XMXT (3), FLOAT (NTT3 (I)))
XMXT (4) =AMAX1 (XMXT (4), FLOAT (NTT4 (I)))
XMNT (1) =AMIN1 (XMNT (1), FLOAT (NTT1 (I)))
XMNT (2) =AMIN1 (XMNT (2), FLOAT (NTT2 (I)))
XMNT (3) =AMIN1 (XMNT (3), FLOAT (NTT3 (I)))
XMNT (4) =AMIN1 (XMNT (4), FLOAT (NTT4 (I)))
150 CONTINUE
DO 160 J=1, 4
XINCT (J) = (XMXT (J) -XMNT (J)) /50.
160 CONTINUE
DO 200 I=1, NBAC
NN=IFIX ( (FLOAT (NTT1 (I)) -XMNT (1)) /XINCT (1)) +1
NN=MIN0 (NN, 50)
NHT (1, NN) = NHT (1, NN) +1
NN=IFIX ( (FLOAT (NTT2 (I)) -XMNT (2)) /XINCT (2)) +1
NN=MIN0 (NN, 50)
NHT (2, NN) = NHT (2, NN) +1
NN=IFIX ( (FLOAT (NTT3 (I)) -XMNT (3)) /XINCT (3)) +1
NN=MIN0 (NN, 50)
NHT (3, NN) = NHT (3, NN) +1
NN=IFIX ( (FLOAT (NTT4 (I)) -XMNT (4)) /XINCT (4)) +1
NN=MIN0 (NN, 50)
NHT (4, NN) = NHT (4, NN) +1

```

```

200 CONTINUE
C
C PRINT TIME HISTOS
C
DO 220 I=1,50
DO 210 J=1,4
210 XH(J)=(XMNT(J)+FLOAT(2*I-1)*.5*XINCT(J))*DTT
WRITE(6,900)(XH(J),NHT(J,I),J=1,4)
220 CONTINUE
C
C ENTRY HISTOGRAMS
C
DO 250 I=1,NBAC
MXN(1)=MAX0(MXN(1),NT1(I)+1)
MXN(2)=MAX0(MXN(2),NT2(I))
MXN(3)=MAX0(MXN(3),NT3(I))
MXN(4)=MAX0(MXN(4),NT4(I))
MNN(1)=MIN0(MNN(1),NT1(I)+1)
MNN(2)=MIN0(MNN(2),NT2(I))
MNN(3)=MIN0(MNN(3),NT3(I))
MNN(4)=MIN0(MNN(4),NT4(I))
250 CONTINUE
DO 260 J=1,4
NDIV(J)=MIN0(50,MXN(J)-MNN(J))
XINCN(J)=FLOAT(MXN(J)-MNN(J))/FLOAT(NDIV(J))
260 CONTINUE
DO 300 I=1,NBAC
NN=IFIX(FLOAT(NT1(I)+1-MNN(1))/XINCN(1))+1
NN=MIN0(NN,50)
NHN(1,NN) = NHN(1,NN)+1
NN=IFIX(FLOAT(NT2(I)-MNN(2))/XINCN(2))+1
NN=MIN0(NN,50)
NHN(2,NN) = NHN(2,NN)+1
NN=IFIX(FLOAT(NT3(I)-MNN(3))/XINCN(3))+1
NN=MIN0(NN,50)
NHN(3,NN) = NHN(3,NN)+1
NN=IFIX(FLOAT(NT4(I)-MNN(4))/XINCN(4))+1
NN=MIN0(NN,50)
NHN(4,NN) = NHN(4,NN)+1
300 CONTINUE
C
C PRINT ENTRY HISTOS
C
DO 360 I=1,50
DO 350 J=1,4
350 XH(J)=FLOAT(MNN(J))+FLOAT(I-1)*XINCN(J)
WRITE(4,900)(XH(J),NHN(J,I),J=1,4)
360 CONTINUE

RETURN

```

END

```
SUBROUTINE PRNPOS (NBAC, X1, X2, X3, A1, A2, C, XP, NTT1, CSUM)
DIMENSION X1 (NBAC), X2 (NBAC), X3 (NBAC), A1 (NBAC), A2 (NBAC)
DIMENSION C (NBAC), XP (NBAC), CSUM (NBAC)
INTEGER*2 NTT1 (NBAC)
WRITE (5) NBAC, X1, X2, X3, A1, A2, C, XP, NTT1, CSUM
RETURN
END
```

```
SUBROUTINE READPO (NBAC, X1, X2, X3, A1, A2, C, XP, NTT1, CSUM)
DIMENSION X1 (NBAC), X2 (NBAC), X3 (NBAC), A1 (NBAC), A2 (NBAC)
DIMENSION C (NBAC), XP (NBAC), CSUM (NBAC)
INTEGER*2 NTT1 (NBAC)
READ (11) NBAC, X1, X2, X3, A1, A2, C, XP, NTT1, CSUM
REWIND (11)
CLOSE (11)
RETURN
END
```

```

C      program EXCON1
C
C      USES ADVECTION OF MOMENTS TO SOLVE A-D
C      EQUATION    STEADY STATE SOLUTION ONLY
C
C      MODIFIED                CHANGES
C      7/88                    ADDED ROTATION AROUND X3
C      8/12/88                 ADDED CALCULATION OF EIGENVECTORS AND VALUES
C      8/15/88                 CHANGED PRINTOUT OF EIGENVECTORS
C                               ADDED ROTATION WITH X1 AND X3 COMPONENTS
C      8/17/88                 ADDED PRINTOUT OF I11 I12 I22
C      8/18                    CHANGED TO EXPLICIT FINITE DIFFERENCE METHOD
C
C      11/8                    CHANGED TO MULTIPLE RUN SETUP
C
C      DIMENSION
XI(3,3,600),E(3),X(5,3,100),C(5,100),DT(600),DIST(5,100)
  DIMENSION C1(100),DME(3),XEIG(3,100),DTMT(600),DN(5,100)
  DIMENSION A(3,3),INDX(3),V(3),B(3),E1(3),TIME(600),XN(3)
  DIMENSION FIR(5,3),DRC(3,3),EE(3,3)
  DIMENSION EVC1(3,3),EVL1(3),CEIG(100)
  DIMENSION EI(3,3),XIN(3,3),XIOL(3,3),AL(3,3),TP(3,3)
  DIMENSION XFI(5),XLAST(5),A1(5),A2(5)
  REAL*8 AJ(3,3),EVC(3,3),EVL(3)
  CHARACTER*1 TAB,TEST,INTR,MTC,EIG,SFIL
  CHARACTER*12 FNAM1,EIGFIL,INFILE,SUMFIL
  DATA EI,XIN,XIOL/27*0./
  DATA XI,X,C/7400*0.0/
  DATA DT,TIME/1200*0.0/
  DATA EVC,EVL,AJ,NROT/21*0.0D0,0/
  DATA N,NPP/3,3/
  DATA E1/3*1./
  DATA DRC,EE/1.,0.,0.,0.,1.,0.,0.,0.,1.,9*0.0/
  DATA TAB/'      '/
C
C      WRITE(*,*) ' LAST MODIFIED  11/09/88 '
C
C      990  FORMAT(A1)
C           XPI=4.*ATAN(1.0)
C           BB=1/(8.*ATAN(1.0))**1.5
C           WRITE(*,*) 'DM (UM**2/S) '
C           READ(*,*)DM
C           DM=1000.
C           WRITE(*,*) ' ENTER INPUT FILENAME '
C           READ(*,970)INFILE
C      970  FORMAT(A12)
C
C      UNIT 9 INPUT FILE
C
C           OPEN(8,FILE=INFILE)
C           READ(8,*)NRUN

```

```

READ (8,*)NPUL
READ (8,990)EIG
READ (8,970)EIGFIL
OPEN (2,FILE=EIGFIL)
READ (8,990)SFIL
READ (8,970)SUMFIL
OPEN (4,FILE=SUMFIL)
WRITE (*,*) ' ENTER CONC AT A=10'
READ (*,*)FLUX
WRITE (*,*) ' ENTER 1 FOR NORMALIZED DIST AND CONC'
READ (*,*)NORM
FLUX=FLUX*40000.*XPI
BB=BB*FLUX
DO 2000 NR=1,NRUN
DO 222 I=1,3
READ (8,*)EE (I,1),EE (I,2),EE (I,3)
222 CONTINUE
EBAR=1.
C EBAR=0.5*(ABS (EE (1,1))+ABS (EE (2,2))+ABS (EE (3,3)))
DBAR=SQRT (DM/EBAR)
CNOT=SQRT (EBAR) /4./XPI/ (DM) **1.5
C
C unit 4 for the all the output data
C
IF (SFIL.EQ. 'Y') WRITE (4,*) 'NR=',NR, ' EBAR=',EBAR
READ (8,*)XMIN,XMAX,EMAX
CALL SETPL1 (TIME,DT,EMAX,DM,XMIN,XMAX,NPUL)
READ (8,*)NP,NAXIS
DO 12 I=1,NAXIS
12 READ (8,*)XFI (I),XLAST (I),A1 (I),A2 (I), (FIR (I,J),J=1,3)
READ (8,970)FNAM1
OPEN (3,FILE=FNAM1)
C
C DO EXPLICIT STEPPING WITH MOMENTS
C
WRITE (*,*) ' PULSE STEPS'
DO 1048 I=1,3
DO 1048 J=1,3
1048 EMAX=AMAX1 (EMAX,ABS (EE (I,J)))
WRITE (*,*) 'EMAX=',EMAX
DO 50 I=1,NPUL
C
C TRANSFER XI TO XIOL
C
IF (I.EQ.1) THEN
DO 24 J=1,3
DO 24 K=1,3
24 XIN (J,K)=0.0
ENDIF
IF (I.GT.1) THEN

```

```

DO 25 J=1,3
DO 25 K=1,3
25 XIN(J,K)=XI(J,K,I-1)
ENDIF
C
C          ADDED INTERNAL LOOP TO LIMIT TIME STEP TO .01*EMAX
C
NS=IFIX(DT(I)/.0051*EMAX)
IF(NS.LT.1)NS=1
IF(MOD(I,10).EQ.0)WRITE(*,*)I,NS
DO 35 II=1,NS
C
C          INITIALIZE
C
DO 30 J=1,3
DO 30 K=1,3
EI(J,K)=0.0
30 XIOL(J,K)=XIN(J,K)
DO 35 J=1,3
DO 35 K=1,3
C
C          EI = SHEAR TIMES OLD MOMENT
C
DO 32 L=1,3
32 EI(J,K)=EI(J,K)+EE(K,L)*XIOL(J,L)+EE(J,L)*XIOL(K,L)
C
C          UPDATE NEW MOMENT
C
35 XIN(J,K)=XIOL(J,K)+DT(I)/FLOAT(NS)*(DRC(J,K)*2*DM+EI(J,K))
DO 50 J=1,3
DO 50 K=1,3
50 XI(J,K,I)=XIN(J,K)
C
C
C          FIND EIGENVALUES AND VECTORS'
C          TRANSFER XI TO DUMMY MATRIX
C
IF(EIG.EQ.'Y')THEN
DO 600 J=1, NPUL
DO 51 K=1,3
DO 51 L=1,3
51 AJ(K,L)=DBLE(XI(K,L,J))
CALL JACOBI(AJ,3,3,EVL,EVC,NROT)
CALL EIGSRT(EVL,EVC,3,3)
DO 52 K=1,3
EVL1(K)=SNGL(EVL(K))
XEIG(K,J)=EVL1(K)
DO 52 L=1,3
52 EVC1(K,L)=SNGL(EVC(K,L))

```

```

600 CONTINUE
C
C
C   FIND FINAL EIGENVECTORS AND TRANSFORMED SHEAR TENSOR
C
  WRITE(*,*) ' NORMALIZED EIGEN VECTORS '
  DO 520 J=1,3
    ED=SQRT (EVC1 (1,J)*EVC1 (1,J)+EVC1 (2,J)*EVC1 (2,J)+EVC1 (3,J) *
* EVC1 (3,J) )
    EVC1 (1,J)=EVC1 (1,J)/ED
    EVC1 (2,J)=EVC1 (2,J)/ED
    EVC1 (3,J)=EVC1 (3,J)/ED
520   WRITE(*,*) J, '      ',EVC1 (1,J),EVC1 (2,J),EVC1 (3,J)
      DO 525 I=1,3
        DO 525 J=1,3
525   AL (I,J)=EVC1 (J,I)
      DO 530 I=1,3
        DO 530 J=1,3

TP (I,J)=AL (I,1)*AL (J,1)*EE (1,1)+AL (I,2)*AL (J,1)*EE (2,1)+AL (I,3) *
1AL (J,1)*EE (3,1)+AL (I,1)*AL (J,2)*EE (1,2)+AL (I,2)*AL (J,2)*EE (2,2) +
2AL (I,3)*AL (J,2)*EE (3,2)+AL (I,1)*AL (J,3)*EE (1,3)+AL (I,2)*AL (J,3)
3*EE (2,3)+AL (I,3)*AL (J,3)*EE (3,3)
530 CONTINUE
  WRITE(*,*) ' TRANSFORMED SHEAR MATRIX '
  DO 535 J=1,3
    WRITE (2,*) TP (J,1), TP (J,2), TP (J,3)
535  WRITE(*,*) TP (J,1), TP (J,2), TP (J,3)
    ENDIF
C
C   START LOOP FOR AXIS
C
  DO 1500 NX=1,NAXIS
    A1 (NX)=A1 (NX)/180.*XPI
    A2 (NX)=A2 (NX)/180.*XPI
    DO 60 I=1,NP
      DIST (NX,I)=XFI (NX) * (XLAST (NX)/XFI (NX)) ** (FLOAT (I-1)/(NP-1))
      X (NX,1,I)=(DIST (NX,I)) *COS (A1 (NX)) *SIN (A2 (NX)) +FIR (NX,1)
      X (NX,2,I)=(DIST (NX,I)) *SIN (A1 (NX)) *SIN (A2 (NX)) +FIR (NX,2)
      X (NX,3,I)=(DIST (NX,I)) *COS (A2 (NX)) +FIR (NX,3)
60   CONTINUE
C
C   ZERO CONCENTRATIONS
C
  DO 65 IP=1,NP
65  C (NX,IP)=0.0
C
C   CALCULATE THE CONCENTRATION

```

```

C          CONTRIBUTION FROM EACH PULSE
C
DO 80 K=1, NPUL
DO 70 I=1, 3
DO 70 J=1, 3
70  A(I, J)=XI(I, J, K)
C    WRITE(*, *) A, N, NPP, INDX, D
    CALL LUDCMP(A, N, NPP, INDX, D)
C
C          ADD THIS CONCENTRATION TO EACH POINT
C
DO 75 IP=1, NP
B(1)=X(NX, 1, IP)
B(2)=X(NX, 2, IP)
B(3)=X(NX, 3, IP)
CALL LUBKSB(A, N, NPP, INDX, B)
ARG=X(NX, 1, IP)*B(1)+X(NX, 2, IP)*B(2)+X(NX, 3, IP)*B(3)
DTMT(K)=A(1, 1)*A(2, 2)*A(3, 3)
C    WRITE(*, *) K, DTMT(K)
C    WRITE(*, *) B, ARG
C    WRITE(*, *) A(1, 1), A(2, 2), A(3, 3), D
75  C(NX, IP)=C(NX, IP)+BB*DT(K)/SQRT(ABS(A(1, 1)*A(2, 2)*A(3, 3))) *
* EXP(-.5*ARG)
80  CONTINUE
1500 CONTINUE
C
C          PRINT CONCENTRATIONS
C
IF(NORM.NE.1) THEN
DBAR=1.
CNOT=1.
ENDIF
DO 85 NX=1, NAXIS
DO 85 I=1, NP
DIST(NX, I)=SQRT(X(NX, 1, I)**2+X(NX, 2, I)**2+X(NX, 3, I)**2)
DN(NX, I)=DIST(NX, I)/DBAR
85  C(NX, I)=C(NX, I)/CNOT
DO 90 I=1, NP
IF(SFIL.EQ.'Y')
*WRITE(4, 1989) (DN(NX, I), C(NX, I), NX=1, NAXIS)
90  WRITE(3, 1989) (DN(NX, I), C(NX, I), NX=1, NAXIS)
1989  FORMAT(5(e11.4, 1x, e11.4, 2x))
2989  FORMAT(5(f7.1, 1x, f7.2, 1x, f7.1, 1x))
X1END=SQRT(ABS(A(1, 1)))
X2END=SQRT(ABS(A(2, 2)))
X3END=SQRT(ABS(A(3, 3)))
DO 1990 I=1, 3
1990 IF(A(I, I).LT.0.0) WRITE(*, '(' A'', I1, '<0'' )' ) I
WRITE(*, *) ' D=', D
WRITE(*, *) 'RUN', NR

```

```

WRITE (*, *) ' X1 MOMENT', X1END
WRITE (*, *) ' X2 MOMENT', X2END
WRITE (*, *) ' X3 MOMENT', X3END
2000 CONTINUE
STOP
END
SUBROUTINE EIGSRT(D, V, N, NP)
REAL*8 D(NP), V(NP, NP)
DO 13 I=1, N-1
  K=I
  P=D(I)
  DO 11 J=I+1, N
    IF (D(J) .GE. P) THEN
      K=J
      P=D(J)
    ENDIF
11 CONTINUE
  IF (K .NE. I) THEN
    D(K)=D(I)
    D(I)=P
    DO 12 J=1, N
      P=V(J, I)
      V(J, I)=V(J, K)
      V(J, K)=P
12 CONTINUE
    ENDIF
13 CONTINUE
RETURN
END
SUBROUTINE JACOBI(A, N, NP, D, V, NROT)
PARAMETER (NMAX=1000)
REAL*8 A(NP, NP), D(NP), V(NP, NP), B(NMAX), Z(NMAX)
DO 12 IP=1, N
  DO 11 IQ=1, N
    V(IP, IQ)=0.
11 CONTINUE
    V(IP, IP)=1.
12 CONTINUE
  DO 13 IP=1, N
    B(IP)=A(IP, IP)
    D(IP)=B(IP)
    Z(IP)=0.
13 CONTINUE
  NROT=0
  DO 24 I=1, 50
    SM=0.
    DO 15 IP=1, N-1
      DO 14 IQ=IP+1, N
        SM=SM+ABS(A(IP, IQ))
14 CONTINUE

```

```

15      CONTINUE
      IF (SM.EQ.0.) RETURN
      IF (I.LT.4) THEN
          TRESH=0.2*SM/N**2
      ELSE
          TRESH=0.
      ENDIF
      DO 22 IP=1,N-1
          DO 21 IQ=IP+1,N
              G=100.*ABS(A(IP,IQ))
              IF ((I.GT.4).AND.(ABS(D(IP))+G.EQ.ABS(D(IP)))
*          .AND.(ABS(D(IQ))+G.EQ.ABS(D(IQ)))) THEN
                  A(IP,IQ)=0.
              ELSE IF (ABS(A(IP,IQ)).GT.TRESH) THEN
                  H=D(IQ)-D(IP)
                  IF (ABS(H)+G.EQ.ABS(H)) THEN
                      T=A(IP,IQ)/H
                  ELSE
                      THETA=0.5*H/A(IP,IQ)
                      T=1./(ABS(THETA)+SQRT(1.+THETA**2))
                      IF (THETA.LT.0.) T=-T
                  ENDIF
                  C=1./SQRT(1+T**2)
                  S=T*C
                  TAU=S/(1.+C)
                  H=T*A(IP,IQ)
                  Z(IP)=Z(IP)-H
                  Z(IQ)=Z(IQ)+H
                  D(IP)=D(IP)-H
                  D(IQ)=D(IQ)+H
                  A(IP,IQ)=0.
              DO 16 J=1,IP-1
                  G=A(J,IP)
                  H=A(J,IQ)
                  A(J,IP)=G-S*(H+G*TAU)
                  A(J,IQ)=H+S*(G-H*TAU)
16      CONTINUE
              DO 17 J=IP+1,IQ-1
                  G=A(IP,J)
                  H=A(J,IQ)
                  A(IP,J)=G-S*(H+G*TAU)
                  A(J,IQ)=H+S*(G-H*TAU)
17      CONTINUE
              DO 18 J=IQ+1,N
                  G=A(IP,J)
                  H=A(IQ,J)
                  A(IP,J)=G-S*(H+G*TAU)
                  A(IQ,J)=H+S*(G-H*TAU)
18      CONTINUE
              DO 19 J=1,N

```

```

          G=V(J,IP)
          H=V(J,IQ)
          V(J,IP)=G-S*(H+G*TAU)
          V(J,IQ)=H+S*(G-H*TAU)
19      CONTINUE
          NROT=NROT+1
          ENDIF
21      CONTINUE
22      CONTINUE
          DO 23 IP=1,N
              B(IP)=B(IP)+Z(IP)
              D(IP)=B(IP)
              Z(IP)=0.
23      CONTINUE
24      CONTINUE
          PAUSE '50 iterations should never happen'
          RETURN
          END
C      TESTING ROT
C
C
C      DIMENSION T(3,3)
C      DATA T /1.,0.,0.,0.,1.,0.,0.,0.,1./
C      WRITE(*,*) ' ENTER T ROW BY ROW'
C      DO 5 I=1,3
C5      READ(*,*) (T(I,J),J=1,3)
C      WRITE(*,*) ' ENTER THETA'
C      READ(*,*) THETA
C      CT=COS(THETA)*COS(THETA)
C      CS=COS(THETA)*SIN(THETA)
C      ST=SIN(THETA)*SIN(THETA)
C      WRITE(*,*) ' C2,CS,S2',CT,CS,ST
C      CALL ROT(T,THETA)
C      DO 11 I=1,3
C      WRITE(*,10) (T(I,J),J=1,3)
C 10      FORMAT(3F10.5)
C 11      CONTINUE
C      STOP
C      END
C
C      FINDS A NEW TENSOR BASED ON ROTATION MATRIX AND OLD TENSORT
C      WITH ROTATION MATRIX DEFINED AS IN VON SCHWIND
C      A(I,J)=COS(XIP,XJ), MUST GIVE ANGLES FROM X3
C
C      DATE                MODIFICATION
C
C      8/15/88             ADDED ROTATION WITH X1 AND X3 COMPONENTS
C      8/17/88             FIXED EARLIER MISTAKES,ANG=0.0 FOR NOW
C
SUBROUTINE ROT(T,ANG,THETA)

```

```

DIMENSION T(3,3),TP(3,3),AL(3,3)
CT=COS(THETA)
ST=SIN(THETA)
CA=COS(ANG)
SA=SIN(ANG)
AL(1,1)=CT
AL(2,2)=CT
AL(3,3)=1
AL(1,3)=0.
AL(2,3)=0.
AL(3,1)=0.
AL(3,2)=-AL(2,3)
AL(2,1)=ST
AL(1,2)=-ST
C   WRITE(*,*)AL
DO 65 I=1,3
DO 65 J=1,3
TP(I,J)=AL(I,1)*AL(J,1)*T(1,1)+AL(I,2)*AL(J,1)*T(2,1)+AL(I,3)*
1AL(J,1)*T(3,1)+AL(I,1)*AL(J,2)*T(1,2)+AL(I,2)*AL(J,2)*T(2,2)+
2AL(I,3)*AL(J,2)*T(3,2)+AL(I,1)*AL(J,3)*T(1,3)+AL(I,2)*AL(J,3)
3*T(2,3)+AL(I,3)*AL(J,3)*T(3,3)
C   WRITE(*,*)' I,J,TP',I,J,TP(I,J)
65  CONTINUE
DO 70 I=1,3
DO 70 J=1,3
70  T(I,J)=TP(I,J)
RETURN
END

C
-C   TESTING MATRIX INVERSIONS
C
C   DIMENSION A(100,100),INDX(100),VV(100),B(100),AINV(100,100)
C 1  WRITE(*,*)' ENTER PHYSICAL AND LOGICAL DIMENSIONS'
C   READ(*,*)NP,N
C   WRITE(*,*)' ENTER A ROW BY ROW'
C   DO 5 I=1,N
C5  READ(*,*)(A(I,J),J=1,N)
C   WRITE(*,10)((I,J,A(I,J),J=1,N),I=1,N)
C10  FORMAT(2I5,F10.2)
C11  FORMAT(2I5,E12.5)
C   CALL LUDCMP(A,N,NP,INDX,D)
C
C   SET UP THE IDENTITY MATRIX
C
C   DO 16 I=1,N
C   DO 15 J=1,N
C 15  AINV(I,J)=0.0
C 16  AINV(I,I)=1.0
C   WRITE(*,11)((I,J,AINV(I,J),J=1,N),I=1,N)
C   DO 20 J=1,N

```

```

C      CALL LUBKSB(A,N,NP,INDX,AINV(1,J))
C 20   CONTINUE
C      WRITE(*,11)((I,J,AINV(I,J),J=1,N),I=1,N)
C      GOTO1
C      END
      SUBROUTINE LUDCMP(A,N,NP,INDX,D)
      PARAMETER (NMAX=100,TINY=1.E-20)
      DIMENSION A(NP,NP),INDX(N),VV(NMAX)
      D=1.
      DO 12 I=1,N
      AAMAX=0.
      DO 11 J=1,N
      IF (ABS(A(I,J)).GT.AAMAX) AAMAX=ABS(A(I,J))
11     CONTINUE
      IF (AAMAX.EQ.0.) PAUSE 'SINGULAR MATRIX'
      VV(I)=1./AAMAX
12     CONTINUE
      DO 19 J=1,N
      IF (J.GT.1) THEN
      DO 14 I=1,J-1
      SUM =A(I,J)
      IF (I.GT.1) THEN
      DO 13 K=1,I-1
      SUM=SUM-A(I,K)*A(K,J)
13     CONTINUE
      A(I,J)=SUM
      ENDIF
14     CONTINUE
      ENDIF
      AAMAX=0.
      DO 16 I=J,N
      SUM=A(I,J)
      IF (J.GT.1) THEN
      DO 15 K=1,J-1
      SUM=SUM-A(I,K)*A(K,J)
15     CONTINUE
      A(I,J)=SUM
      ENDIF
      DUM=VV(I)*ABS(SUM)
      IF (DUM.GE.AAMAX) THEN
      IMAX=I
      AAMAX=DUM
      ENDIF
16     CONTINUE
      IF (J.NE.IMAX) THEN
      DO 17 K=1,N
      DUM=A(IMAX,K)
      A(IMAX,K)=A(J,K)
      A(J,K)=DUM
17     CONTINUE

```

```

D=-D
VV(IMAX)=VV(J)
ENDIF
INDX(J)=IMAX
IF(J.NE.N) THEN
IF(A(J,J).EQ.0.) A(J,J)=TINY
DUM=1./A(J,J)
DO 18 I=J+1,N
A(I,J)=A(I,J)*DUM
18 CONTINUE
ENDIF
19 CONTINUE
IF(A(N,N).EQ.0.) A(N,N)=TINY
RETURN
END
SUBROUTINE LUBKSB(A,N,NP,INDX,B)
DIMENSION A(NP,NP),INDX(N),B(N)
II=0
DO 12 I=1,N
LL=INDX(I)
SUM=B(LL)
B(LL)=B(I)
IF(II.NE.0) THEN
DO 11 J=II,I-1
SUM=SUM-A(I,J)*B(J)
11 CONTINUE
ELSEIF(SUM.NE.0.) THEN
II=I
ENDIF
B(I)=SUM
12 CONTINUE
DO 14 I=N,1,-1
SUM=B(I)
IF(I.LT.N) THEN
DO 13 J=I+1,N
SUM=SUM-A(I,J)*B(J)
13 CONTINUE
ENDIF
B(I)=SUM/A(I,I)
14 CONTINUE
RETURN
END
SUBROUTINE LUINV(A,N,NP,INDX,D,Y)
DIMENSION A(NP,NP),Y(NP,NP),INDX(NP)
DO 12 I=1,N
DO 11 J=1,N
Y(I,J)=0.
11 CONTINUE
Y(I,I)=1.
12 CONTINUE

```

```

CALL LUDCMP (A,N,NP,INDX,D)
DO 13 J=1,N
C   CALL LUBKSB (A,N,NP,INDX,Y(1,J))
13  CONTINUE
RETURN
END
SUBROUTINE LUDET (A,N,NP,INDX,D)
DIMENSION A (NP,NP),INDX (NP)
CALL LUDCMP (A,N,NP,INDX,D)
DO 11 J=1,N
D=D*A (J,J)
11  CONTINUE
RETURN
END

C
C   PROGRAM TO SET POSITION OF PULSES
C
C   MODIFIED VERSION TO RUN WITH EXMOMCON1
C
SUBROUTINE SETPL1 (TIME,DT,EMAX,DM,XMIN,XMAX,N)
DIMENSION DT (600),TIME (600),VV (3)
C=1./FLOAT (N-1)*ALOG (XMAX/XMIN)
DO 10 I=1,N
DT (I)=(XMIN*EXP (C*FLOAT (I-1)))**2
C   WRITE (*,*)DT (I)
10  CONTINUE

C
C   FIND THE TIMES
C
IF (EMAX.NE.0.0) THEN
DO 20 I=1,N
TIME (I)=.5/EMAX*ALOG (1.+EMAX*DT (I)/DM)
C   WRITE (*,*)TIME (I)
20  CONTINUE
ELSE
DO 30 I=1,N
TIME (I)=DT (I)*DT (I)/2./DM
C   WRITE (*,*)TIME (I)
30  CONTINUE
ENDIF

C
C   FIND THE TIME STEPS
C
DO 40 I=N,2,-1
DT (I)=TIME (I)-TIME (I-1)
C   WRITE (*,*)DT (I)
40  CONTINUE
DT (1)=TIME (1)
C   WRITE (*,*)DT (1)
RETURN

```

END